

Additive Manufacturing of Sacrificial Cores for Liquid Moulding of Composites

by

Linus Lehnert

B. Eng, McGill University, 2016

Department of Mechanical Engineering

McGill University, Montreal

A thesis submitted to McGill University
in partial fulfillment of the requirements of the degree of
Master of Engineering



March 2019

© Linus Lehnert, 2019

Abstract

Out-of-autoclave techniques such as liquid moulding of complex carbon fibre reinforced polymer structures find many applications in the fabrication of aerospace components. With current structures being assembled from multiple composite parts, a more flexible and cost-effective manufacturing process is of interest. For the development of a novel one-shot moulding process, the usage of sacrificial cores becomes imperative. In this work, a method for the fabrication of additive manufactured sacrificial cores, tailored for liquid moulding of composites, is proposed.

The 3D printed sacrificial cores presented are made from polyvinyl-alcohol copolymers. To determine operational temperature, the coefficient of thermal expansion and the mechanical strength, material characterization was performed. Following, proof-of-concept structures were fabricated to validate the proposed method and identify key challenges for the implementation in a production environment. Time effective core removal was determined as one of the largest difficulties. Therefore, two washout approaches were characterized, tested and implemented to determine optimal parameters for core removal. With an optimized processing method in place, a simple demonstrator structure was designed and fabricated to validate the moulding capabilities of the developed core technology. The results showed that the proposed method was capable of moulding composite structures with comparable quality to conventional moulding methods, while adding the geometrical freedom inherent to additive manufacturing. Lastly, a cost analysis was performed that evaluated the cost of the 3D printer sacrificial core technology and compared it to conventional sacrificial moulding solutions.

The proposed method successfully outlines the application of additive manufactured sacrificial cores in the fabrication of liquid moulded composite structures. Although exhibiting a higher price point than conventional core solutions, the added benefits make this process a feasible solution for low to medium volume production of complex structures.

Abrégé

Les procédés hors autoclave comme le moulage liquide sur renfort de structures complexes en polymère renforcé de fibres de carbone sont couramment utilisés pour la fabrication de pièces pour l'aérospatiale. La majorité des structures sont présentement assemblées à partir de nombreuses pièces en matériaux composites. Le développement d'un procédé de fabrication plus flexible et plus économique présente donc un grand intérêt. Ainsi, l'utilisation de noyaux sacrificiels devient nécessaire afin de fabriquer ces structures en une seule opération. Dans ce travail, l'élaboration d'une méthode de production de noyaux sacrificiels par fabrication additive adaptée au moulage liquide sur renforts est proposée.

Des noyaux sacrificiels imprimés en 3D sont fabriqués à partir de copolymères d'alcool polyvinylique. Afin de déterminer la plage de température pour la fabrication, le coefficient de dilatation thermique et la résistance mécanique ont été mesurés. Ensuite, des prototypes ont été fabriqués pour valider la méthode proposée et identifier les principaux défis pour la mise en œuvre dans un environnement de production. L'élimination efficace du noyau a été identifiée comme étant la plus grande difficulté du procédé. Par conséquent, deux approches de dissolution ont été étudiées afin de déterminer les paramètres optimaux d'élimination du noyau. Avec une méthode de traitement optimisée en place, une structure de démonstrateur simple a été conçue et fabriquée pour valider les capacités de moulage de la technologie de base développée. Les résultats ont montré que le procédé proposé était capable de fabriquer une structure composite avec une qualité comparable aux méthodes de moulage conventionnelles, tout en ajoutant la liberté géométrique inhérente à la fabrication additive. Enfin, une analyse des coûts a été réalisée pour évaluer le coût de la technologie de base sacrificielle pour imprimantes 3D et le comparer aux solutions de moulage sacrificielles classiques.

Le procédé développé dans ce travail illustre avec succès l'utilisation de noyaux sacrificiels par fabrication additive pour la mise en forme de structures composites moulées par injection sur renforts. Bien que leur coût soit supérieur comparativement aux solutions conventionnelles, les avantages associés à cette nouvelle technologie font de ce processus

une solution envisageable pour la production de structures complexes de faible et moyenne série.

Acknowledgements

First and foremost, I would like to thank Professor Pascal Hubert for taking me on as a master's student and providing me with this great opportunity. I am very grateful for the guidance and advice he provided throughout this project and I have been fortunate to have him as my supervisor and mentor.

I would also like to thank Martin Levesque and Antonin Leclair-Marechal at Hutchinson for the guidance, help and resources they provided to ensure this project remained on track. I am very thankful to them for integrating me into their work environment, allowing me to grow on an educational as well as professional level.

I would further like to sincerely thank Louis Grou and Derek Harvey; I am very happy to have such great colleagues and friends. Not only were they a great resource to exchange ideas with and offer new insights, they also assisted me greatly in my work when needed.

To all the other members of the McGill Structures and Composite Materials group, I would like to extend my thanks, most notably to Lucie Riffard and Adam Smith for their assistance and help. Furthermore, I would like to thank Steve Hypolite and Franck Guillemand at Hutchinson for their assistance and knowledge in fabricating composite structures.

Lastly, I would like to greatly acknowledge the financial support provided by the Consortium for Aerospace Research and Innovation in Canada (CARIC), the Consortium for Research and Innovation in Aerospace in Quebec (CRIAQ), the Research Centre for High Performance Polymer and Composite Systems (CREPEC), Mitacs, and industrial partner Hutchinson Aerospace & Industry. Without their support, this project would have not been possible.

Table of contents

Abstract	II
Abrégé.....	III
Acknowledgements	V
Table of contents.....	VI
List of Figures	X
List of Tables.....	XV
1 Introduction	1
1.1 Motivation	2
1.2 Research Objectives and Thesis Organization	4
2 Technology Review	7
2.1 Flyaway Cores	8
2.2 Removable Inserts.....	9
2.2.1 Rigid Inserts	9
2.2.2 Inflatable Cores.....	10
2.3 Sacrificial Cores	11
2.3.1 Eutectic Salt Cores	11
2.3.2 Plaster-Based Cores	12
2.4 Additive Manufacturing	13
2.4.1 Binder Jetting.....	14
2.4.2 Fused deposition modelling	15
2.5 Technology Summary & Proposal of Thesis Direction	18
3 Process Methodology and Material Characterization	20
3.1 Process Overview	20

3.1.1	Fused Deposition Modelling Parameters	21
3.1.2	Core Requirements	23
3.2	Material characterization	24
3.2.1	Additive Manufacturing Equipment.....	25
3.2.2	Operational Temperature of Cores	27
3.2.3	Coefficient of thermal expansion.....	30
3.2.4	Compressive Strength and Compressive Modulus	33
3.3	Summary of Material Properties	38
4	Evaluation of Sacrificial Core Technologies.....	40
4.1	Handlebar Stem Benchmark	40
4.1.1	Geometry and Tooling.....	41
4.1.2	Core Fabrication	42
4.1.3	Composite Fabrication.....	44
4.1.4	Results and Key Findings.....	46
4.2	Linear Omega Benchmark.....	48
4.2.1	Geometry & Fabrication Process	48
4.2.2	Core Fabrication.....	51
4.2.3	Results & Discussion.....	53
4.2.4	Key Findings	56
5	Dissolution Rate Characterization	58
5.1	Washout Approaches.....	58
5.2	Methodology.....	59
5.3	Results & Discussion	62
5.4	Redesigned Dissolution Experiments.....	63

5.5	Key Findings	65
6	Composite Fabrication using 3D printed Sacrificial Cores	66
6.1	Complex Stiffened Double-Curvature Panel	66
6.1.1	Structure Design & Geometry	66
6.1.2	Implementation of Wash-Out Approaches	67
6.1.3	Composite Fabrication.....	69
6.1.4	Results & Discussion.....	71
6.1.5	Key Findings	74
6.2	X-shaped Stiffened Panel.....	76
6.2.1	Structure Design & Geometry	76
6.2.2	Fabrication Process and Tooling	76
6.2.3	Cores and Processing Parameters.....	77
6.2.4	Study #1	78
6.2.5	Study #2	83
6.2.6	Study #3	87
7	Cost Analysis	91
7.1	Methodology.....	91
7.1.1	Investment.....	91
7.1.2	Production cost.....	92
7.2	Cost assessment	94
7.2.1	Case Study.....	94
7.2.2	Process Analysis	95
7.3	Cost Comparison	106
7.4	Key Findings	108

8	Conclusions & Future Work.....	109
8.1	Conclusions.....	109
8.2	Future Work.....	112
9	References.....	114

List of Figures

Figure 1.1. Boeing 787 Dreamliner - 50% composite usage by weight [2].....	1
Figure 1.2: Hybrid glareshield assembly containing several sub-assemblies [3].....	2
Figure 1.3. Large picture objective: One-shot, net-shape structure fabrication by unitization of key manufacturing aspects. Conventionally, the glareshield structure shown is assembled from 46 separate parts. The novel one-shot process would combine these into a single moulded structure.	3
Figure 1.4. Thesis progression to develop sacrificial cores for liquid moulding of composites.	5
Figure 2.1. Overview of conventional core technologies for the fabrication of hollow composite structures.....	7
Figure 2.2. Water-soluble sacrificial core for the fabrication of hat-stiffened panel [14].....	12
Figure 2.3. Overview of additive manufacturing technologies [16].....	13
Figure 2.4. Surface finish of parts fabricated by binder jetting. Process-inherent are sand-like surface finishes and relatively high part porosity.....	15
Figure 2.5. Visualization of fused deposition modelling process.	16
Figure 2.6. 3D printed ULTEM tool used for the fabrication of composite UAV fan blade [20].	17
Figure 2.7. 3D printed sacrificial tooling used for fabrication of hollow composite structure [22]. 3D printed core (left) and finished hollow composite structure (right).	17
Figure 3.1. Process overview of additive manufacturing of cores for complex hollow composite structures.....	20
Figure 3.2. Schematic of fused deposition modelling process [27].	22
Figure 3.3. Overview of infill patterns offered in slicing software. (a,b,c) 2D infill patterns shown in grey and solid shell shown in black. (d,e) Infill types created by pattern variation in build direction.....	23

Figure 3.4. Additive manufacturing system used to fabricate samples and cores.	25
Figure 3.5. Build orientation for 3D printed structures using fused deposition modelling.	27
Figure 3.6. Storage modulus vs. temperature data from DMA analysis for FDM-C material. Onset and inflection point are used to determine the glass transition temperature.	29
Figure 3.7. Glass transition temperature of water-soluble thermoplastic filaments.	29
Figure 3.8. Dimensional change versus temperature data set obtained from TMA testing of FDM-C. The CTE before and after the glass transition temperature are extracted.	32
Figure 3.9. Coefficient of thermal expansion of 3D printed FDM-C.	32
Figure 3.10. Load versus displacement data set obtained from compression testing of FDM-C. Compressive modulus and compressive strength are indicated.	35
Figure 3.11. Compressive strength of 3D printed core materials.	35
Figure 3.12. Compressive modulus of 3D printed core materials.	36
Figure 3.13. Failure modes of compressive strength samples.	36
Figure 4.1. Carbon fibre bicycle stem [30]	40
Figure 4.2. Design overview of handlebar stem [30]	41
Figure 4.3. Overview of stem resin transfer moulding tooling [30]	42
Figure 4.4. Overview of 3D printed cores for stem prototype.	42
Figure 4.5. 3D printed core structure for bicycle stem.	44
Figure 4.6. Resin transfer moulding setup for bicycle stem moulding/	44
Figure 4.7. Carbon fibre bicycle stem after demoulding and trimming.	45
Figure 4.8. Solvent entry point for dissolution of PVA stem core.	46
Figure 4.9. Bicycle stem cross-section showing 3D printed sacrificial core.	46
Figure 4.10. Linear omega benchmark geometry with cut-out section.	48
Figure 4.11. Overview of omega benchmark geometry.	48
Figure 4.12. Vacuum assisted resin infusion setup for omega benchmark fabrication.	49

Figure 4.13. Insert geometries of omega benchmark. Overview of assembly with silicone core (a), 2.5D inserts Type A (b) and insert with integrated C-lip (c).....	50
Figure 4.14. Type C core geometry of omega benchmark. Complete omega core with integrated cut-out features.	51
Figure 4.15. Results of Omega Benchmark Core 1.	53
Figure 4.16. Results of Omega Benchmark <i>Core 2</i>	54
Figure 4.17. Cast ceramic inserts. The inserts show a highly porous structure and are very brittle. Damage-free demoulding was not achieved after several attempts.....	55
Figure 4.18. 3D printed ceramic core made using binder jetting process.....	55
Figure 4.19. Omega benchmark with 3D printed ceramic core.	56
Figure 5.1. Experimental setups to investigate rate of dissolution.	61
Figure 5.2. Comparison of effective dissolution rate of FDM-A material for different solvents.	62
Figure 5.3. Effective dissolution rate for agitated water and ultrasonic cleaning approach at different temperatures.	63
Figure 5.4. Redesigned dissolution setup.....	64
Figure 6.1. Optimized demonstrator panel.....	67
Figure 6.2. 3D printed PVOH mandrels of complex stiffener benchmark.....	68
Figure 6.3. Water agitation approach: Composite structure and circulation pump before bath is filled with water.....	68
Figure 6.4. Ultrasonic cleaning approach: Composite structure mounted in ultrasonic cleaning bath.....	69
Figure 6.5. Surface finish and porosity of 3D printed PVOH core.....	70
Figure 6.6. Demoulded composite structures.....	72
Figure 6.7. Geometry of X-shaped benchmark panel.	76

Figure 6.8. Sacrificial core geometry with net-shape cut-out section – X-shape stiffener, study #1.	79
Figure 6.9. Preform after binder melting prior to trimming (a), net-shape preform after trimming operation.	80
Figure 6.10. Dissolution setup for X-shaped stiffener. (a) Panel submerged and connected to water inlets. (b) Flow pattern through stiffener during dissolution.	81
Figure 6.11. X-shaped composite panel – Study #1.	82
Figure 6.12. Fabrication defects in X-shaped stiffened panel.	83
Figure 6.13. Redesigned X-shaped stiffener for Study #2. Added features include smooth end sections and larger transition radius between stiffener legs.	84
Figure 6.14. X-shaped composite panel with sacrificial core – Study #2.	86
Figure 6.15. Resin starvation on skin of X-shaped stiffened panel Study #2.	86
Figure 6.16. Resin rich stiffener ends of X-shaped stiffened panel Study #2.	86
Figure 6.17. Redesigned X-shaped stiffener features for Study #3.	88
Figure 6.18. Results of X-shaped composite panel – Study #3.	89
Figure 6.19. Comparison of fabrication quality of stiffener ends.	89
Figure 7.1. Omega benchmark structure selected as case study for the cost analysis.	94
Figure 7.2. Core geometry with dimensions used for cost analysis study.	94
Figure 7.3. Process steps for casting a sacrificial core.	96
Figure 7.4. Comparison of recurring cost analysis results for cast cores.	100
Figure 7.5. Process steps for fabrication of 3D printed cores.	102
Figure 7.6. Comparison of recurring-cost analysis results for 3D printed cores.	105
Figure 7.7. Production cost versus production volume for sacrificial core technologies. Low volume production ranging from 0-30 parts (top) and medium volume production ranging from 0-350 parts (bottom).	107

Figure 8.1. Workflow of covered work.	110
--	-----

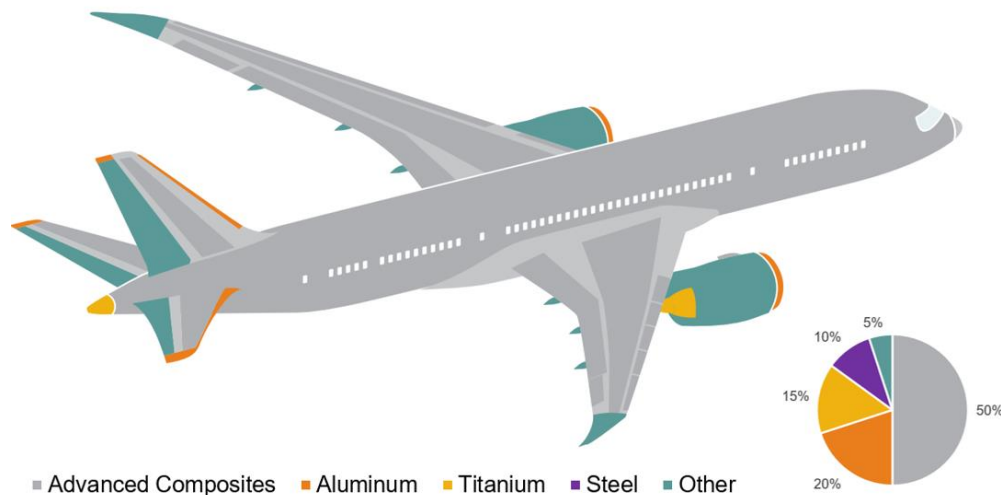
List of Tables

Table 3.1. Critical parameters for cores used in liquid moulding of composites.....	24
Table 3.2. Overview of sacrificial material for fused deposition modelling.....	24
Table 3.3. Raise3D N2 printer specification	26
Table 3.4. Experimental parameters for DMA characterization.....	28
Table 3.5. Test parameters for TMA analysis.....	31
Table 3.6. Compression test: Sample and test parameters.....	34
Table 3.7. Material properties summary. FDM-A, FDM-B and FDM-C have been characterized; all other information was gathered from manufacturer datasheets.	39
Table 4.1. Manufacturing information of 3D printed cores for stem prototype.....	43
Table 4.2. Resin transfer moulding parameters for bicycle stem.	45
Table 4.3. Fabrication parameters of omega benchmark.....	49
Table 4.4. Core test matrix for omega benchmark.....	51
Table 4.5. Omega insert fabrication parameters.	52
Table 5.1. Test matrix for dissolution characterization.....	60
Table 5.2. Sample geometry and fabrication parameters of specimens used in dissolution characterization.....	60
Table 6.1. Core parameters for 3D printing.....	70
Table 6.2. Summary of proof-of-concept fabrication parameters.....	71
Table 6.3. Dissolution approaches and cycle times.	72
Table 6.4. Additive manufacturing parameter for X-shape panel case study.....	78
Table 6.5. Fabrication parameters of X-shaped composite panel for study #1.....	80
Table 6.6. Fabrication parameters of X-shaped composite panel for Study #2.....	85
Table 7.1. Standardized cost rates.....	95

Table 7.2. Cost of casting tools for sacrificial cores via casting.....	96
Table 7.3. Fabrication cost analysis of cast cores.....	98
Table 7.4. Material cost analysis of cast cores	99
Table 7.5. Fabrication cost analysis of 3D printed sacrificial cores.	103
Table 7.6. Material cost for 3D printed cores.....	104

1 INTRODUCTION

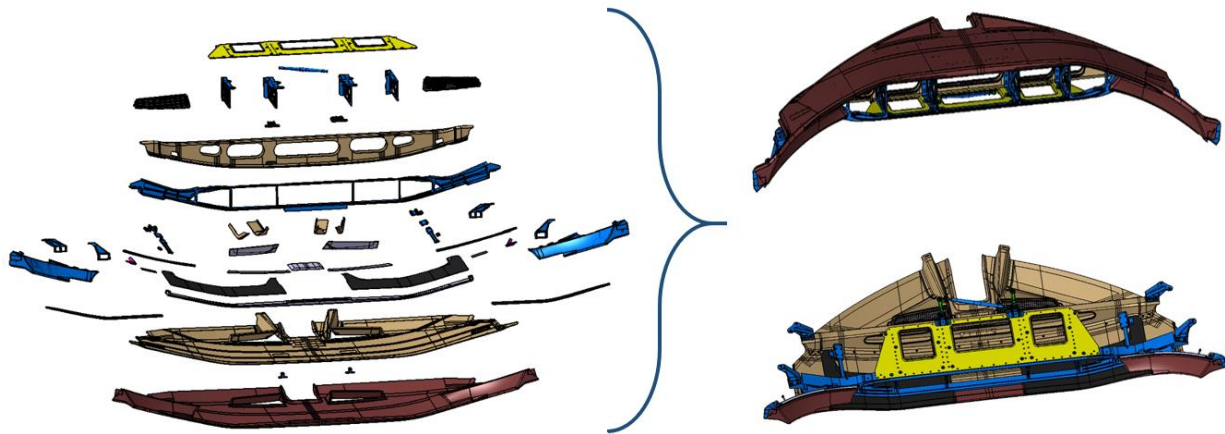
Complex carbon fibre reinforced polymer (CFRP) structures find many applications in the aerospace industry due to their excellent mechanical properties, low weight and corrosion resistance. Starting with the first patent on carbon fibres in 1961, the processing knowledge and application field has steadily grown. Although at first only having limited applications in the aerospace sector due to challenges in processing as well as high material and manufacturing cost, modern composite structures are now widely spread in personal, military and commercial aircrafts. For example, the Boeing 777 introduced in 1994 featured a total of 12% composite material by weight, while the Boeing 787 Dreamliner released in 2012 featured as much as 50 percent composite material by weight [1] as shown in Figure 1.1.



Reproduced with permission from The Boeing Company

Figure 1.1. Boeing 787 Dreamliner - 50% composite usage by weight [2].

Most of these CFRP structures consist of multiple assembled parts forming complex sub-assemblies that are mounted to the frame of the aircraft. In this context, complex structures are defined as hybrid assemblies, that mostly consist of CFRP parts combined with hardware and inserts made from metal and polymers such as the interior cockpit panel shown in Figure 1.2.



Reproduced with permission from Hutchinson Aerospace & Industry

Figure 1.2: Hybrid glareshield assembly containing several sub-assemblies [3].

Often featuring complex shapes, the traditional manufacturing process consists of an elaborate multi-step process including the fabrication of several single composite parts, assembly using mechanical fastening or adhesives, as well as an array of trimming and finishing steps. This excessive number of processing steps translates into long manufacturing times, high production cost as well as unoptimized designs that are heavy and struggle to achieve a high repeatability.

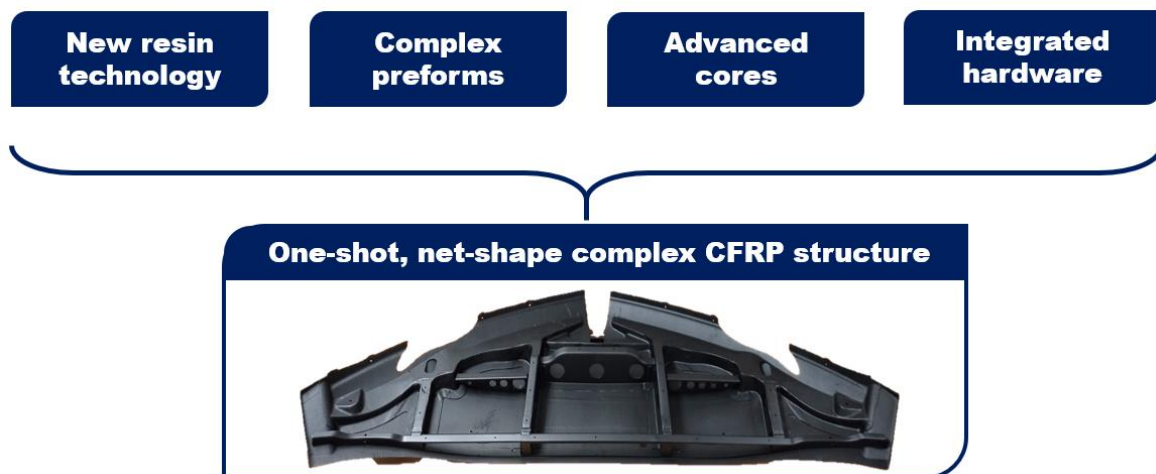
With recent advancements in composite manufacturing, the aerospace industry is moving towards a variety of out-of-autoclave (OOA) processing techniques. Resin Transfer Moulding (RTM) and its lower pressure variant Vacuum Assisted Resin Transfer Moulding (VARTM), also often referred to as Vacuum Assisted Resin Infusion (VARI), show promising potential as an effective fabrication process for complex CFRP structures. Due to its comparatively low price point and excellent surface finish, RTM and VARI are especially of interest for manufacturing complex interior aircraft structures that are visible and require a high level of aesthetics.

1.1 Motivation

One of the largest drivers in today's aerospace industry is remaining cost-competitive by the implementation of novel manufacturing technologies. Next to the ability of fabricating high-

quality structures at low cost, flexible manufacturing processes adapted to low to medium production volumes are in high demand. Geometries and requirements are steadily evolving, making adjustable production lines crucial. The manufacturing process for complex structures currently in place struggles to keep up with these demands, motivating the industry to invest into the development of more optimized and advanced ways to fabricate complex CFRP structures. Recent advances in resin technology, fibre preforming as well as additive manufacturing have widened the design space and offer prospects that could overcome these challenges.

The large picture objective is the development of a net-shape, one-shot moulding process that combines most assembly and finishing steps into a one-step fabrication process as shown in Figure 1.3.



Reproduced with permission from Hutchinson Aerospace & Industry

Figure 1.3. Large picture objective: One-shot, net-shape structure fabrication by unitization of key manufacturing aspects. Conventionally, the glareshield structure shown is assembled from 46 separate parts. The novel one-shot process would combine these into a single moulded structure.

Currently, the glareshield structure shown in Figure 1.3 is assembled from 46 separate parts. The one-shot approach would unitize these several parts into one single moulded structure featuring highly complex geometries. This unitization would not only result in a cost-effective fabrication process but would also eliminate various fasteners and adhesives. In addition, with the use of preforming technologies and novel cores, net-shape feature

moulding would be enabled. Furthermore, integration of metallic fasteners and placeholder inserts would not only improve dimensional tolerances, but also eliminate the need for additional machining operations. To develop such a process, a significant development effort is required in several fields.

One main component is the development and integration of hollow cores and tooling technologies. New materials and processes introduced by the industry, as well as additive manufacturing, demonstrate novel approaches that may be translated to the liquid moulding of composites. While these technologies offer a much higher level of design freedom than comparable alternatives, many of them are relatively new and their application is not well documented. The level of maturity as well as financial feasibility of these technologies, especially in combination with liquid moulding of large and complex assemblies, is unknown.

1.2 Research Objectives and Thesis Organization

This research contribution aims to advance the state of the art in application of freeform core technologies and additive manufacturing in the composite manufacturing field. In this context, *core* is defined as tooling surrounded by reinforcement and resin during the fabrication process. Generally rigid or semi-rigid, cores fill and shape the composite part from the inside, similar to tooling shaping the outside. A cylindrical core is often referred to as *mandrel*.

The objective of this thesis is to analyse, evaluate and integrate novel core technologies and additive manufacturing approaches in conjunction with liquid moulding. The main focus of this work is on developing a method for the fabrication of sacrificial cores by additive manufacturing, more specifically fused deposition modelling (FDM), that would enable the fabrication of complex and hollow composite structures. However, other suitable core technologies are reviewed and briefly investigated as alternative technologies.

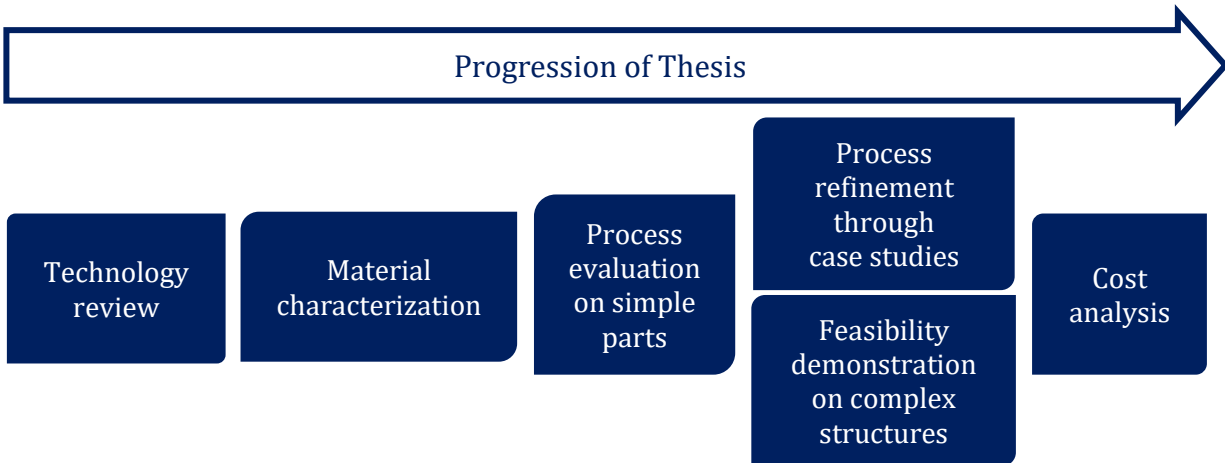


Figure 1.4. Thesis progression to develop sacrificial cores for liquid moulding of composites.

Figure 1.4 depicts the progression of this thesis by outlining the five milestones addressed. According to these milestones, this thesis is divided into several chapters which split the progression of the works as follows:

- Chapter 2 - Technology Review: A generalized review on core technologies for composite manufacturing as well as on additive manufacturing processes is conducted. Literature and case studies are consulted to identify the most promising technologies applicable to liquid moulding, as well as to identify possible risk and challenges.
- Chapter 3 – Process Methodology and Material Characterization: Background knowledge of fused deposition modelling is provided and a fabrication process for sacrificial cores is proposed. Relevant material testing is conducted, determining the operational temperature, the coefficient of thermal expansion and the compression strength of the selected materials.
- Chapter 4 - Evaluation of Sacrificial Core Technologies: Selected technologies are evaluated for their technical feasibility on simple geometries. Several small case studies are fabricating to identify processing issues and limitations.
- Chapter 5 - Dissolution Rate Characterization: Two different washout approaches are introduced, and dissolution conditions are analyzed. Optimized dissolution parameters are developed for time-efficient core removal.

- Chapter 6 - Composite Fabrication using 3d Printed Sacrificial Cores: The developed process is further analyzed and refined using experimental methods. Using a complex geometry, the technical feasibility of 3D printed sacrificial cores is validated.
- Chapter 7 – Cost Analysis: An approach to determining the cost of different core technologies is introduced. By comparing the cost of the developed process to conventional core technologies, financial feasibility is verified.
- Chapter 8 – Conclusion: The application state of 3D printed sacrificial cores is reviewed and perspectives for future work are discussed.

2 TECHNOLOGY REVIEW

To obtain an overview of different core technologies that are potentially suitable for the moulding of hollow complex composite structure, a technology review was carried out. The aim of this review was to create a compilation of core solutions currently offered on the market. Furthermore, a review of additive manufacturing processes was conducted to understand which technologies are most suited for the creation of 3D printed cores.

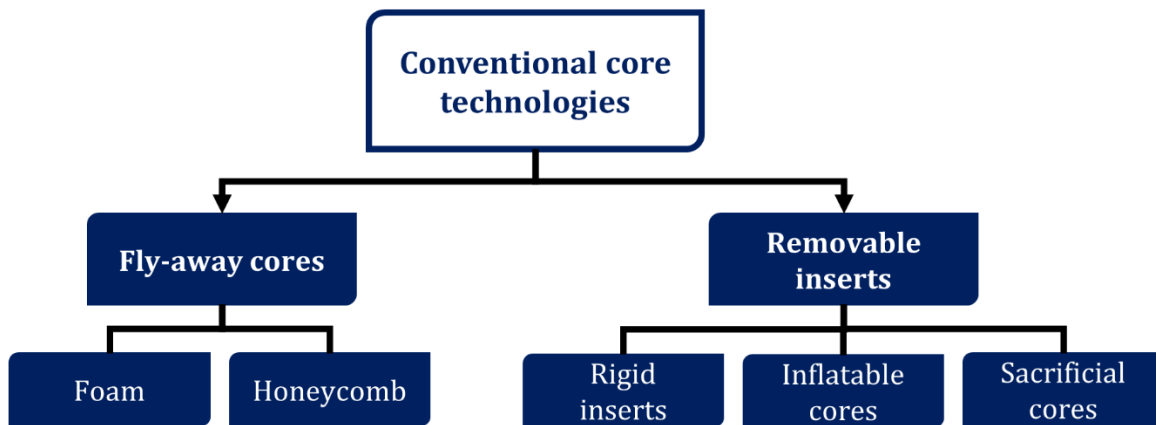


Figure 2.1. Overview of conventional core technologies for the fabrication of hollow composite structures.

The scope of the search encompassed all types of technologies that are offered as a core or sandwich material for the fabrication of composite structures. Figure 2.1 depicts an overview chart showing all reviewed technologies [4] .

These core technologies can be separated into two categories, namely *flyaway cores* and *removable inserts*. In this context, *flyaway cores* are defined as cores that remain in the composite structure throughout its lifetime. *Removable inserts* are defined as temporary cores that are removed during fabrication to yield a hollow composite structure.

2.1 Flyaway Cores

The two most popular variants of *flyaway cores* are honeycomb and foam cores. Although honeycomb is one of the most popular materials used in the fabrication of composite sandwich panels, the nature of the material makes the shaping into complex three-dimensional structures difficult. Furthermore, the open-cell structure poses a challenge in combination with liquid moulding. These drawbacks make honeycomb cores not well suited for complex three-dimensional hollow structures.

Foam is a type of cellular material in which cells are arranged in a three-dimensional space rather than a two-dimensional space as in honeycomb [4]. While many materials can be produced as a cellular solid, polymers are the most common. For complex composite structures, only rigid foams are of interest. Most commonly found rigid foam materials are polyvinyl (PVC), polyurethane (PU), polymethacrylimide (PMI) and epoxy foams. For aerospace applications, the required flame-smoke-toxicity (FST) rating narrows the material choices to PMI and epoxy foams, however, recent advances in polymer composition also introduced PU foams that pass FST regulations while offering a competitive price point [5].

Most foam materials are supplied in blocks and hence the most common methods to fabricate complex shaped cores are subtractive manufacturing processes such as multi-axis milling or turning. While this allows for high core complexity and accurate tolerances, computer numerically controlled (CNC) machining of cores is associated with significant fabrication cost.

In-mould foaming is a cost-effective alternative for creating complex-shaped cores [6]. Rather than the material being foamed into a block at the supplier's facility, the material is directly foamed into the desired shape, producing a net-shape foam core. This not only reduces material waste, but also eliminates any costly machining operations. Depending on the material choice, the foaming processes might require elevated temperatures and high pressure, making the process similar to compression moulding, or can be conducted at room temperature and low pressure, comparable to casting. However, only a limited material selection is currently available on the market that offers this manufacturing option.

One notable material is castable, closed-cell syntactic epoxy foam [7]. This type of foam is based on an epoxy resin system, offering high strength and stiffness. Furthermore, the closed cell structure makes this foam ideal for liquid moulding applications since the core is inherently sealed from resin infiltration. In addition, incorporated flame retardants fulfil the required fire resistance for aerospace usage. Lastly, the low pressure and low temperature casting conditions make this material ideal for low volume production while offering a competitive price point.

Foam cores with closed-cell structure have been successfully used with liquid moulding processes. A study conducted on landing gear doors of a Dornier 728, compared a honeycomb core to a closed-cell PMI foam core [8]. Next to demonstrating the successful combination of liquid moulding and foam cores, the study showed a 25% reduction in manufacturing cost and 19% overall weight saving compared to a prepreg structure using a honeycomb core.

2.2 Removable Inserts

Removable inserts can be further separated into three categories, namely rigid inserts, inflatable cores and sacrificial cores.

2.2.1 Rigid Inserts

Rigid inserts for moulding hollow cavities into composite structures are collapsible or deformable solid tools made from metals, composites or polymers [4]. Similar to lay-up or RTM tooling, they provide a rigid surface that shapes the inside of the composite structure. After curing the composite structure, the tool is removed either by pull-out or by disassembly of the core, comparable to a jig-saw puzzle. The largest advantage of using rigid inserts is their reusable nature and the high dimensional control.

Cores fabricated from metals and rigid polymers provide excellent dimensional control and high durability, however, often do not exert consolidation pressure when combined with rigid outer tooling made from the same material, therefore inducing processing defects. Alternatively, solid mandrels made from elastomeric compounds, such as silicon, rely on the difference of coefficient of thermal expansion (CTE) between core and the surrounding

tooling to generate pressure between tooling surfaces. A common usage of these cores are hat-stiffeners for self-stiffened composite parts. The application of rigid inserts is generally limited to easily accessible cavities for extraction. Furthermore, while cores such as hat-stiffeners are simple to fabricate, multi-part cores for complex cavities, especially when made from metals, are expensive and challenging to design and manufacture. Furthermore, multi-part inserts often leave interior seams or ridges in the final part. This tooling technology is often only applicable for manufacturing large production volumes of simple geometries where tool life is the driving factor.

2.2.2 Inflatable Cores

Inflatable cores or bladder tooling consist of an elastomeric compound that is inserted into the layup process and inflated during the cure phase to expand and compress the laminate against the outer tooling [4]. The high elongation capabilities of the used materials make it possible to deflate the tool after curing and remove it completely from the complex structure, leaving a hollow cavity. Several types of inflatable cores exist, namely open bladders, sealed bladders, and shape memory polymers.

Open bladders are filled with a gas over an injection port which expands the bladder and compresses the laminate. After curing, the pressure is released, and the bladder can be removed. Drawbacks include limitations to certain geometries that allow for bladder removal, as well as more complex outer tooling design to accommodate for ports and fixtures to provide gas to the bladder.

Sealed bladders are made from an elastomeric compound and contain a liquid or gel. During the composite fabrication, compression of the bladder by the outer tool leads to a pressure increase in the bladder. If compression is not possible, the bladder can be filled with fluids that have a high coefficient of thermal expansion. Once the core is heated up by the surrounding tooling as part of the moulding process, the liquid will expand and provide the required consolidation pressure. This technology avoids the additional need for ports and seals.

Shape memory polymer (SMP) is an advanced mandrel material with shape recovering properties. It is preformed to a certain shape before the composite fabrication and recovers

its original shape under external stimuli such as heat [9]. First, a blank of SMP material is put into a mould, heated, pressurized and cooled down to yield a mandrel of the desired shape. It is then used as a typical mandrel in the layup process. During the curing phase, the mandrel is again pressurized to consolidate the laminate. After the cure is completed, the mandrel is depressurized at an even higher temperature than the activation temperature and recovers to its original shape, allowing for its removal from the finished composite structure [10].

When used with rigid tooling on the outside, bladders can provide high dimensional tolerances. Inflatable cores have been well established with RTM processes [11] and process parameters have been refined to achieve high quality structures. However, the application field of inflatable cores is restricted to easily accessible geometries and therefore not suitable for complex cavities that don't feature a large opening for core removal. Furthermore, the rigid tooling requirement makes many of the inflatable core approaches not suitable for lower cost liquid moulding processes, such as infusion, that depend on soft shells or vacuum bags.

2.3 Sacrificial Cores

Sacrificial cores, also referred to as soluble or *washout* cores, are rigid structures designed to be disintegrated and removed after the composite fabrication is completed. This is generally achieved by using a core material that has no interaction with the matrix material, however, disintegrates being exposed to a solvent material that in return does not interact with the composite structure. The materials most documented are salt-based and plaster-based.

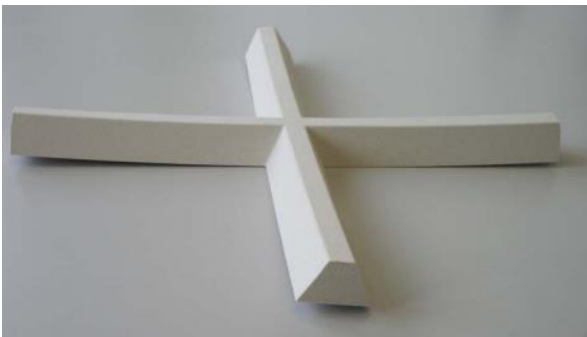
2.3.1 Eutectic Salt Cores

Eutectic salt is an established material for sacrificial cores. The salt is cast in a molten state to the desired shape. This process requires a preheated metal tool, for example heated to approximately 120°C, in which the salt is poured at temperatures of about 260°C [12]. Once cooled down, the product is a high density and brittle core with a smooth, non-porous surface finish. After the composite fabrication process, a high-pressure water stream is required to remove the core. The produced waste water stream is corrosive and

environmentally unfriendly. Although very high tolerances can be achieved with this method, the core production and especially the washout phase are labour-intensive processes.

2.3.2 Plaster-Based Cores

Plaster-based cores are made from a mix of mostly plaster blended with additives and fillers, such as microspheres, to improve heat resistance and fabrication characteristics. These materials are available in several forms such as solid blocks or castable solutions [12, 13]. To fabricate a core from the solid block form, subtractive manufacturing identical to the machining of foam cores is used. The castable version uses a low pressure and low temperature casting process to create a shaped sacrificial core. However, an additional curing step is required, in which the material shrinks significantly. Although offsets in tooling can counteract this shrinkage, dimensional accuracy is comparatively low to other sacrificial core technologies. Lastly, finishing steps such as filling larger porosity with fillers and wrapping the core in sealant tape require additional labour. An example of a plaster-based washout core is shown in Figure 2.2.



(a) Machined plaster-based core before moulding.



(b) Washout of core from moulded composite structure using water

Reproduced with permission from Aero Consultants AG

Figure 2.2. Water-soluble sacrificial core for the fabrication of hat-stiffened panel [14].

2.4 Additive Manufacturing

Additive manufacturing (AM) is a fabrication process that enables the manufacturing of a three-dimensional computer aided design (3D CAD) without the need for elaborate process planning or tooling [15]. The general idea is that the designed model is manufactured by adding thin layers of material over each other, building up the desired geometry layer by layer. This offers large geometrical freedom during the design process and allows to produce highly complex geometries. A large variety of 3D printing technologies have been developed for a variety of materials, including polymers, metals and ceramics. Figure 2.3 gives a general overview of the most common additive manufacturing technologies.

Vat photopolymerization and associated technologies such as stereolithography (SLA) and digital light processing (DLP) functions by curing a photo-reactive resin using a light source, such as a laser or projector. Parts produced with this technology offer good mechanical strength as well as very high accuracy and surface finish. However, the material selection is limited to few selected thermoset resins and the overall fabrication cost is comparatively high.

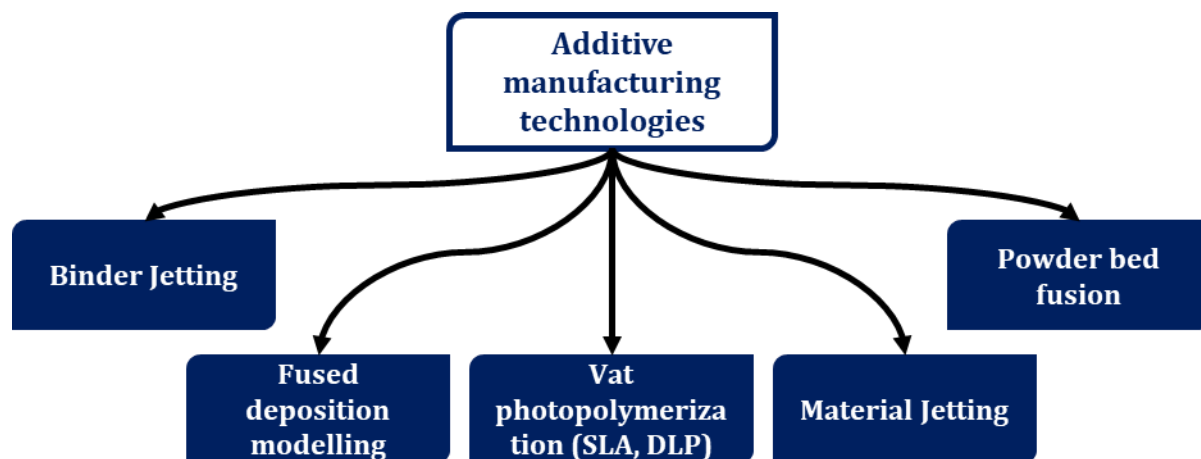


Figure 2.3. Overview of additive manufacturing technologies [16]

Material jetting relies on a similar working principle as an inkjet printer. It uses a print head to deposit liquid material onto a build platform, which is subsequently cured using an energy source such as a UV light. Advantages of this technology are the high print speed, as well as

the option to print multiple materials or colours simultaneously. As with VAT polymerization, the material choice is limited to a few specialty thermoset resins.

Powder bed fusion entails methods such as selective laser sintering (SLS) and selective laser melting (SLM). In this process, thin layers of powder are spread, and the desired part geometry is traced using a high-powered laser. Depending on the process, the powder is then fused or melted together. Common materials are both polymers and metals. Powder bed fusion offers fast production speeds and resulting parts offer good mechanical strength. Disadvantages are the rough surface finish and lower accuracy, as well as the very high operating cost.

After review, binder jetting and fused deposition modelling were deemed as the most suitable for the fabrication of flyaway and sacrificial cores. The following presents a deeper introduction of both technologies and their applicability for the fabrication of cores used with liquid moulding processes.

2.4.1 Binder Jetting

In binder jetting, thin layers of powder are deposited and hardened to the desired geometry using a small stream of binder [16]. The powders offered are most often metal or ceramic materials. Since the entire build area is filled with powder, the geometry itself is supported and no extra support is needed, reducing material cost and print time significantly. Therefore, this additive technology is one of the fastest and cost-effective for building larger structures. Parts printed from ceramics are often used in investment casting as disposable tooling, while metal prints undergo an additional sintering process to be used as functional parts. Compared to other AM methods such as fused deposition modelling, the surface finish is significantly rougher as shown in Figure 2.4, part accuracy is lower and small features can often not be printed.



Figure 2.4. Surface finish of parts fabricated by binder jetting. Process-inherent are sand-like surface finishes and relatively high part porosity.

One commercial option is currently marketed towards sacrificial cores for composite fabrication. The cores are manufactured using silica powder and a water-soluble binder, allowing for the dissolution of the core using water. Proof-of-concept parts, such as cylindrical vessels, demonstrate the technical feasibility with composite fabrication techniques such as prepreg layup and filament winding [17]. However, successful application with liquid moulding has not been demonstrated to the author's knowledge.

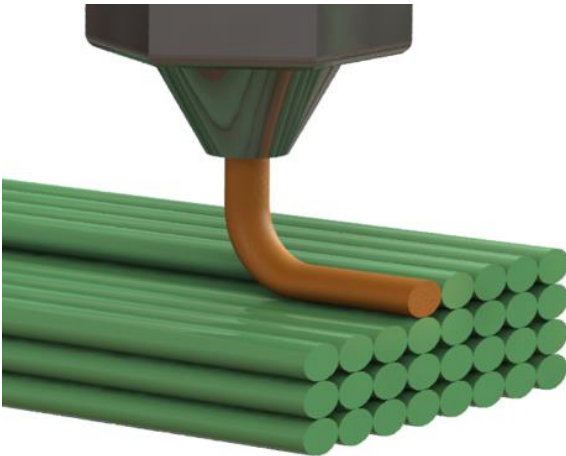
One big challenge in using cores fabricated by binder jetting is the high porosity of the 3D printed part. Although a barrier coat is applied to seal the porous surface, a small leak or crack in the coating will drive significant amounts of resin into the core during liquid moulding. Although suppliers have developed proprietary coating processes that supposedly prevent any resin infiltration, the technical feasibility of these cores in conjunction with liquid moulding of composites must be validated.

2.4.2 Fused deposition modelling

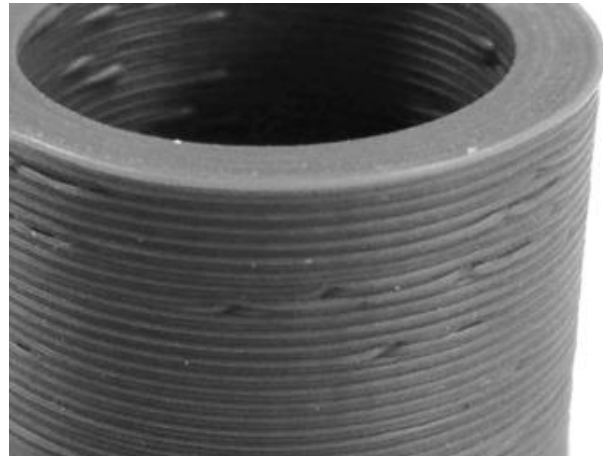
Fused Deposition Modelling (FDM) or Fused Filament Fabrication (FFF) belongs to the group of extrusion based additive manufacturing (EBAM) and is one of the most widely used

additive manufacturing technologies [16]. In this manufacturing process, a polymer is molten and extruded through a small nozzle. The resulting structure is therefore formed by fusing beads of thermoplastic material together, as shown in Figure 2.5-a, to ultimately build up a layered structure as shown in Figure 2.5-b.

FDM is known as one of the strongest polymer-based additive manufacturing processes [15]. The material selection for this process is strictly limited to thermoplastics. Next to commodity plastic, higher performance materials include Nylon, polyetherimide (PEI) and polyether ether ketone (PEEK).



(a) Molten extrusions of thermoplastic material are deposited adjacent to each other to build up a structure.



(b) Surface finish of 3D printed structure showing layered surface finish.

Figure 2.5. Visualization of fused deposition modelling process.

The concept of using FDM technology to create tooling for composite fabrication has gained increasing attention in the literature over the past years. Li H. et al [18] have investigated properties such as dimensional accuracy and surface roughness of FDM tooling for application in VARI. T. Schniepp et al. showed characterization efforts for the development of a design guide to use FDM to fabricate tooling for composite fabrication with high-performance polymers such as ULTEM [19]. They specifically investigated dimensional

accuracy and stability of 3D printed tools after thermal cycling to estimate tool life. The 3D printed tool under investigation is shown in Figure 2.6.



Reproduced with permission from Stratasy

Figure 2.6. 3D printed ULTEM tool used for the fabrication of composite UAV fan blade [20].

To the knowledge of the author, only one commercial supplier offers a dissolvable thermoplastic that is specifically marketed for the use of sacrificial tooling material to produce composite structures [21]. The polymer is based on proprietary technology and requires the use of an alkaline cleaning agent for dissolution. It is suitable for autoclave and out-of-autoclave processes and successful manufacturing in combination with prepreg material has been reported. An application example is the duct shown in Figure 2.7.



Reproduced with permission from Stratasy

Figure 2.7. 3D printed sacrificial tooling used for fabrication of hollow composite structure [22]. 3D printed core (left) and finished hollow composite structure (right).

Polyvinyl-alcohol (PVOH) based materials are commonly used in FDM as support materials for printing complex geometries. Many suppliers have developed PVOH-copolymer filaments for this purpose and they are freely available for most current FDM systems, offering a competitive price-point to proprietary material systems [23-25]. These materials show good potential to be used as sacrificial cores for liquid moulding of composites.

Although many aspects in the field of additive manufacturing have been explored, the usage of 3D printed sacrificial mandrels using FDM is still a new application which is not well covered in the literature. One study by N. Lakshman et al. investigated the influence of HIPS and PVOH mandrels on the mechanical strength of composite structures and demonstrated the usage of PVOH mandrels in combination with wet-layup [26]. They determined that there was no significant impact on the composite strength when using PVOH-based mandrels.

To the knowledge of the author, no work so far has outlined or proven a manufacturing process involving sacrificial 3D printed mandrels in combination with liquid moulding of composites.

2.5 Technology Summary & Proposal of Thesis Direction

From the technologies and solutions discussed so far, the following conclusions are drawn:

- Limited commercially available core options are on the market suitable for liquid moulding of composite structures
- Foam cores are well established, but require high-cost multi-axis machining to achieve complex geometries
- Castable foam materials offer a low-cost fabrication alternative for complex geometries
- Rigid and inflatable pull-out cores are most suitable for simple and easy accessible features
- Sacrificial cores offer the highest geometrical complexity combined with a simple integration into the moulding process
- Plaster-based sacrificial cores are most common, but pose processing issues when combined with liquid moulding

- 3D printed ceramic cores offers a promising sacrificial core solution for complex geometries, but material porosity might pose processing issues when combined with liquid moulding
- Fused deposition modelling is gaining popularity in tool and core fabrication for composite processing
- No applications have successfully proven sacrificial FDM cores combined with liquid moulding
- PVOH-based materials exhibit high potential for cost-effective 3D printed sacrificial cores

To recall, the objective of this work is to evaluate and develop core technologies that are suitable for the fabrication of composite structures using a liquid moulding process. While some of the reviewed technologies offer a technically feasible option, the main driver is commercial feasibility. Weight reduction and overall performance increase in composite structures by using complex shaped cores is only of interest for industrial applications if the associated cost is competitive to alternative manufacturing processes. The target application defined by the industrial partner is the low-volume production of secondary and tertiary aerospace structures, such as interior aircraft panels [3]. Many of the presented technologies require expensive 5-axis machining steps that are not suitable for truly complex geometries or have financially infeasible material costs. While some technologies, such as cast foam cores and cast sacrificial cores, seem to meet the given requirements, no successful application has been shown in combination with liquid moulding. Therefore, it was concluded that the most suitable approach is to focus on 3D printed sacrificial cores.

In this thesis, a process is developed and proposed to fabricate sacrificial cores via fused deposition modelling applicable to composite fabrication via liquid moulding. Commercially available PVOH-copolymer materials were chosen for this development.

3 PROCESS METHODOLOGY AND MATERIAL CHARACTERIZATION

This chapter will introduce the proposed process to create complex shaped sacrificial cores via FDM. Manufacturing details as well as the necessary background information of FDM is provided. Relevant requirements for cores used with liquid moulding are discussed. The process methodology selected to fabricate 3D printed cores is outlined and material characterization to determine relevant material properties is conducted.

3.1 Process Overview

The manufacturing process to create complex shaped sacrificial cores generally consists of five major steps as outlined in Figure 3.1.

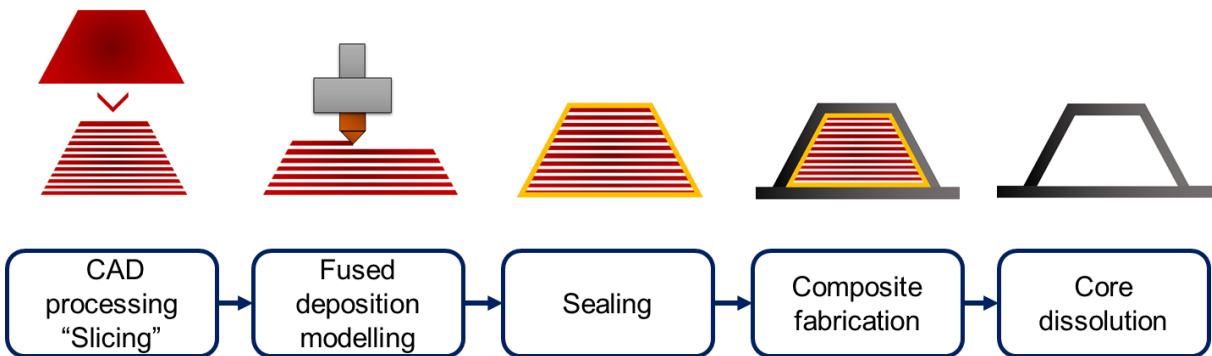


Figure 3.1. Process overview of additive manufacturing of cores for complex hollow composite structures.

The process starts with a 3D CAD model of the complex shaped core. Then, the core geometry is prepared for 3D printing in a step called *slicing*. In this step, various design and process parameters are selected and defined for the 3D printing process. The result is an output file containing the toolpath and extrusion head behaviour that is directly fed to the 3D printer. A more complete description and analysis of this step are provided below. In the next step, the core is printed from the desired thermoplastic material.

Once the core is fabricated, the next step is the sealing process. Since most sacrificial cores present a certain level of porosity, the sealing is necessary to prevent resin infiltration during the moulding process to retain the cores integrity as well as the soluble characteristic. This can be achieved by a spray or brush on coating, by wrapping the core in a sealant tape, or by combining both.

Finally, the fibre preform is combined with the sealed core to fabricate the composite structure using a liquid moulding process such as RTM or VARI. Once the structure is completely cured, it can be demoulded to reveal the final part with the core inside.

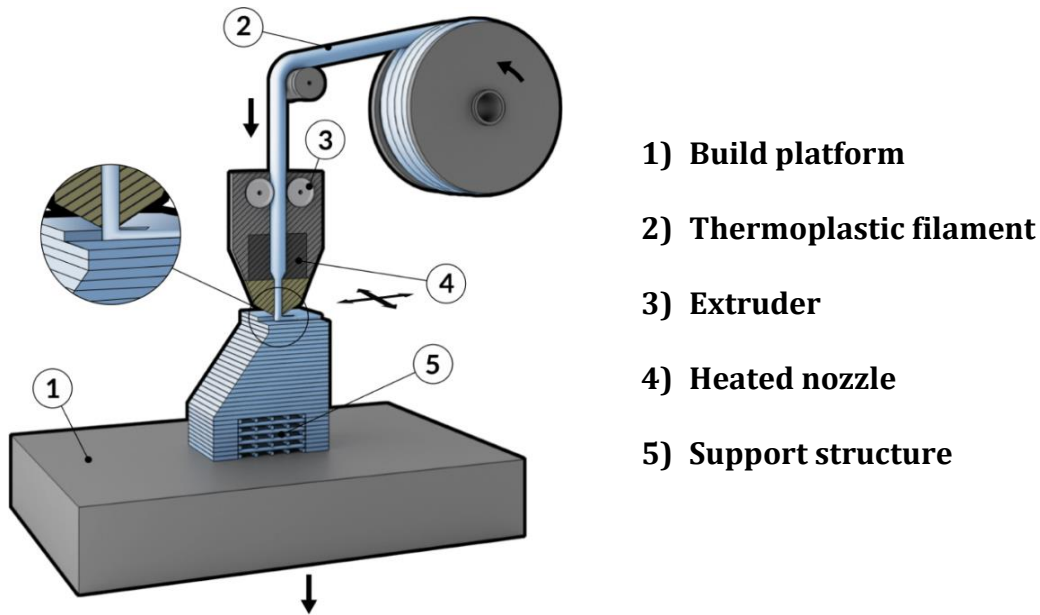
The last step of this process consists of dissolving and therefore removing the sacrificial core. The result is a complex hollow composite structure.

3.1.1 Fused Deposition Modelling Parameters

To design an efficient and functional soluble mandrel, an understanding of the composition of parts created by FDM is necessary.

The basic components of an FDM 3D printer are outlined in Figure 3.2. In the printing process, a thermoplastic filament is fed by an extruder through a heated nozzle controlled in three-dimensional space. The molten and liquefied polymer is deposited layer by layer onto a build platform, starting with the outer perimeter of the part followed by a repetitive pattern to fill the inside. The position of the nozzle is controlled by a computer numerically controller (CNC) motions systems.

To program the 3D printer from the CAD geometry, a processing software, referred to as a *slicer*, is used. The slicer automatically creates a geometry separated into a shell and infill component and generates the toolpath for the 3D printer. The shell is a thin layer of solid polymer forming an outer hull of the desired geometry, while the infill is an internal structure occupying the hollow cavity of the part. An example is shown in Figure 3.3-a, where the infill pattern is represented in grey, while the solid shell is represented by the black outline. Although the infill could be solid, it is often of advantage to use a lightweight and material-saving microstructure. The purpose of the infill is not only to increase the mechanical properties of the part, but it is also required as a support for the deposition of the shell geometry during the printing process.



Reproduced with permission from Manufacturing Guide

Figure 3.2. Schematic of fused deposition modelling process [27].

Most slicers offer 2-dimensional infill patterns that are oriented perpendicular to the build direction. Typical infill patterns are rectilinear, honeycomb and triangular as shown in Figure 3.3-a,b,c. One additional option is the use of continuous infill or sparse infill patterns. In continuous infill, the entire infill pattern is deposited for every printed layer, while in sparse infill the pattern is split into sections which are printed in alternating order every other layer. This creates a lattice type microstructure as shown in Figure 3.3-e. While the continuous infill provides significantly more strength, the sparse infill reduces material usage and print time. The density of the infill pattern is usually specified as a nominal percentage value.

Next to the pattern choice, other design parameters include the shell thickness, the thickness of the most outer layer, the layer height, the height of each layer deposited, and the extrusion width, the width of each bead of polymer extruded. These sets of parameters are selected depending on design requirements and must be defined for each structure printed.

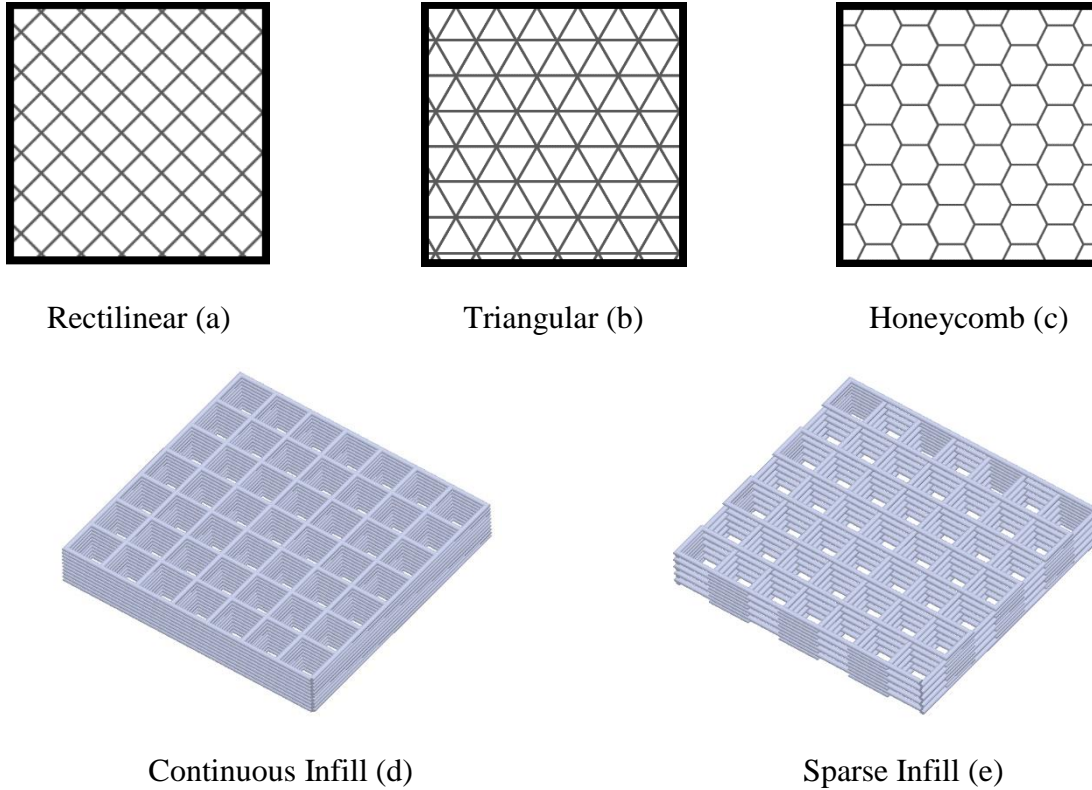


Figure 3.3. Overview of infill patterns offered in slicing software. (a,b,c) 2D infill patterns shown in grey and solid shell shown in black. (d,e) Infill types created by pattern variation in build direction.

3.1.2 Core Requirements

The first step to evaluate and integrate novel tooling materials and technologies is to understand the requirements needed for a core used in conjunction with liquid moulding of CFRP composites. In the most basic form, the core must be resistant to the process specific temperatures and pressures [4]. However, many other factors, such as core porosity and thermal expansion, can alter the effectiveness of the core, as well as affect the quality of the composite structure. In addition, since not only materials, but also the FDM manufacturing process is evaluated, further parameters such as dimensional accuracy and geometrical complexity are of importance. An overview of all critical parameters for core materials and their manufacturing processes is summarized in Table 3.1. These parameters form the guideline for the material characterization and experimental procedures conducted throughout this work.

Table 3.1. Critical parameters for cores used in liquid moulding of composites.

	Parameter	Description
Material	Processing temperature	Heat deflection temperature (HDT) for short cycle processes and glass transition temperature (T_g) for longer cycles processes must be higher than infusion temperature to prevent core deformation and/or creep.
	Compressive strength	Compressive strength must be sufficient to prevent core deformation
	Thermal expansion	Thermal expansion of core material suitable for high temperature processes
	Solubility	Degree of solubility to ensure fast core washout and low cycle times
	Cost	Raw material cost of core
Process	Surface porosity	Surface porosity or sealing solution must be adequate to prevent resin infiltration during moulding process
	Dimensional accuracy	Dimensional accuracy of final core
	Geometrical freedom	Geometrical freedom and flexibility in core fabrication
	Cost	Investment, non-recurring & recurring cost of process

3.2 Material characterization

Table 3.2 outlines four sacrificial polymers that are compatible with FDM systems. As discussed in Chapter 2, the selected materials for fabricating the sacrificial cores are polymers based on PVOH chemistry. Overall, three selected commercially available materials are investigated, namely FDM-A, FDM-B, and FDM-C. A proprietary sacrificial material referred to as FDM-D is included for referencing purposes.

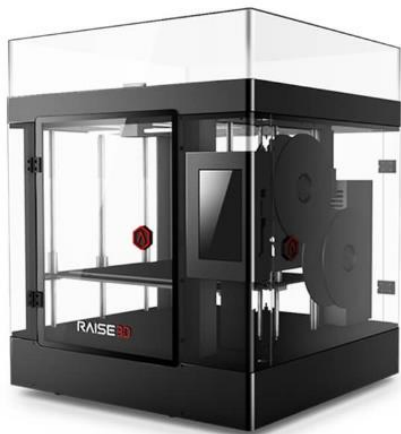
Table 3.2. Overview of sacrificial material for fused deposition modelling

Identifier	FDM - A	FDM - B	FDM - C	FDM-D
Material Type	PVOH blend	PVOH co-polymer blend	BVOH blend	Proprietary polymer
Form	Filament - 1.75 mm diameter			

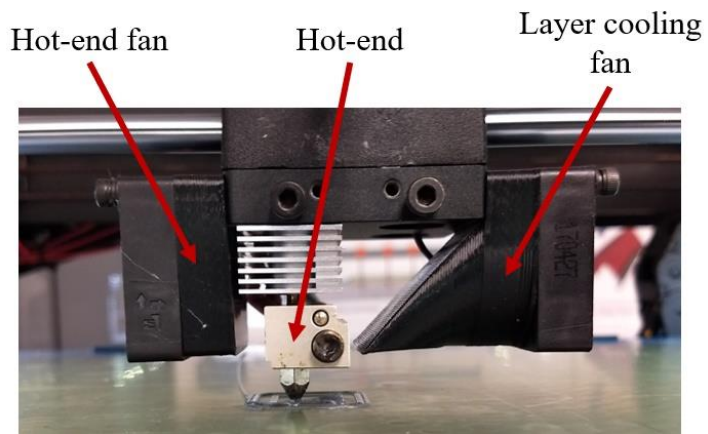
PVOH-copolymers can be used on most available open and closed source FDM systems, and, furthermore, can be procured in filament form or in pellets. Especially the availability in pellet form allows for a scalable manufacturing process, since filament can be produced in-house, or a pellet-feed extrusion head can be used on a AM system, both significantly lowering per-part cost. Since these materials are typically only used as support materials for additive manufacturing, available material properties are very limited. To understand limitations and ensure success using these materials, basic material characterization is required.

3.2.1 Additive Manufacturing Equipment

All samples and cores in this thesis are printed on a Raise 3D N2 printer shown in Figure 3.4-a. Basic printer specifications, such as the build envelope size and maximum extrusion temperature, are listed in Table 3.3. Raise3D N2 printer specification



(a) Raise 3D N2 printer



(b) Modified hot-end configuration

Figure 3.4. Additive manufacturing system used to fabricate samples and cores.

Table 3.3. Raise3D N2 printer specification

Parameter	Value
Build envelope	305 mm x 305 mm x 305 mm
X-Y resolution	12.5 μm
Z resolution	10 μm
Filament diameter	1.75 mm
Maximum extruder temperature	300 °C
Maximum build plate temperature	100 °C
Enclosure	Yes
Slicer software	Simplify3D

This specific printer was modified from the factory setup to provide a more controllable printing performance. First off, the second extruder was removed to reduce weight of the moving gantry, enabling faster printing speeds with less part distortion. The original layer cooling fan used to be merged with the heat sink fan of the hot end, constantly being enabled and running at full speed. This configuration was redesigned and replaced with a dedicated layer cooling fan as shown in Figure 3.4-b, that can be dynamically controlled through the slicing process. Furthermore, the original BuildTak build surface was removed and replaced with a 0.38 mm thick PEI film to provide better adhesion to the build plate with certain materials. The slicing software Simplify3D was used to process and prepare all geometries for printing.

Each material requires a specific extrusion temperature as well as a specific build plate temperature. Most material manufacturers provide a range for both temperatures and the final temperatures are adjusted to the specific 3D printer used.

In this work, the build orientation of a sample is defined as the direction parallel to the testing direction based on the coordinate system indicated in Figure 3.5. For example, a sample build in z-direction will be tested in the direction normal to each deposited layer.

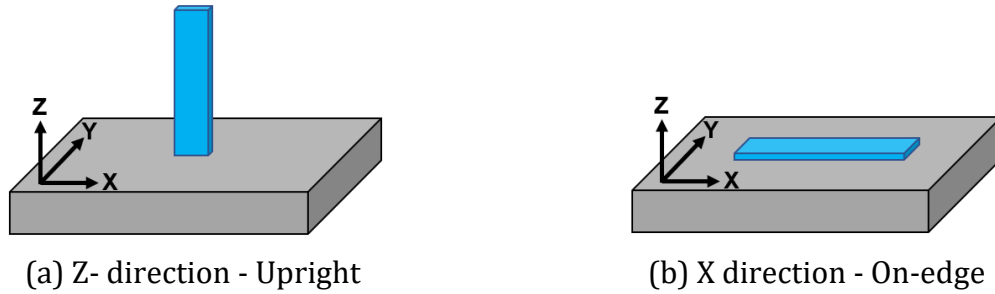


Figure 3.5. Build orientation for 3D printed structures using fused deposition modelling.

3.2.2 Operational Temperature of Cores

The glass-transition temperature (T_g) was selected as an indicator for the maximum operational temperature of 3D printed polymer cores. If the processing temperature exceeds this temperature during the composite manufacturing process, the core will be exposed to loading during a polymer transition phase, inducing permanent deformation by creep. To avoid this, the T_g was determined for the selected sacrificial polymers to define their respective operational temperature limits.

3.2.2.1 Methodology

Dynamic mechanical analysis (DMA) was used to determine the T_g of the materials. The equipment used for these tests was a DMA Q800 made by TA Instruments.

The sample dimension was 12.5 mm by 60.0 mm by 2.0 mm, which was produced with the 3D printing parameters listed in Table 3.4. Due to dimensional variations in the 3D printing process, each sample was measured using a digital caliper to verify actual dimensions. The double cantilever test fixture was used for all tests, and parameters such as ramp rate and frequency, are listed in Table 3.4.

Table 3.4. Experimental parameters for DMA characterization

		FDM - A	FDM - B	FDM - C
3D printing	Extrusion temperature	215°C	215°C	215°C
	Bed temperature	50°C	50°C	70°C
	Nozzle diameter	0.6 mm		
	Extrusion width	0.6 mm		
	Layer height	0.3 mm		
	# of top layers / # of bottom layers	2/2		
	Infill pattern	100% Rectilinear infill		
	Build direction	On-edge		
DMA	Dimension	12.75 mm x 2.06 mm	12.73 mm x 2.08 mm	12.91 mm x 2.10 mm
	Cantilever length	35.00 mm		
	Ramp Rate	3.00 °C/min		
	Frequency	1 Hz		
	Oscillation Strain	0.5%		

3.2.2.2 Results

The glass transition temperature was determined from the onset and inflection points extracted from the storage modulus versus temperature graph provided from the DMA test. A typical data set obtained from the DMA test and the respective T_g points are shown in Figure 3.6. The T_g points for the three materials investigated are graphed in Figure 3.7.

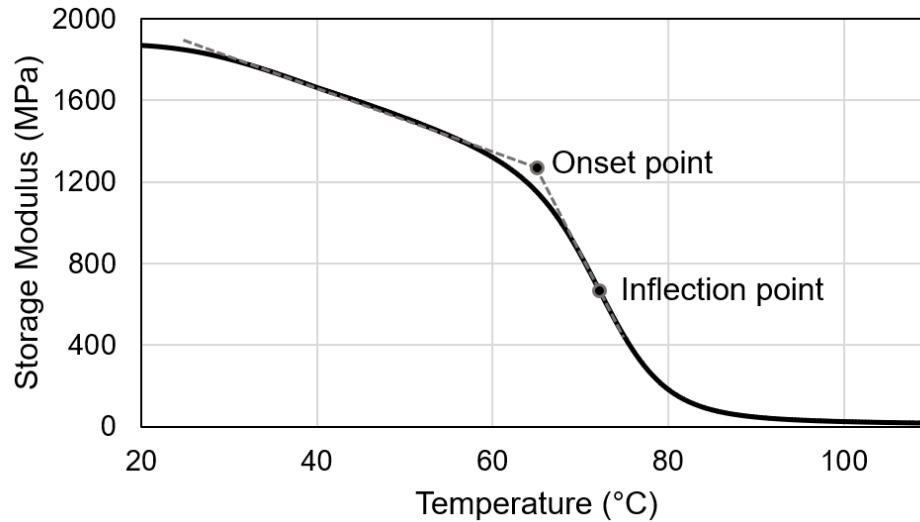


Figure 3.6. Storage modulus vs. temperature data from DMA analysis for FDM-C material. Onset and inflection point are used to determine the glass transition temperature.

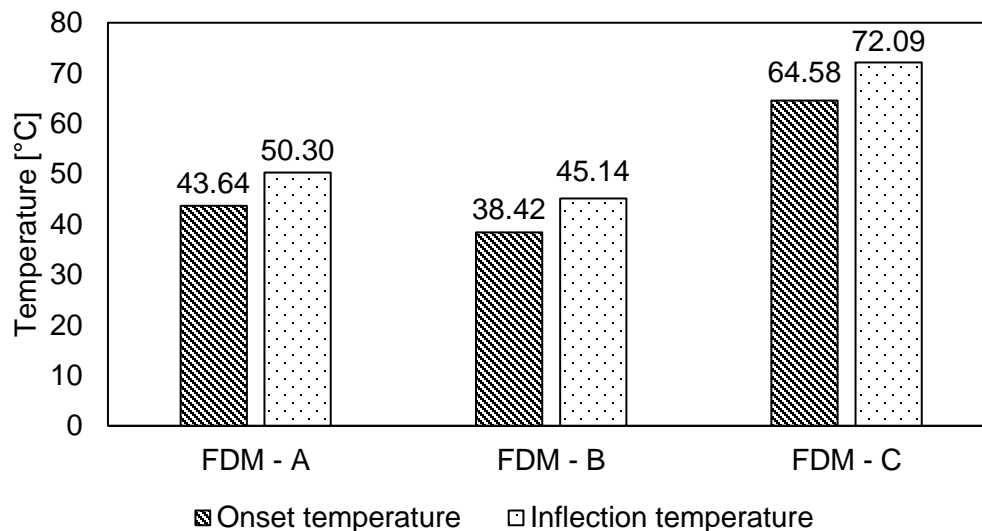


Figure 3.7. Glass transition temperature of water-soluble thermoplastic filaments.

Basing the T_g on the onset temperature, the FDM-C filament shows the highest T_g and therefore best temperature resistance of up to 64°C. This is followed by the FDM-A filament with 43.6°C and lastly, the FDM-B material with a T_g of only 38.4°C. It appears that the addition of fillers and other polymers to ease the processing has lowered the T_g slightly.

Furthermore, the distance between onset and inflection temperature shows that the transition stage for the FDM-C is the largest, while the transition stage for both, FDM-A and FDM-B filaments, appear identical.

These results show that the only material suitable for an above room-temperature moulding process is FDM-C with a limit of 64 °C. The low glass transition temperature of the other two filaments makes them suitable for room-temperature infusion processes only.

3.2.3 Coefficient of thermal expansion

The coefficient of thermal expansion (CTE) is of importance for cores if the process temperature during composite fabrication is above room temperature. For example, in resin transfer moulding, the composite thickness is given by the gap between the core and the outer mould surface, hence any dimensional variation can lead to a change in composite quality and induce processing issues. For VARI, the dimensional changes will have an impact on final part dimensions of the finished structures. To offset the effect of thermal expansion, the coefficient of thermal expansion was determined for suitable materials.

3.2.3.1 Methodology

Thermomechanical analysis (TMA) was used to determine the CTE of *FDM-C* material. In the previous test it was determined that *FDM-C* is the only material suitable for usage at temperatures above 25 °C, and hence was the only material tested.

The equipment used for this test was a TMA Q400 made by TA Instruments. The probe used was the expansion probe designed for determining the CTE of materials. The sample dimension was 6 mm by 6 mm by 6 mm. Three samples with upright direction and three samples with on-edge direction were tested. All 3D printing parameters as well as test parameters are listed in Table 3.5.

Table 3.5. Test parameters for TMA analysis

3D printing parameters	Parameter	Value
	Material	FDM-C
	Extrusion temperature	215
	Bed temperature	70
	Extrusion nozzle diameter	0.40 mm
	Extrusion width	0.48 mm
	Layer height	0.15 mm
	# of top layers / # of bottom layers	2 / 2
	Infill pattern	100 % solid rectilinear
	Dimension	6 mm x 6 mm x 6 mm
TMA parameters	Probe type	Expansion
	Probe force	0.10 N
	Ramp rate	a. C/min

3.2.3.2 Results

The properties measured in the TMA test are dimensional change versus temperature. A typical data set is shown in Figure 3.8. Using the slope before and after the T_g , the CTE was extracted. The resulting CTE measurements of FDM-C material are shown in Figure 3.9.

Figure 3.9 shows that the CTE above the glass transition temperature is significantly higher than below. The maximum expansion was measured for the on-edge samples with 208.73 ppm/K, while the upright samples had only minor deviations above the inflection point. Below the T_g , difference of CTE between the two testing directions were found. The upright testing direction exhibits an average CTE of 135.77 ppm/K, while the on-edge direction measured a lower CTE of 97.58 ppm/K. While these discrepancies appear large, it should be noted that the samples tested were all manufactured by 3D printing. Inherent to the process, the 3D printed samples contain porosity varying according to the build direction, which

could be a potential source of these variations. A similar CTE behaviour has also been shown by tests conducted on commercial soluble support material [21].

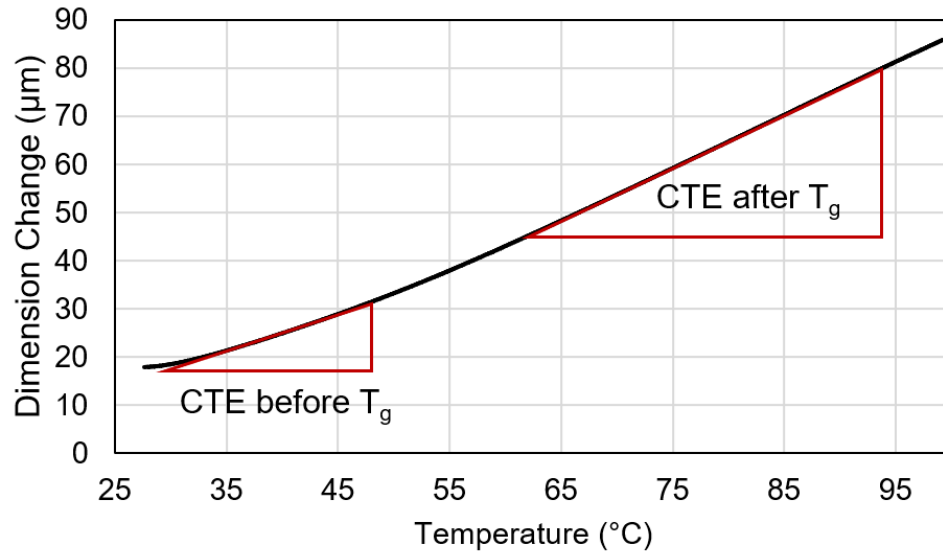


Figure 3.8. Dimensional change versus temperature data set obtained from TMA testing of FDM-C. The CTE before and after the glass transition temperature are extracted.

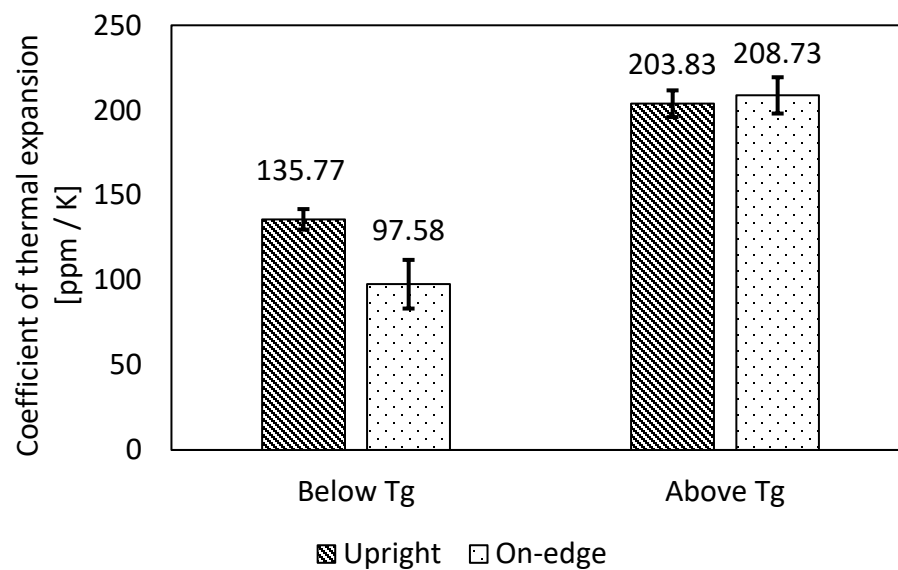


Figure 3.9. Coefficient of thermal expansion of 3D printed FDM-C.

3.2.4 Compressive Strength and Compressive Modulus

Liquid moulding processes such as RTM and VARI rely on pressure exerted by tooling or a vacuum bag to consolidate the reinforcement, hence the core will be exposed to compressive forces. The compressive strength of the core material is an indicator if the core will sustain these compressive forces during the moulding process. The compressive modulus will indicate how much deformation the core will experience when compressed.

3.2.4.1 Methodology

Compression testing was conducted according to ASTM D695 [28], a standard test method for compressive properties of rigid plastics. It should be noted that the sample was not solid, and a representative infill was chosen to determine the compressive strength of a 3D printed structure rather than the bulk material properties. The test was conducted in the upright and on-edge direction. Each sample was measured using digital calipers to verify dimensional variance between the modelled and printed samples. The test frame used was a Test Resource Universal Testing frame with a 30kN calibrated load cell. The displacement recorded is the crosshead displacement of the testing frame. Sample properties and testing parameters are outlined in Table 3.6.

Table 3.6. Compression test: Sample and test parameters.

		FDM - A		FDM - B		FDM - C	
General	Sample direction	Upright	On edge	Upright	On edge	Upright	On edge
	Number of samples	5	5	5	5	5	5
3D printing	Extrusion temperature	215 °C		215 °C		215 °C	
	Bed temperature	50 °C		50 °C		70 °C	
	Extrusion nozzle diameter	0.6 mm					
	Extrusion width	0.6 mm					
	Layer height	0.3 mm					
	# of top layers / # of bottom layers	4 / 4					
	Infill pattern	20% triangular – sparse					
	Sample geometry	Rectangular prism: 12.7 mm x 12.7 mm x 25.4 mm					
Comp. test	Load cell	30kN Calibrated – TCTN-9110					
	Control	Displacement controlled					
	Compression speed	1.3 mm/min					

3.2.4.2 Results

From the load versus displacement data collected by the compression test, the compressive strength and the compressive modulus were calculated. A typical data set is shown in Figure 3.10. The results for all three materials are shown in Figure 3.11 and Figure 3.12.

For upright compressive loads, the failure mode was buckling, while for the on-edge direction the failure mode was interlaminar failure between the deposited layers. A representative sample for both failure modes is shown in Figure 3.13.

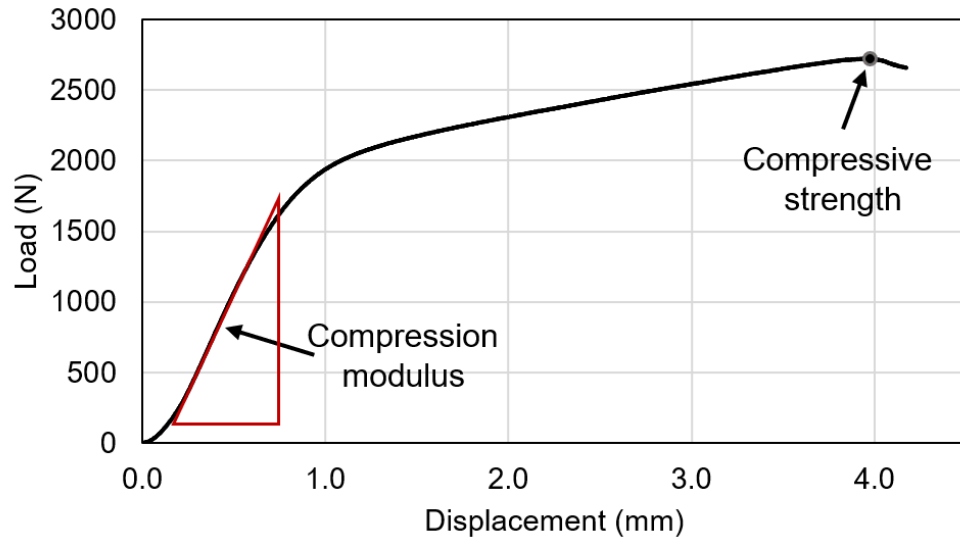


Figure 3.10. Load versus displacement data set obtained from compression testing of FDM-C. Compressive modulus and compressive strength are indicated.

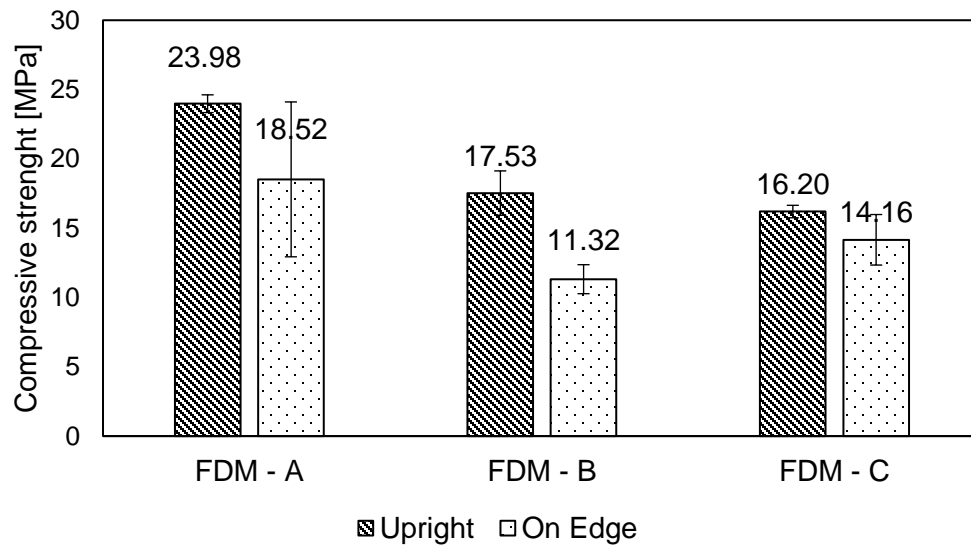


Figure 3.11. Compressive strength of 3D printed core materials.

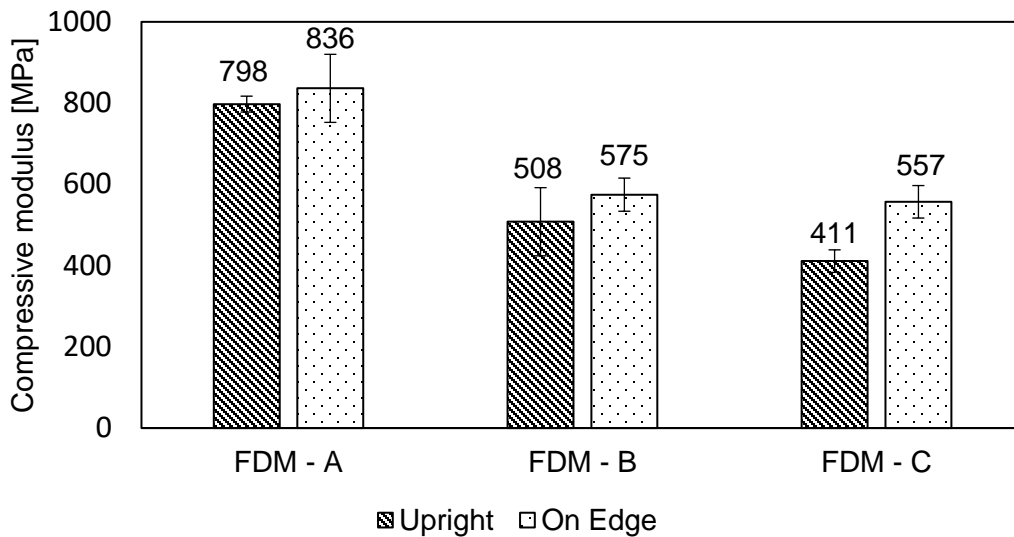
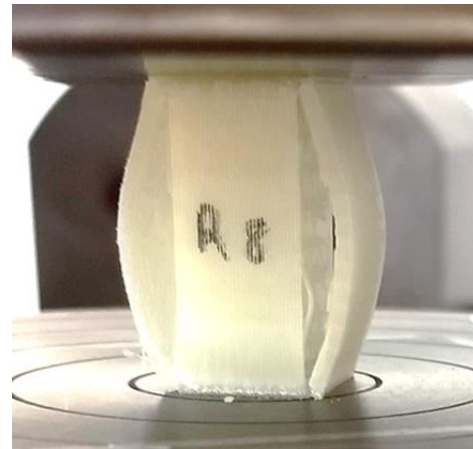


Figure 3.12. Compressive modulus of 3D printed core materials.



(a) Upright – buckling



(b) On Edge - interlaminar failure

Figure 3.13. Failure modes of compressive strength samples.

The results show that *FDM-A* had the highest compressive strength with 23.98 MPa and 18.52 MPa in upright and on-edge direction respectively. *FDM-C* followed with 16.20 MPa in upright and 14.16 MPa in on-edge, while *FDM-B* had the lowest compressive strength. While the standard deviation of the upright samples was low, the on-edge samples showed more variation. This is most likely due to the additive manufacturing process that can heavily influence the interlayer adhesion of the final structure. The results found were consistent

with experiences from 3D printing these materials. In general, *FDM-B* showed very little interlaminar strength and was prone to failure during handling, while *FDM-C* and *FDM-A* showed better handling resistance.

A core in liquid moulding must resist two sources of pressure. First, when the tool is closed containing the core and fibres, the mould closure pressure will compact the dry fibre while exerting a certain pressure on the core. For example, dry fibre compaction tests [4] of a 3K plain weave graphite fabric have shown that to achieve a fibre volume fraction above 0.55, the compaction pressure lies between 0.3-0.4 MPa. The second source of pressure is the pressure experienced during the injection of the resin. Generally, for infusion processes this pressure is negligible at 0.1 MPa, or 1 atmosphere. However, for resin transfer moulding, this pressure becomes more significant. Generally, pressures between 1 MPa and 2 MPa are common, while some high-pressure processes even achieve pressures up to 12 MPa [29].

In context to the core materials tested, the compressive strength for all tested materials was deemed sufficient, often by magnitudes. The lowest value determined was the on-edge *FDM-B* sample with 11.32MPa, which theoretically withstands 10 Bar injection pressure.

Another factor to investigate is the degree of deformation the cores experience under the pressure. The compressive modulus chart in Figure 3.12 shows that *FDM-A* had the highest compressive modulus with 798 MPa and 836 MPa in the upright and on-edge directions, respectively. *FDM-B* and *FDM-C* had similar compressive moduli, with *FDM-B* being slightly higher at 508 MPa for upright and 575 MPa for on-edge direction.

In a vacuum assisted infusion process with a compaction pressure of 0.1 MPa, this would correspond for the lowest modulus material, *FDM-C*, to a strain of 2.43×10^{-4} . On the scale and precision of the 3D printing process, it was deemed that this was not a significant dimensional change. However, for higher pressure processes such as HP-RTM, this might become an issue and would require further investigation. It should be noted that the stiffness of the core can be further increased by using a higher infill percentage at the penalty of manufacturing time and dissolution speed.

3.3 Summary of Material Properties

Table 3.7 is a summary chart for the three PVOH-based materials characterized. As a reference, material properties of conventional core materials, such as cast plaster cores and cast foams, are provided as well. In comparison to conventional sacrificial core technologies, the sacrificial polymers tested had consistently lower operational temperatures, while also exhibiting consistently higher compressive strengths. While many composite fabrication processes require these high temperatures, infusion-based processes often only require elevated temperatures during the post-cure of the structure, but not during the infusion step. Hence the three polymers tested were deemed suitable for the application intended.

Table 3.7. Material properties summary. FDM-A, FDM-B and FDM-C have been characterized; all other information was gathered from manufacturer datasheets.

	Material	Technology	Maximum operational temperature	Coefficient of thermal expansion	Compressive strength	Compressive modulus
Sacrificial Cores	Cast-A	Cast plaster	200 °C	6.5 PPM/K	1.51 MPa	N/A
	Cast-B	Cast plaster	175 °C	9 PPM/K	>10.34 MPa	N/A
	BJC-A	Binder Jetting	175 °C	19.6 PPM/K	>3.45 MPa	N/A
	FDM-A	FDM	43 °C	N/A	18.52 MPa	798 MPa
	FDM-B	FDM	38 °C	N/A	11.32 MPa	508 MPa
	FDM-C	FDM	64 °C	98 - 136 PPM/K	14.16 MPa	411 MPa
	FDM-D	FDM	132°C	88 - 107 PPM/K	14.50 MPa	N/A
Fly Away cores	Foam-A	Cast foam	150 °C	N/A	1.72 MPa	53.78 MPa

4 EVALUATION OF SACRIFICIAL CORE TECHNOLOGIES

The focus of this chapter is to experimentally evaluate the suitability of the proposed 3D printed sacrificial core technology by fabricating and evaluating proof-of-concept structures. A variety of different geometries were tested in combination with different composite manufacturing processes. Although the focus of this thesis is 3D printed cores via FDM, other materials were briefly investigated for reference. These include a 3D printed core via binder jetting and a cast plaster-based core. Overall, two different geometries, namely a handlebar stem and an omega stiffened flat panel, are evaluated. Since the combination of 3D printed cores and liquid moulding is a novel application, very limited knowledge and best practices are available. The goal of this chapter is to develop a better understanding of the manufacturing process and its associated challenges.

4.1 Handlebar Stem Benchmark

A handlebar stem, as shown in Figure 4.1, is a bicycle component that acts as the joint between the fork holding the front wheel and the handlebar. This component is generally manufactured from metal alloys, however, the trend towards lighter high-performance bicycle components has led to designs incorporating composite materials.



Figure 4.1. Carbon fibre bicycle stem [30]

This specific handlebar stem and the associated composite manufacturing process has been developed by Lessard and Thouin in 2004 as part of an industrial project with True Temper Sports at McGill University [30]. Since a detailed manufacturing process as well as the physical tooling was readily provided by L. Lessard, the development phase for a new component could be skipped, allowing for a rapid initial assessment of a 3D printed washout core in a liquid moulding application.

4.1.1 Geometry and Tooling

The geometry of the handlebar stem is shown in Figure 4.2. The original stem design consists out of two cast inserts made from polyurethane, with the upper insert being completely made from polyurethane, while the lower insert being reinforced with a machined aluminum core to provide mounting points for the end-cap bracket. The hollow section shown in green was originally moulded using a latex bladder.

The tooling used the mould the stem is a multi-piece aluminum tooling as shown in Figure 4.3. The tool consists out of two halves shaping the outer geometry of the handlebar stem as well as internal components such as the bladder holder and the steerer alignment tube. The injection inlet and outlet are positioned as outlined in Figure 4.3.

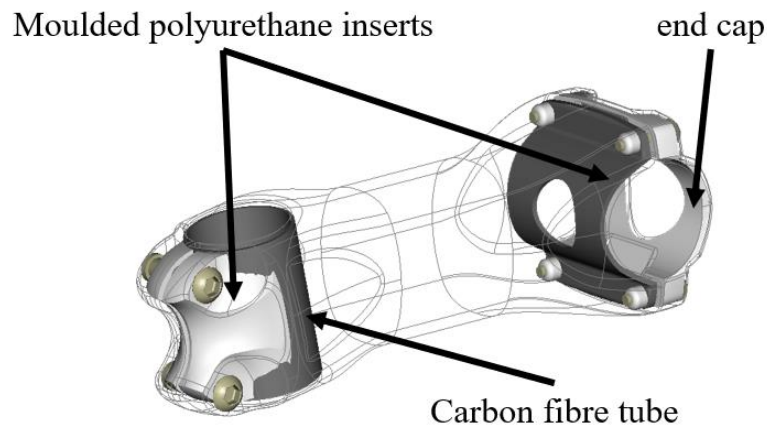


Figure 4.2. Design overview of handlebar stem [30]

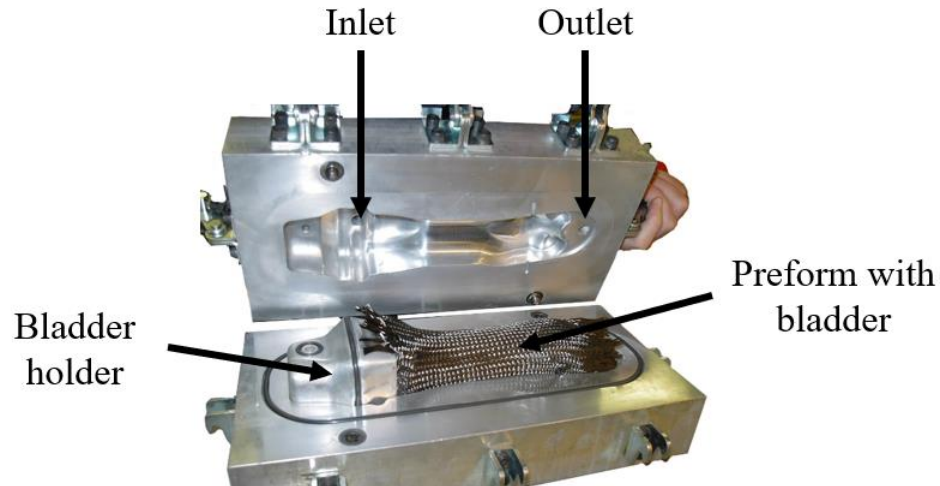


Figure 4.3. Overview of stem resin transfer moulding tooling [30]

4.1.2 Core Fabrication

The core fabrication methodology as outlined in Chapter 3 was applied. Compared to the original fabrication method, the process was slightly adjusted and simplified with the usage of 3D printed cores. All polyurethane inserts were replaced with 3D printed inserts to avoid the labour-intensive moulding process. Since the goal of this study is to investigate 3D printed sacrificial cores rather than creating a functional structure, the integration of reinforcements into the cores were omitted.

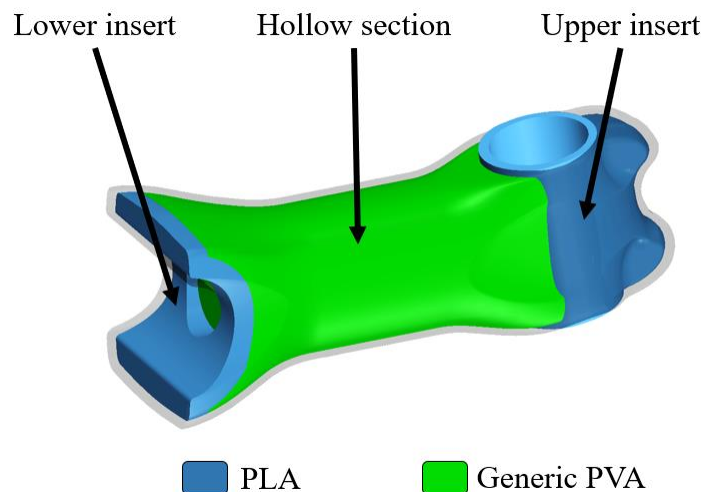

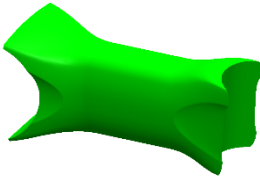
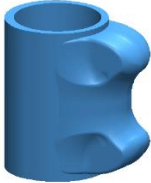


Figure 4.4. Overview of 3D printed cores for stem prototype

The original CAD drawings were used to create a total of three core geometries. The lower insert remained identical to the original core, however, the upper insert was merged with the carbon fibre tube to yield one single part. All permanent inserts were printed using polylactic acid (PLA). The cavity originally occupied by the bladder was filled with a third core made from water-soluble material. Figure 4.4 shows an overview of the core layout, while Table 4.1 provides more detailed manufacturing information about the three cores.

Table 4.1. Manufacturing information of 3D printed cores for stem prototype.

	Lower insert	Hollow section	Upper insert
			
Material	PLA	FDM-A	PLA
Nozzle diameter	0.40 mm	0.40 mm	0.40 mm
Extrusion width	0.48 mm	0.48 mm	0.48 mm
Layer height	0.15 mm	0.20 mm	0.15 mm
Nominal infill percentage	30%	20%	30%
Infill pattern	Full honeycomb	Full honeycomb	Full honeycomb

After printing, the three cores were assembled using cyanoacrylate-based adhesive to form a single core structure as shown in Figure 4.5.

The final step to complete the core was sealing. The lower and upper inserts were printed with 30% nominal infill and the hollow section with only 20% nominal infill, making all cores partially hollow. To seal surface porosity and prevent resin infiltration during the moulding process, the core was sealed by manually brushing the same epoxy resin used later for the injection on the surface of the core using a foam brush. The principal idea was for the high

viscosity resin to bridge small gaps and holes on the surface without penetrating the core and filling the hollow structure, effectively sealing the core without adding a different material.



Figure 4.5. 3D printed core structure for bicycle stem.

4.1.3 Composite Fabrication

The next step to fabricate the composite bicycle stem was the assembly of the preform. The preform was formed directly on the 3D printed core using a braided biaxial carbon fibre reinforcement. Several incisions were made, and smaller pieces were cut to wrap the upper stem section. Overall, a total of four plies were build up onto the core assembly. To ease with the draping and keep the preform in shape, Super 77 adhesive by 3M was used as a sprayable tackifier. Resin transfer moulding was used to fabricate the composite stem. The complete setup is depicted in Figure 4.6.

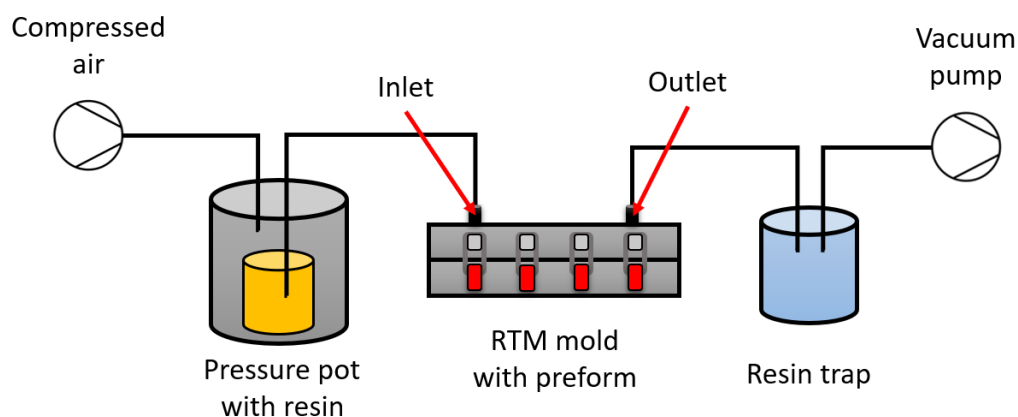


Figure 4.6. Resin transfer moulding setup for bicycle stem moulding/

Table 4.2. Resin transfer moulding parameters for bicycle stem.

Parameter	Value
Fibre architecture	Biaxial Carbon Fibre braid
Number of plies	4
Resin system	Epoxy system
Tackifier	3M Super77 Adhesive
Degassing time	5 minutes
Injection pressure gradient	$\Delta 6.89$ kPa
Injection temperature	21°C
Post cure	24h @ 21°C

A pressure pot was used to inject the resin on the inlet side, while a vacuum pump was connected to the outlet side to further increase the driving pressure gradient. Injection parameters are summarized in Table 4.2.

The tool was sealed using Zyvac Sealer GP and treated with Zyvac EnviroShield release agent prior to moulding. The preform was mounted to the bladder holder and placed into the two-part tooling described earlier. After closing the tool, a pressure test was conducted to ensure no leaks were present in the tooling setup. With a total injection pressure gradient of 6.89 kPa, the part was injected and once completed, cured for 24 hours at room temperature prior to being released. Post demoulding, excess resin flash was trimmed manually using a rotary tool. The final stem is shown in Figure 4.7.



Figure 4.7. Carbon fibre bicycle stem after demoulding and trimming.

4.1.4 Results and Key Findings

Figure 4.7 shows that the resin transfer moulding of the bicycle stem with the usage of a 3D printed sacrificial core was successful. The core did not deform and kept the desired shape, yielding a satisfying result in terms of external geometry.

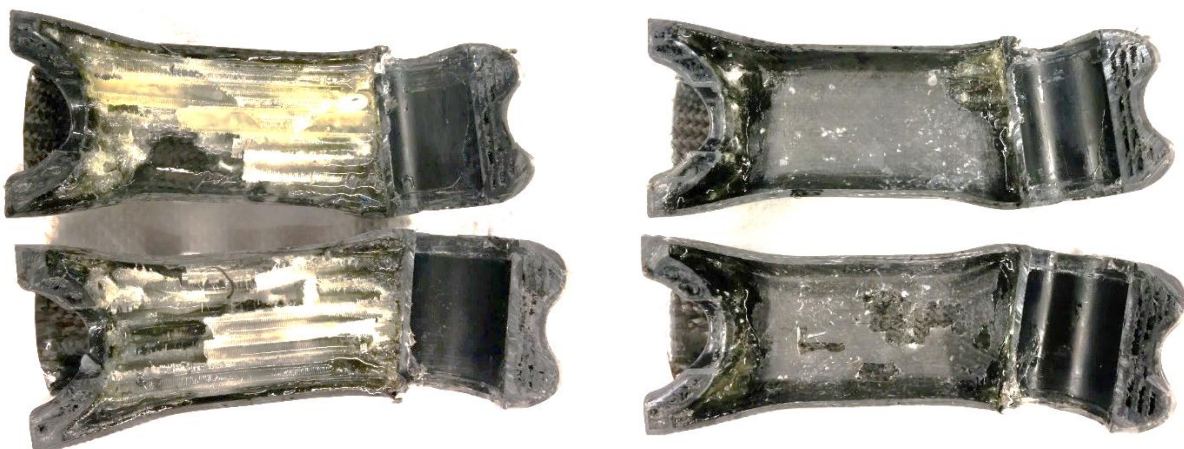
To dissolve the 3D printed core material, resin flash at the entry point of the original bladder was trimmed using a rotary tool to provide an entry opening for the solvent. The entire structure was



Figure 4.8. Solvent entry point for dissolution of PVA stem core.

submerged in a bucket of tap water at a temperature of 25°C for a time of >36h to disintegrate the core. The water was not externally agitated; however, it was ensured that the inside of the core was filled with water rather than being occupied with trapped air. At several occasions, the part was moved and agitated to circulate the water inside the core.

Even after 36 hours, the core had not dissolved, and the original structure still appeared intact as shown in Figure 4.8. Subsequently, the composite part was cut down the centre to reveal both sides and investigate the stage of dissolution as shown in Figure 4.9-a.



(a) Before mechanical core removal

(b) After mechanical core removal

Figure 4.9. Bicycle stem cross-section showing 3D printed sacrificial core.

The dissolution of a 3D printed washout core occupying a dead-end cavity, without any agitation or flow, was not successful. While small parts of the core had been dissolved, most of it remained. Furthermore, resin infiltration was evident, which made parts of the core not dissolvable. After mechanical removal and additional washing, most of the core was released from the structure to yield the result shown in Figure 4.9-b. However, small sections, especially in the corners, could not be removed due to the mix of core and resin. The key findings are summarized as follows:

- Successful resin transfer moulding using additive manufactured washout core
- No visual deformation of sacrificial core
- Acceptable internal surface quality of cavity
- Resin infiltration (either during sealing or injection) prevented complete core removal
- Slow and unfeasible core removal in resting, room temperature water bath

These key findings show that the general process is suitable to fabricate composite structures using liquid moulding. However, they also identify challenges for a successful application. First off, the sealing process requires improvement to ensure no resin will be driven into the core. Furthermore, a more feasible dissolution approach must be developed to ensure efficient core removal in an industrial setting, increasing robustness while reducing overall dissolution time.

4.2 Linear Omega Benchmark

The linear omega section as shown in Figure 4.10 was chosen as a benchmark geometry that represents a simple but common problem in the fabrication of CFRP composite structures.

Omega sections, also referred to as hat stiffeners, are used to increase the stiffness of thin panels. While the moulding of linear constant cross-section stiffeners together with the skin is a well-developed process, adding net-shape cut-out sections still pose a challenge. Usually, hat stiffeners are fabricated using an elastomeric mandrel that is pulled out of the structure post fabrication. However, if the stiffener itself requires cut-out sections as the one shown in Figure 4.10, for example to provide openings for wiring, additional machining operations are required. This benchmark focuses to evaluate core technologies that can eliminate this additional machining operation and have the capability to produce hat stiffeners with net-shape moulded cut-out sections.



Figure 4.10. Linear omega benchmark geometry with cut-out section.

4.2.1 Geometry & Fabrication Process

The benchmark geometry consists of three main features, namely the skin, the omega stiffener and the cut-out section within the stiffener. An overview of this geometry is depicted in Figure 4.11.

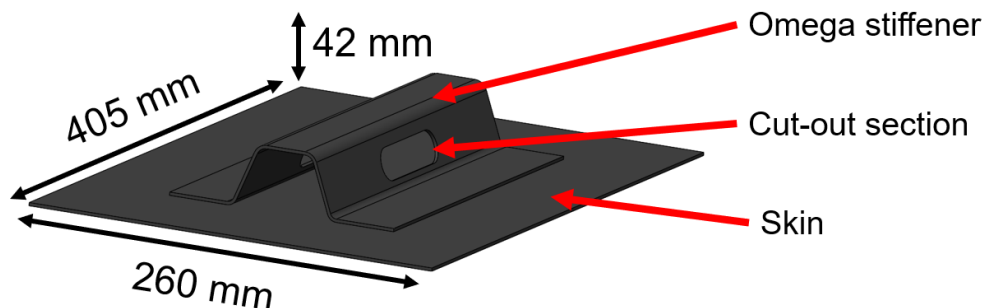


Figure 4.11. Overview of omega benchmark geometry.

Vacuum assisted resin infusion (VARI) was the selected liquid moulding process for this benchmark. A treated flat plate was used as the moulding surface for the skin. The omega stiffener and the cut-out section are solely formed by the core. The fabrication setup is shown in Figure 4.12, while injection parameters and materials are listed in Table 4.3.

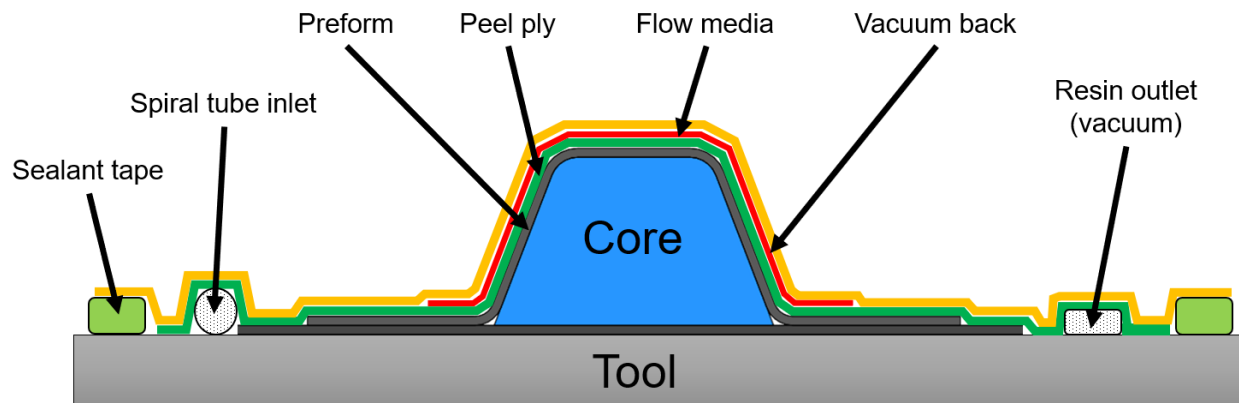


Figure 4.12. Vacuum assisted resin infusion setup for omega benchmark fabrication.

Table 4.3. Fabrication parameters of omega benchmark.

Parameter	Value
Tool	Aluminium plate @ 40°C
Resin	Epoxy System
Fibre architecture	Carbon – 5HS + Binder – 4540
Skin Layup	3 plies, non-consolidated
Omega stiffener	3 plies, preformed to stiffener shape
Preforming step	Vacuum bag, 15 minutes @ 120°C
Injection temperature	25°C
Vacuum pressure	101.35 kPa absolute
Poste cure	24h @ 25°C

Prior to moulding, the aluminum plate was sealed using Zyvax Sealer GP and treated with Zyvax EnviroShield release agent. While the preform of the skin was not consolidated prior to injection, the preform of the stiffener itself was consolidated and shaped using a silicone core and a vacuum bag to help with draping and improve the quality of the cut-out sections. The skin and consolidated stiffener were only combined at the moulding stage. Flow media was applied over the stiffener to aid with resin flow. The injection was conducted at a tool temperature of 40°C and an injection temperature of 25°C.

In this benchmark, three different types of cores were tested. *Type A* and *Type B* are both sacrificial inserts forming the net-shape cut-out sections and are held in place by a cast silicone carrier core. Both insert types clip into the core as shown in Figure 4.13-a. The insert geometry of *Type A* is a 2.5D geometry with a flat edge around the perimeter. Insert geometry *Type B* is featuring a C-shaped lip around the perimeter to clip the fibre preform in place and to achieve a smoother net-shape edge. Both insert geometries and their respective dimensions are shown in Figure 4.13-b and Figure 4.13-c.

Type C is the full-size stiffener core as shown in Figure 4.14. This core includes features to mould the cut-out section as well as shape the omega stiffener itself.

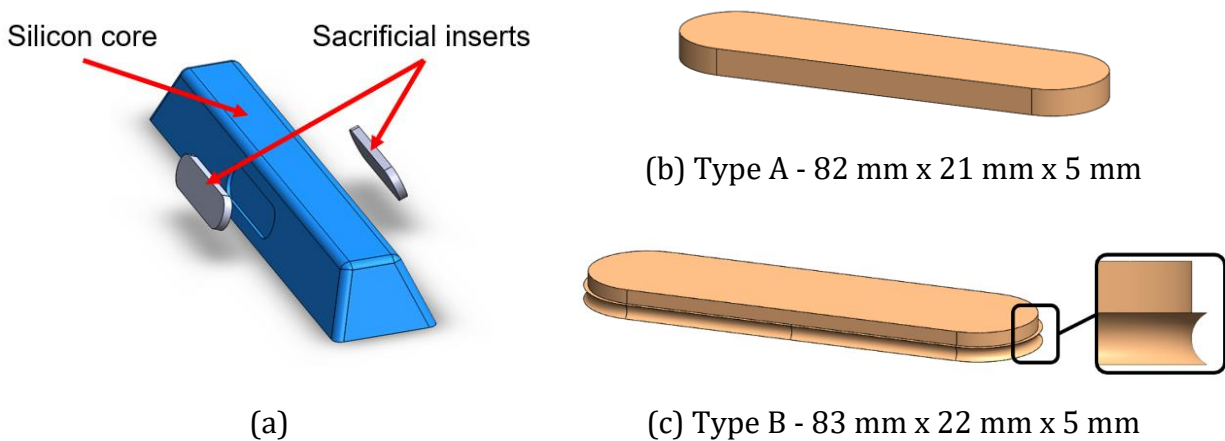


Figure 4.13. Insert geometries of omega benchmark. Overview of assembly with silicone core (a), 2.5D inserts Type A (b) and insert with integrated C-lip (c).

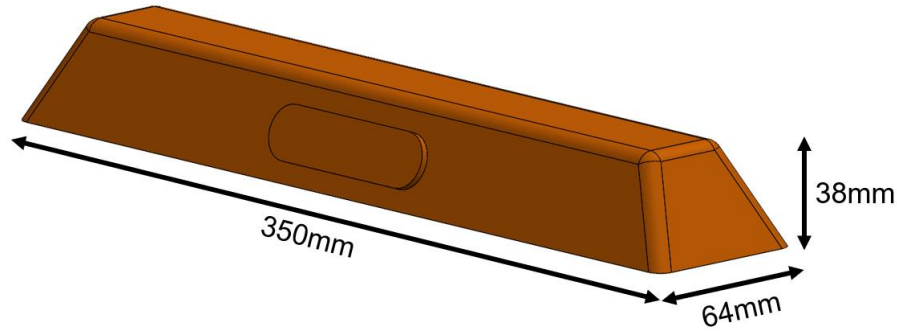


Figure 4.14. Type C core geometry of omega benchmark. Complete omega core with integrated cut-out features.

4.2.2 Core Fabrication

Three different core materials were investigated, namely 3D printed FDM-A inserts, cast plaster inserts, and a 3D printed ceramic core. The core test matrix is shown in Table 4.4.

Table 4.4. Core test matrix for omega benchmark

	Core Type	Fabrication process	Material	Sealing Process
Core 1	Type A	FDM	FDM-A	Water spray
Core 2	Type B	FDM	FDM-A	Water spray
Core 3	Type A	Room-temperature casting	Cast-A	PVOH coating
Core 4	Type C	Binder Jetting	BJC-A	PVOH coating

Core 1 and *Core 2* were manufactured from *FDM-A* material. Due to the sealing issues experienced in the fabrication of the bicycle stem, a different sealing approach was applied.

The *water spray sealing* approach works by coating the sacrificial core with a thin film of water. Due to the nature of PVOH-based polymers, the core does not rapidly dissolve, but

rather swells and creates a viscous gel layer. Without active water flow, the gel layer is stagnant and rests on the surface of the core. This gel layer is then redistributed using a foam brush to fill any porosity induced by the 3D printing process. Subsequently, the core is dried at a temperature below the maximum operating temperature to evaporate the water and leave a non-porous surface.

The fabrication parameters of *Core 1* and *Core 2* are listed in Table 4.5.

Table 4.5. Omega insert fabrication parameters.

	Core 1	Core 2
Material	FDM A	FDM A
Extrusion diameter	0.4 mm	0.4 mm
Layer height	0.1 mm	0.2 mm
Infill pattern	30% Full honeycomb	30% Full honeycomb
Sealing method	Water spray sealing	
Drying procedure	30 min @ 25°C	

Core 3 was fabricated by casting plaster-based sacrificial core material, as referenced in Chapter 3, into a silicone mould. The material was prepared according to the manufacturer's processing guidelines and poured into the mould cavity. After the recommended cure cycle, the inserts were removed from the tool. To seal the inherent porosity of the core, a PVOH based sealing agent was to be brushed onto the core.

Core 4 was 3D printed via binder jetting using silica sand and a proprietary binder solution. Post-printing, the core was sealed using a proprietary sealant, followed by a spray-on PVOH coat to provide a porosity free surface.

4.2.3 Results & Discussion

Core 1

The moulded part including *Core 1* is shown in Figure 4.15-a. The 3D printed core showed no defects in the core fabrication and the *water spray sealing* process was successful in preventing any resin infiltration during the moulding process. After submerging the structure in room-temperature water, the insert softened rapidly and was easily pried out from the cavity within five minutes. The resulting net shape cut-out is shown in Figure 4.15-b. It should be noted that the complete dissolution of the insert did not occur within a feasible time. After being submerged for 30 minutes in the water bath, only the outer surface of the insert had dissolved, leading to the assumption that complete dissolution of the inserts will require unfeasibly long cycle times with the current dissolution approach.



(a) Core and composite structure after demoulding.



(b) Net-shape cut-out section after dissolving and removing the sacrificial core.

Figure 4.15. Results of Omega Benchmark Core 1.

Overall, the desired cut-out geometry was achieved using *Core 1*. However, the edge finish on the composite part was suboptimal, with sharp edges, resin flash all around the perimeter, as well as unimpregnated fibres. To improve on these manufacturing defects, the C-lip design as seen in *Core 2* was realized.

Core 2

The 3D printed insert quality of *Core 2* was similar to *Core 1* and is shown in Figure 4.16-a. The insert was successfully sealed, and no resin infiltration was noticed during the composite fabrication process. Again, after softening the core in a water bath, it was effortlessly removed to yield the net-shape cut-out shown in Figure 4.16-b. Due to the soluble nature of the insert, the trapped C-lip geometry encasing the edge posed no demoulding issue.



(a) 3D printed core sealed with flash tape before moulding. The dry preform is clipped into the c-shaped groove.



(b) Truly net-shape mounted cut-out section after core removal.

Figure 4.16. Results of Omega Benchmark *Core 2*.

Similar to *Core 1*, the desired cut-out geometry was achieved, however, the net-shape finish was significantly better. The edge finish was smooth without any resin flash, and the contour was well impregnated. No additional finishing operations were required, confirming the feasibility of moulding a true net-shape cut-out feature.

Core 3

The casting of the ceramic material for *Core 4* was not successful. Even after multiple attempts of drying the cast core and releasing the inserts from the casting tool, no intact core could be fabricated. The dried core was highly brittle and porous, and even though high care was taken during demoulding, no complete insert could be released. The attempts are shown in Figure 4.17. It should be noted that even if the inserts would have released without issues, the high surface porosity would require an additional step to seal major porosity before applying the low viscosity PVOH sealant coat.

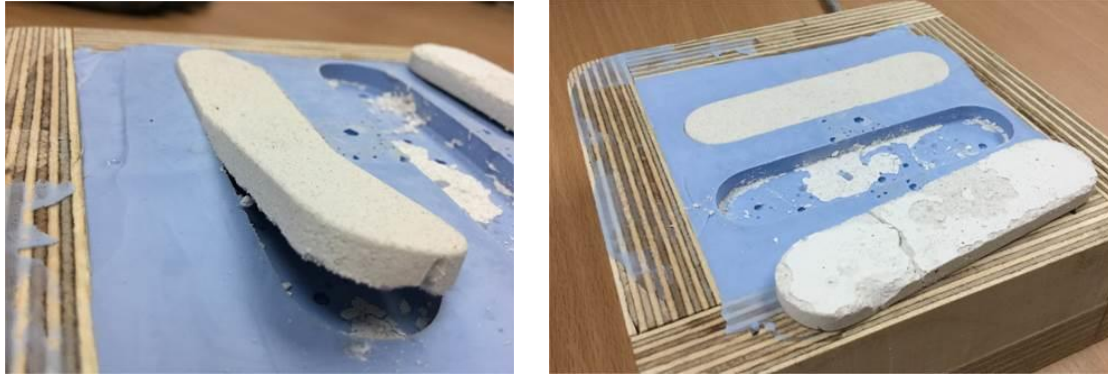


Figure 4.17. Cast ceramic inserts. The inserts show a highly porous structure and are very brittle. Damage-free demoulding was not achieved after several attempts.

It was concluded that thin inserts and delicate structure are not suitable for the cast ceramic based sacrificial moulding material. While manufacturing error is not to be ruled out, this specific approach was not deemed as a feasible solution to fabricate the inserts for this study.

It should be kept in mind that literature has shown that larger structures have been manufactured successfully using the cast ceramic material and prepreg composite parts have been fabricated using this approach.

Core 4

The 3D printed *Core 4* is shown in Figure 4.18. The fabrication process of the core showed that thin features and small detail is difficult to achieve with this ceramic-based material. For example, the C-lip featured in *Core 2* could not be accurately manufactured using the binder jetting process. According to the manufacturer, the dimensional accuracy of the 3D printed core is within $\pm 0.5mm$.



(a) Complete core with PVA sealant coat prior to infusion.

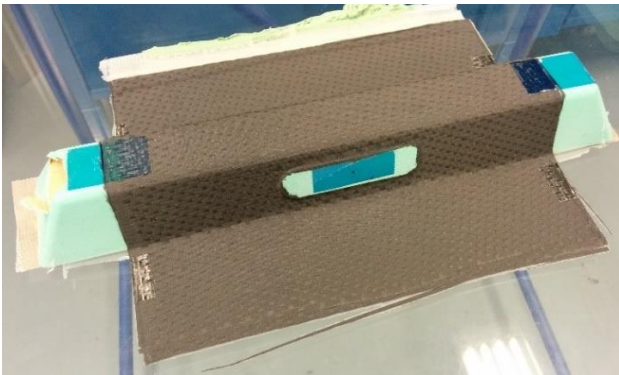


(b) Insert section showing low feature quality and visual surface roughness.

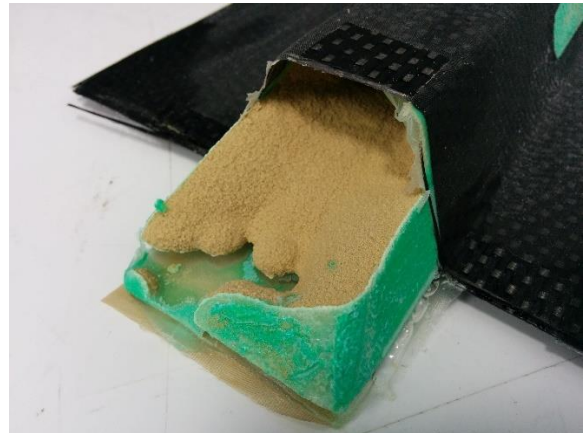
Figure 4.18. 3D printed ceramic core made using binder jetting process.

Visual inspection did not find any major porosity on the core surface. However, after the composite part was injected, it became evident that the core had wicked up resin and was partially solidified. This indicated that either the highly brittle core experienced micro-cracking that allowed resin to infiltrate, or that the surface was not entirely sealed. The resin infiltrated sections could not be removed from the composite structure.

None-the-less, certain parts of the core were dissolved effortlessly in a room-temperature water bath. Once the core was subjected to water, the un-infiltrated sections transformed from a solid, highly brittle structure to a wet sand-like consistency that could be easily removed. The moulded structure before dissolution and the result after the dissolution attempt is shown in Figure 4.19.



(a) Structure after demoulding containing Core 4.



(b) Partially dissolved core showing resin-infiltrated base.

Figure 4.19. Omega benchmark with 3D printed ceramic core.

4.2.4 Key Findings

The omega stiffener benchmark produced valuable results about the different core technologies investigated. Key challenges were identified, and the findings were used for future development of the 3D printed sacrificial core process. Key findings for each technology from this study are listed below:

3D printed PVOH-based inserts – Core 1 & Core 2

- Design freedom enabled by 3D printing allows for trapped designs to mould net-shape features in composite parts

- Good geometry retention during moulding process (no visual collapse or deformation)
- The *water spray sealing* approach offers a robust and effective way to seal cores from resin infiltration
- Fast water absorption of PVOH softens inserts quickly, allowing for rapid physical removal
- Relatively slow washout, complete dissolution of inserts appears inefficient with current process

Cast ceramic inserts – Core 3

- Highly porous core material requires several sealing steps
- Challenging demoulding process did not produce functional cores
- Cast ceramic inserts might only be feasible for larger, simpler core structures

3D printed ceramic cores – Core 4

- Highly rigid core material with excellent geometric retention
- Better suited for large volume cores rather than detailed or complex structures
- Highly soluble core material with excellent washout properties.
- Non-robust sealing process causes resin infiltration and prevents core removal

5 DISSOLUTION RATE CHARACTERIZATION

The successful washout of sacrificial cores is crucial to the manufacturing process. While the main priority is complete washout to ensure no foreign part contamination in the composite structure, a time-efficient core dissolution is required to achieve a feasible fabrication time. If the removal process requires several days or has a high chance that parts of the core remain in the structure, the process will be rendered unfeasible for most industrial applications. As shown in Chapter 4, the washout approaches applied so far did not yield satisfactory results. This chapter will investigate two different dissolution approaches, namely *water agitation* and *ultrasonic cleaning*. To characterize the effectiveness of both approaches, a set of small-scale lab experiments was conducted. The overall objective is to evaluate the dissolution rates of PVOH-copolymers for different washout conditions.

Dissolution rates of PVOH-copolymers have been investigated in the literature, however, mostly in relation to thin films for medical or packaging applications. One exception is the dissolution experiments carried out by Duran C. et al. [31], who investigated 3D printed PVOH structures. Their results indicate a linear increase in average dissolution rate with increase in solvent temperature as well as with increase in flow velocity. They recommend dissolving PVOH structures at a high temperature and high flow rate to achieve optimal dissolution.

To the knowledge of the author, *ultrasonic cleaning* has not been applied or investigated for dissolving sacrificial polymers.

5.1 Washout Approaches

The *water agitation* approach uses a stream of water that is forced through the core structure to disintegrate and dissolve the core. In contrast to having stagnant water, this approach relies on carrying dissolved material away from the core's surface and diluting it within the water bath. In addition, elevated water temperatures are used to further speed up the dissolution of the polymer.

In the *ultrasonic cleaning* approach, a commercial ultrasonic cleaner is used to dissolve the core. This approach relies on the idea of the cavitation cleaning action, created by ultrasonic waves, to carry away material from core's surface by "gently scrubbing" away the disintegrated polymer. Again, elevated water temperatures are used to further speed up the dissolution process.

5.2 Methodology

To determine the dissolution rate of 3D printed PVOH-copolymers, a simple small-scale experiment was designed and conducted that measures the mass loss over time of a sample during dissolution. Overall, two different test series were conducted with different objectives, as outlined in Table 5.1. Test series DT-1 has the objective to obtain a comparative measurement between water and water mixed with ethanol, methanol and ethyl acetate. Test series DT-2 has the objective to compare the dissolution rate at different temperatures, as well as between the two dissolution approaches. Information about the sample geometry and fabrication parameters are listed in

Table 5.2.

Table 5.1. Test matrix for dissolution characterization.

Test series	DT-1				DT-2		
Test number	1	2	3	4	5	6	7
Investigated parameter	Solvent type				Solvent temperature, dissolution method		
Dissolution approach	Water agitation				Water agitation	Water agitation	Ultrasonic cleaning
Solvent temperature	25 °C				25 °C	90 °C	25 °C
Solvent type (by volume)	100% Water	80% Water, 20% Ethanol	80% Water, 20% Methanol	80% Water, 20% Ethyl Acetate	100% Water		

Table 5.2. Sample geometry and fabrication parameters of specimens used in dissolution characterization.

	Parameter	Value
Sample	Material	FDM-A
	Geometry	Cubic
	Dimension	14.4 mm x 14.4 mm x 14.4 mm
	Volume	3000 mm ³
3D printing	Extrusion temperature	215°C
	Bed temperature	40°C
	Nozzle diameter	0.4 mm
	Extrusion width	0.4 mm
	Layer height	0.1 mm
	Infill pattern	100% Rectilinear infill

The two setups representing the two dissolution approaches are depicted in **Figure 5.1**. The agitated water approach was simulated by submerging the specimens into a beaker containing temperature-controlled water, agitated by a magnetic stirrer. The beaker was filled for each test with 250 mL of fresh solvent. In the ultrasonic cleaning approach, the sample is submerged into an ultrasonic cleaner, model 2510 by Branson, filled with water as a solvent.

The following experimental method to measure the mass loss over time was applied:

1. Measure dry sample mass using digital scale
2. Expose sample to solvent for fixed amount of time
3. Remove sample from solvent and remove residual solvent using compressed air
4. Measure sample mass and determine mass loss
5. Repeat starting at step 2 using the same sample

To calculate the effective dissolution rate from the measured mass loss, an even material removal rate across the surface of the sample was assumed. Using the average density of the material, the reduction of surface area during the dissolution was accounted for. The resulting effective dissolution rate is hence independent of sample size and is given in units of mass per surface area per time.

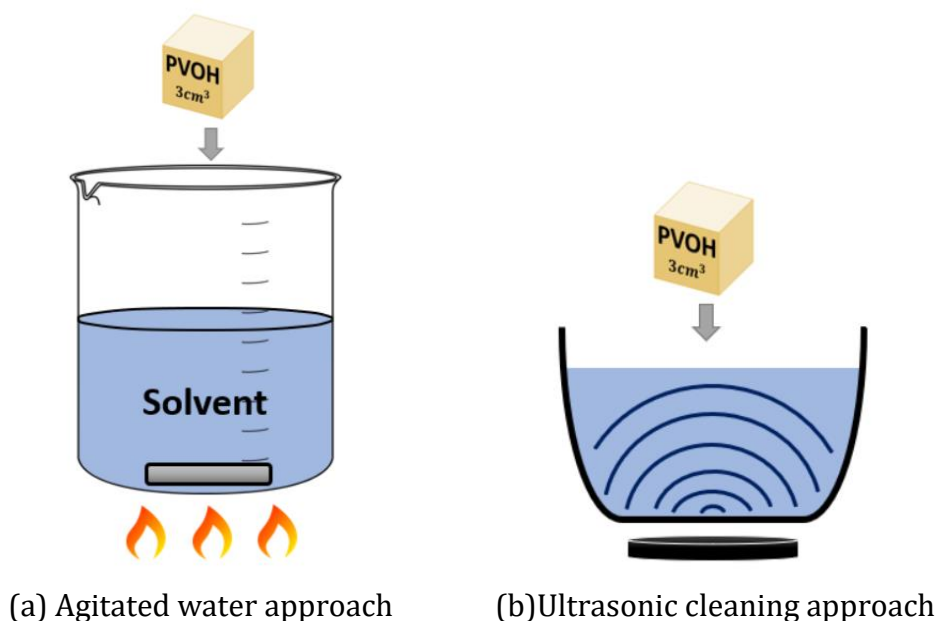


Figure 5.1. Experimental setups to investigate rate of dissolution.

5.3 Results & Discussion

The results for test series DT-1 are shown in Figure 5.2. Due to the heating system used, the bath temperature could not be kept constant and hence small variations occurred as indicated. Solely water as a solvent showed the highest dissolution rate, followed by a water and ethanol mixture and water and methanol mixture. The lowest dissolution rate was experienced using water and ethyl acetate. The assumption that adding an additional solvent to the water bath would accelerate the dissolution process had been proven incorrect. For the PVOH-copolymers used in this study, using solely water was determined as the best approach.

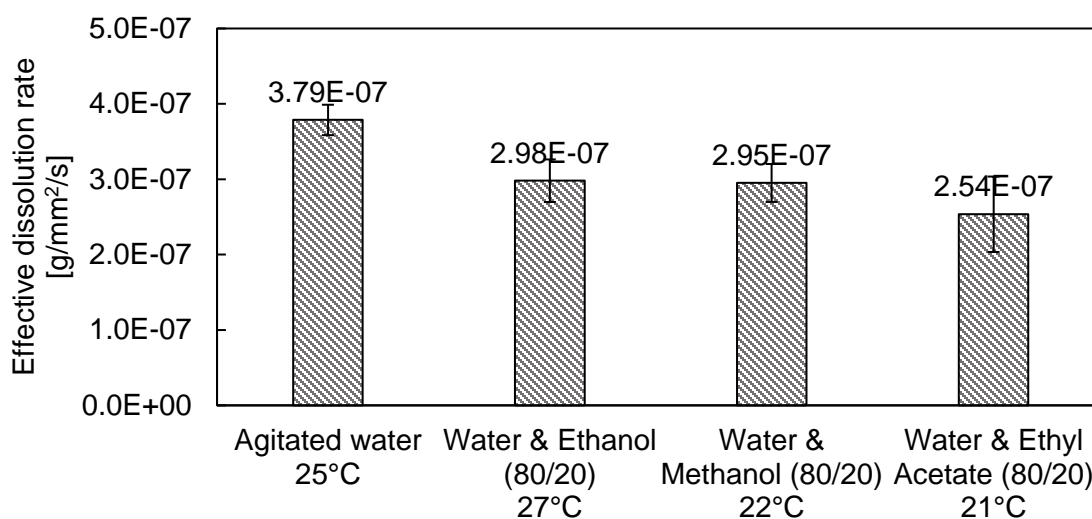


Figure 5.2. Comparison of effective dissolution rate of FDM-A material for different solvents.

The effective dissolution rates of test series DT-2 are shown in Figure 5.3. The results indicate that an increase in water temperature also yields an increase in effective dissolution rate. These findings are in agreement with the work presented by Duran C. et al. [31]. This increase in dissolution rate of more than 55% shows that the elevated solvent temperatures can significantly accelerate the dissolution process.

Furthermore, a test at 29 °C was conducted in the ultrasonic cleaner to compare the two approaches directly. The measured effective dissolution rate was significantly higher using the ultrasonic cleaning approach compared to the agitated water approach at a similar

temperature. These results indicate that ultrasonic cleaning might be a suitable approach to decrease washout times. It should be noted that the deviation between measurements was considerably higher for the ultrasonic cleaning approach.

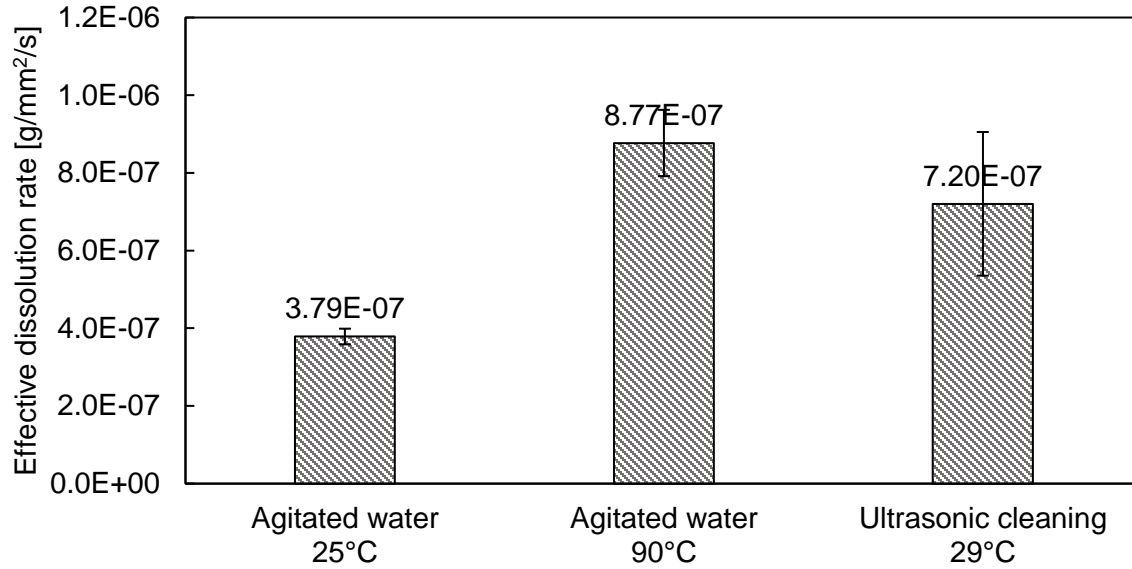


Figure 5.3. Effective dissolution rate for agitated water and ultrasonic cleaning approach at different temperatures.

While the conducted experiments gave insight into trends that influence the effective dissolution rate of a core printed from PVOH-copolymers, several challenges were encountered that prevent accurate dissolution rate measurement. For one, the free-floating sample approach resulted in the sample touching the beaker at several occasions and being hit by the stirrer. This could potentially result in mechanical removal of material from the sample, hence skewing the results. Furthermore, the removal of moisture from the specimen after the dissolution process could be improved by incorporating a post-condition step to remove any moisture remaining in the material.

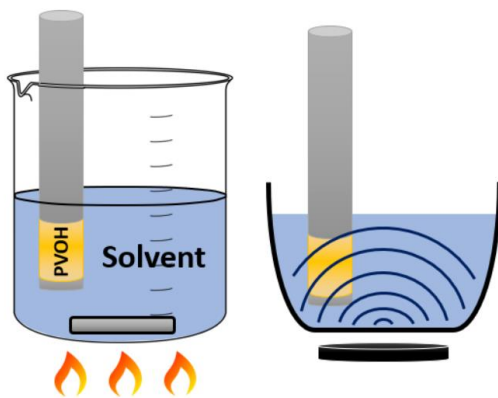
5.4 Redesigned Dissolution Experiments

To obtain more accurate effective dissolution rate measurements to potentially develop a simple numerical model to estimate washout time for larger structures, the experimental setup was redesigned [32].

The sample geometry was changed from a cubic sample to a cylindrical sample that is mounted onto a holding fixture as shown in Figure 5.4-a, to prevent any contact between test specimen and dissolution setup. Furthermore, this setup allowed for repeatable positioning of the sample in each experiment. In addition, a pre-conditioning and post-conditioning step was added to ensure no moisture was left in the sample when measuring the mass loss.

After testing several specimens with both dissolution approaches and at different temperatures, it became evident that determining an effective dissolution rate measurement was not feasible.

Using the agitated water approach, the dissolution rate was strongly affected changing experimental parameters, such as the location of the sample in the beaker and the surface roughness of the specimen. However, these parameters will inherently vary and cannot be controlled when dissolving a complex mandrel geometry.



(a) Cylindrical specimen mounted on fixed holder for improved control of experimental conditions.



(b) Beginning of dissolution of a specimen submerged in ultrasonic cleaner.

Figure 5.4. Redesigned dissolution setup.

For the ultrasonic cleaning approach, the results obtained showed that some experimental runs yielded a very high dissolution rate, while others did not. The data collected showed a strong correlation between position in the ultrasonic cleaner and dissolution rate. Although data was too scattered to quantitatively characterize dissolution rate throughout the cleaner, some qualitative observations were made. At the beginning of each test, visible diffusion at

the sample-solvent interface was noticeable, as shown in Figure 5.4-b. However, as the test progressed, and a thick gel layer formed, the dissolution rate appeared to decrease. In addition, removing the basket from the cleaner greatly increased the observed dissolution rate.

Overall, while these further experiments did not yield quantitative measurements, deeper insight into both dissolution approaches was gained.

5.5 Key Findings

From the experiments conducted, the following key findings were drawn.

Agitated water approach

- Increase in solvent temperature results in increased dissolution rate
- Water is the best solvent for the material tested
- High variance in dissolution rate related to surface roughness and geometry of structure

Ultrasonic cleaning approach

- Potentially highest overall dissolution rate achievable
- Reduced dissolution over time due to gel layer formation
- High variance in dissolution rate related to position within the cleaner

From these key findings, it was concluded that using solely water at an elevated temperature will result in the fastest washout of the sacrificial core structure. However, no clear determination of which dissolution approach is better suited for the washout of larger structures could be made. While the agitated water approach produced robust but slower washout, the ultrasonic cleaning approach produced rapid, but highly uneven, core removal. Further investigation with proper composite structures is suggested.

6 COMPOSITE FABRICATION USING 3D PRINTED SACRIFICIAL CORES

Basic functionality of 3D printed sacrificial cores fabricated via fused deposition modelling has been demonstrated in Chapter 4 and suitable washout processes have been identified and characterized in Chapter 5. With the material properties being sufficient for many liquid moulding applications, and the *water spray sealing approach* giving satisfactory results in the omega benchmark trial, the fabrication of composite structures using PVOH-copolymer core solutions are further explored in this chapter. The objective of these studies is to implement and evaluate effective washout approaches and identify design and fabrication issues when upscaling to relevant geometries. This section is separated into two main investigations. First, a complex stiffened double-curvature panel design is fabricated to explore and implement different dissolution approaches. Secondly, an X-shaped stiffened panel is fabricated with the objective of achieving a composite quality comparable to conventional manufacturing methods encountered in the industry.

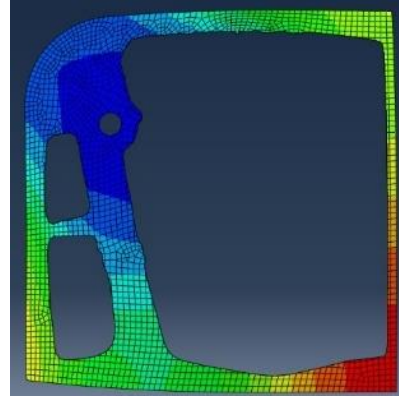
6.1 Complex Stiffened Double-Curvature Panel

6.1.1 Structure Design & Geometry

The geometry for this case study shown in Figure 6.1-a consists of a double-curvature panel, depicted in beige, reinforced by an optimized composite stiffener, depicted in red. Double-curvature panels like this are often encountered in the aerospace industry. However, limitations in manufacturing usually result in the usage of constant cross-section stiffeners only. For this specific demonstrator, the stiffener geometry was inspired by an optimization based on a typical load case, conducted using ABAQUS FEA. The result of this optimization is shown in Figure 6.1-b. While this demonstrated design might not be the most optimized solution, it provides a challenging manufacturing case for 3D printed sacrificial cores.



(a) Double curvature panel



(b) Optimization result (quarter panel only)

Figure 6.1. Optimized demonstrator panel.

Due to manufacturing limitations, such as the size of the washout equipment available, only a section was manufactured as part of this case study; however, the developed approach remains scalable to the entire structure. The 3D printed mandrel shown in Figure 6.2-a conforms to a selected section of the proposed stiffener but includes extrusions to create openings in the composite structure. These openings are required to washout the core and are located strategically to ensure flow throughout the entire stiffener structure. The mandrel shown in Figure 6.2-b is a redesigned version of the original mandrel, allowing for better drapability and dissolution.

6.1.2 Implementation of Wash-Out Approaches

Water agitation

The *water agitation* approach is implemented by forcing a stream of water through the core structure to disintegrate and dissolve the core. In this setup, the composite structure with the core is submerged into an isothermal bath of tap water. The setup for this approach is shown in Figure 6.3. A water pump with a flow rate of 36 litres/minute is used to circulate water throughout the core structure. While no active heating was used in the bath itself, the water is preheated to the indicated temperature. For washout setups in industrial applications, it is recommended to add a heating system to the bath to keep an elevated bath temperature throughout the entire dissolution phase.



(a) Core 1 – Original geometry



(b) Core 2 – Improved geometry for better drapability

Figure 6.2. 3D printed PVOH mandrels of complex stiffener benchmark.

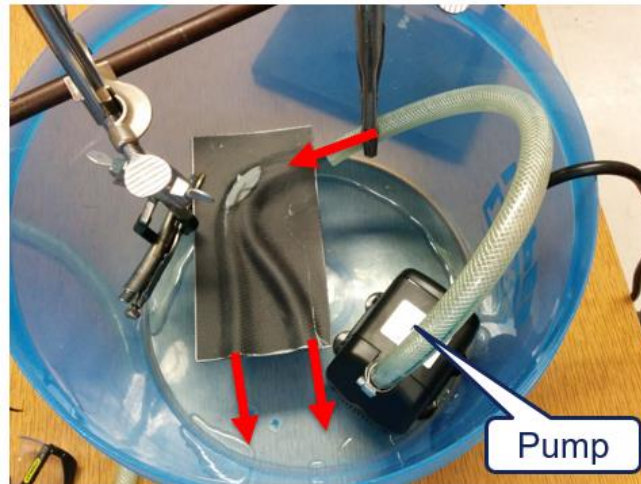


Figure 6.3. Water agitation approach: Composite structure and circulation pump before bath is filled with water.

Ultrasonic cleaning

For the *ultrasonic cleaning* approach, a commercial ultrasonic cleaner with a capacity of 2.84 L and a frequency of 40 Hz was used. The stainless steel cleaning basket was removed, and the composite structure was mounted independently to prevent any contact with the cleaning tank itself. Again, the solvent used is tap water without any additional cleaning agents. The ultrasonic cleaner has a build-in tank heater that was able to achieve a constant water temperature of up to 55°C. The entire setup is shown in Figure 6.4.



Figure 6.4. Ultrasonic cleaning approach: Composite structure mounted in ultrasonic cleaning bath.

6.1.3 Composite Fabrication

Two 3D printed cores shown in Figure 6.2 were printed and sealed using *FDM-B* material and with the design parameters listed in Table 6.1. A core shell thickness of 0.8 mm was selected. Experimental investigations determined that thinner shell thicknesses resulted in too much porosity causing issues during the sealing process. A layer height of 200 μm was determined as suitable for the application regarding manufacturing time and surface finish of the 3D printed core.

The *water spray sealing approach* discussed in Chapter 4 was applied as shown in Figure 6.5. As seen, small pores and gaps on the surface are sealed off, while the shape of the core is insignificantly altered.

Table 6.1. Core parameters for 3D printing

	Parameter	Value
Design	Infill architecture	Triangular - Sparse
	Infill percentage	15%
	Extrusion width	0.4 mm
	Shell thickness	0.8 mm
	Layer height	0.2 mm



Before sealing (a)



After sealing (b)

Figure 6.5. Surface finish and porosity of 3D printed PVOH core.

Fabrication parameters for each mandrel and their respective composite structure are summarized in Table 6.2. For the fabrication of the composite parts of the two case studies, a 6k 5-harness carbon fibre architecture and a 3k 4-harness carbon fibre architecture were chosen. The stack-up consisted of two plies, followed by the core and another two plies forming the stiffener. The shape of the stiffener preform was produced from the CAD model using a commercially available 3D flattening software. A room temperature cure epoxy resin system was used for the vacuum-assisted resin infusion due to the low processing temperature of the FDM-B material.

Table 6.2. Summary of proof-of-concept fabrication parameters

	Parameter	Core 1	Core 2
3D printed core	Material	<i>FDM - B</i>	<i>FDM - B</i>
	Dimensions	186 mm x 100 mm x 17 mm	186 mm x 146 mm x 18 mm
	Printing time	123 min	150 min
	Sealing time	~30 min	~30 min
	Material usage	29.06 cm ³	29.61 cm ³
	Weight	34.58 g	35.24 g
Composite	Reinforcement	6k 5-harness carbon fibre	3k 4-harness carbon fibre
	Matrix	Room temperature cure epoxy resin	Room temperature cure epoxy resin
	Infusion temperature	25 °C	25 °C

6.1.4 Results & Discussion

The moulded composite structures of *Core 1* and *Core 2* are shown with and without the sacrificial core in Figure 6.6. The dissolution approach used, and the resulting total cycle times, are summarized in Table 6.3. Both structures were moulded without any issues. No resin infiltration or core collapse occurred during the manufacturing process. It should be noted that since neither core is identical and varies in geometry and slightly in mass, this is not to be seen as a direct comparison. The results of this study are more of qualitative nature rather than a quantitative metric comparing dissolution speeds.



Case study 1 with core (a)



Case study 1 without core (b)



Case study 2 with core (c)



Case study 2 without core (d)

Figure 6.6. Demoulded composite structures.**Table 6.3. Dissolution approaches and cycle times.**

	Parameter	Case Study 1	Case Study 2
Dissolution approach	Approach	Ultrasonic cleaner	Water agitation
	Water temperature	55 °C	45 °C
	Comments	No basket	Flow rate: ~36L/min
	Infill removal time	5 min	5 min
	Total dissolution time	>90 min	~60 min

Core 1 – Results

The dissolution of this core was achieved using the *ultrasonic cleaner approach*. At the locations of the openings in the composite structure, the exposed shell was cut to reveal the infill structure. The part was submerged in the tank and cleaned for a total of 90 minutes.

After approximately five minutes of cleaning, the infill structure was completely dissolved, only leaving the shell to be removed. Most of the shell was dissolved after a total of 90 minutes in the cleaner. However, the channel with the smallest cross-section of the core had clogged and could not be dissolved. Even after leaving the structure in a water bath soaking for 24 hours and restarting the ultrasonic cleaning process, the channel could not be cleared.

Generally, it was found that the dissolution rate of the core reduced over time. In its rigid state at the beginning of the dissolution process, the apparent mass removal rate was high, but once the core soaked up water and formed a gel layer on the surface, the dissolution rate appeared to decrease. This is further supported by the excellent cleaning performance of a thin PVOH film on a rigid substrate, such as residue from the core washout on the composite structure. One hypothesis for this phenomenon is that the formed gel layer on the surface acts as a protective barrier that absorbs the cavitation action. Since no macro-flow is present in the cleaner, this gel layer is not carried away and only slowly diffuses in the surrounding water.

Furthermore, cavitation damage to the composite structure was found. Upon visual inspection, the skin, especially in the area located directly above the transducers of the ultrasonic cleaner, showed signs of porosity that were not present before cleaning. Although no deeper investigation, such as determining the degree of cure and performing microscopic analysis before and after the dissolution process were conducted, this result indicates a high risk of damage to the composite structure. One option to mitigate this damage is to insert the stainless steel mesh basket into the cleaner or change the ultrasonic output frequency to reduce the cleaning power. However, this will also result in longer dissolution times.

Concluding, the *ultrasonic cleaning approach* did not turn out to be a preferable method for dissolving the PVOH copolymer core. Next to the issues of clogging and missing macro-flow,

the high risk of damage to the composite structure makes this process not favourable, especially when aiming to produce high quality aerospace structures.

Core 2 – Results

For case study 2, the *water agitation approach* was applied. Again, the openings in the composite structure were cut to reveal the infill structure. The part was fixed to a holder, submerged in a water bath at 45 °C and a circulation pump was used to achieve a steady flow throughout the porous infill of the mandrel.

As with the ultrasonic cleaner, the infill structure was removed after approximately 5 minutes, leaving only the shell behind. After a time of approximately 60 minutes, the core had been completely dissolved according to visual inspection. The macro-flow avoided any clogging issues as those present with the ultrasonic cleaning approach.

The water agitation approach was deemed suitable for this application. The final composite structure did not reveal any visible damage after the dissolution process and the total cycle time of dissolution was satisfactory.

6.1.5 Key Findings

In conclusion, these two case studies investigated two different dissolution approaches using two different geometries that represent an industrial relevant structure. The key findings are summarized below:

- Successful composite fabrication using VARI in conjunction with 3D printed PVOH copolymer core
- Reproducible sealing process prevented resin infiltration into core

Ultrasonic cleaning

- Infill structure of core dissolves rapidly, while shell structure dissolves slowly
- Small features tend to clog due to lack of macro-flow
- High variance in dissolution rate with respect to position of ultrasonic transducer
- Cavitation poses high risk of damage to composite structure after prolonged exposure

Water agitation approach

- Infill structure of core dissolves rapidly, shell structure dissolves slower, but faster compared to ultrasonic cleaning
- Macro-flow prevents any clogging issues
- Gentle cleaning action poses low risk of damage to composite structure

6.2 X-shaped Stiffened Panel

The motivation of the X-stiffener case study is the design and manufacturing of a simple structure with industrial relevant features. The objective is to fabricate a high-quality composite structure that integrates the benefits of sacrificial cores via fused deposition modelling, while achieving the same composite quality obtained with traditional moulding methods such as elastomeric mandrels or multi-step assembly. Combining the knowledge of core fabrication and washout methods obtained from previous case studies, this case study focuses on the design and fine-tuning of the developed process to present and validate the moulding capabilities of sacrificial cores via FDM.

6.2.1 Structure Design & Geometry

The geometry is a flat panel reinforced by a complex hollow stiffener. The stiffener geometry is a cross-shaped pattern with a non-constant cross-section which renders the inside cavity trapped and therefore requires a sacrificial core. Furthermore, the top features a net-shape cut-out section, offering a better view inside the hollow structure once the core is removed. Figure 6.7 shows a drawing of the composite part.

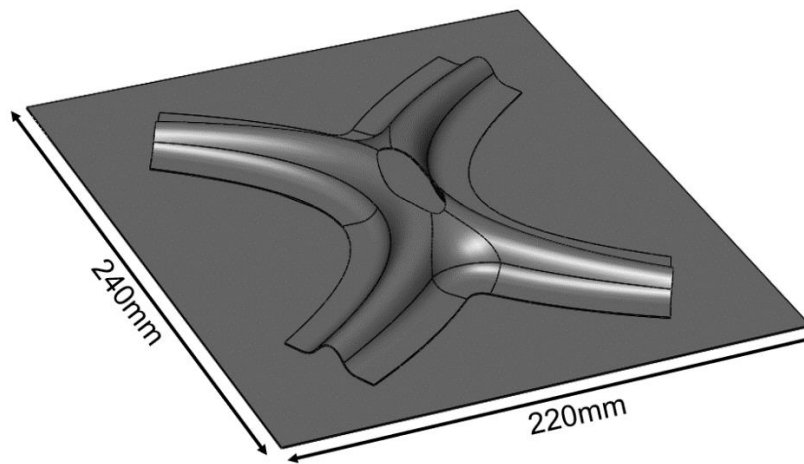


Figure 6.7. Geometry of X-shaped benchmark panel.

6.2.2 Fabrication Process and Tooling

The fabrication process chosen is vacuum assisted resin infusion combined with the sacrificial core process described in Chapter 3. A flat, polished and treated aluminum plate

is used as the rigid tool to shape the skin. The preform tool and the sacrificial core went through several iterations to improve on encountered processing issues. More details on the different core iterations are described below for each study.

For this geometry, a net-shape preform is fabricated. The preforming process consists of several steps, namely pattern cutting, binder application, draping, consolidation and melting. First, a flat pattern of the dry reinforcement for the skin and the stiffener is cut. The cut-to-shape dry reinforcement is referred to as a preform. To transform this 2D, flat preform into a 3D net-shape preform, a binder or tackifier is used. A binder is generally a thermoplastic or thermoset resin that is solid at room temperature. The dry reinforcement is coated with the binder and then draped to its final shape using a preform tool. In this study, the preform is consolidated by vacuum pressure using a traditional vacuum bag approach.

Lastly, the entire setup is placed into an oven and heated. The heat melts the binder and allows for impregnation into the fibres. Upon cooling, the resin will then form a physical bond between the fibres and plies, keeping the preform in the desired shape. The result is a dry fibre reinforcement that is semi-rigid and flexible, but net-shaped to the final geometry.

For designing the preform tool and selecting the correct material, the preform cure cycle temperature is the critical property. The binders used in this case study are Cytec 7720 and EMS D1365, requiring a temperature of at least 80°C to melt. Since the process applies constant pressure over extended periods of time, the glass transition temperature was used as a metric to ensure no heat induced creep will occur in the preform tool. Acrylonitrile styrene acrylate (ASA) was chosen as the preform tool material, due to its glass transition temperature of 100°C.

Lastly, for the core removal, the water agitation washout approach as outlined earlier in this chapter is applied.

6.2.3 Cores and Processing Parameters

All sacrificial cores in this study were printed using FDM-C material. Due to its high glass-transition temperature it is the most versatile material, allowing for slightly elevated temperatures during the infusion process. All additive processing parameters used for the

core as well as for the preform tool fabrication are outlined in Table 6.4. To seal the core from resin infiltration, the *water spray sealing approach* discussed in Chapter 4 was applied.

Table 6.4. Additive manufacturing parameter for X-shape panel case study.

Parameter	Sacrificial Core	Preform Tooling
Material	FDM - C	ASA
Extrusion temperature	215°C	240°C
Bed temperature	60°C	100°C
Print speed	3600 mm/min	3000 mm/min
Infill architecture	Triangular - Sparse	Triangular - Solid
Infill percentage	15%	30%
Extrusion width	0.48 mm	0.48
Layer height	0.25 mm	0.25 mm

6.2.4 Study #1

Core design

The core was designed according to the desired geometry of the stiffener and features an extruded section to accommodate the net-shape cut-out. The perimeter of the extrusion was lined with a C-shaped lip as in core Type B discussed in Chapter 3 for an improved edge finish. The core geometry is depicted in Figure 6.8.

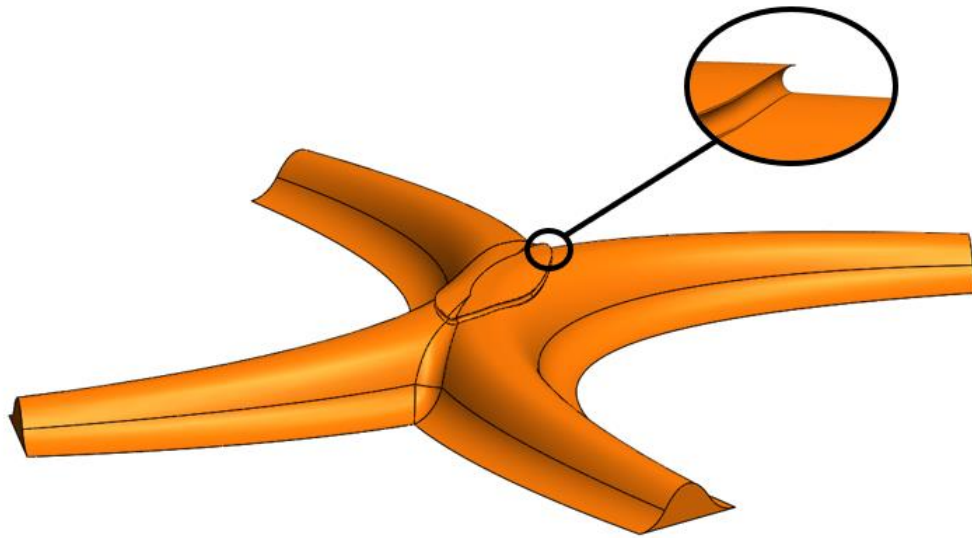


Figure 6.8. Sacrificial core geometry with net-shape cut-out section - X-shape stiffener, study #1.

Composite Fabrication

The panel of study #1 was fabricated using 5HS-6k carbon fibre reinforcement. The material came pre-impregnated with Cytec 7720 binder; hence the binder application step was skipped. The layup consisted of 2 plies for the skin and 2 plies for the stiffener. The stiffener was net-shaped as described earlier, while the skin was not consolidated prior to injection. The stiffener preform, before and after trimming, is shown in Figure 6.9. The infusion setup used is identical to the setup shown in Figure 4.12 in Chapter 4. All layup and infusion parameters used for this study are listed in Table 6.5.

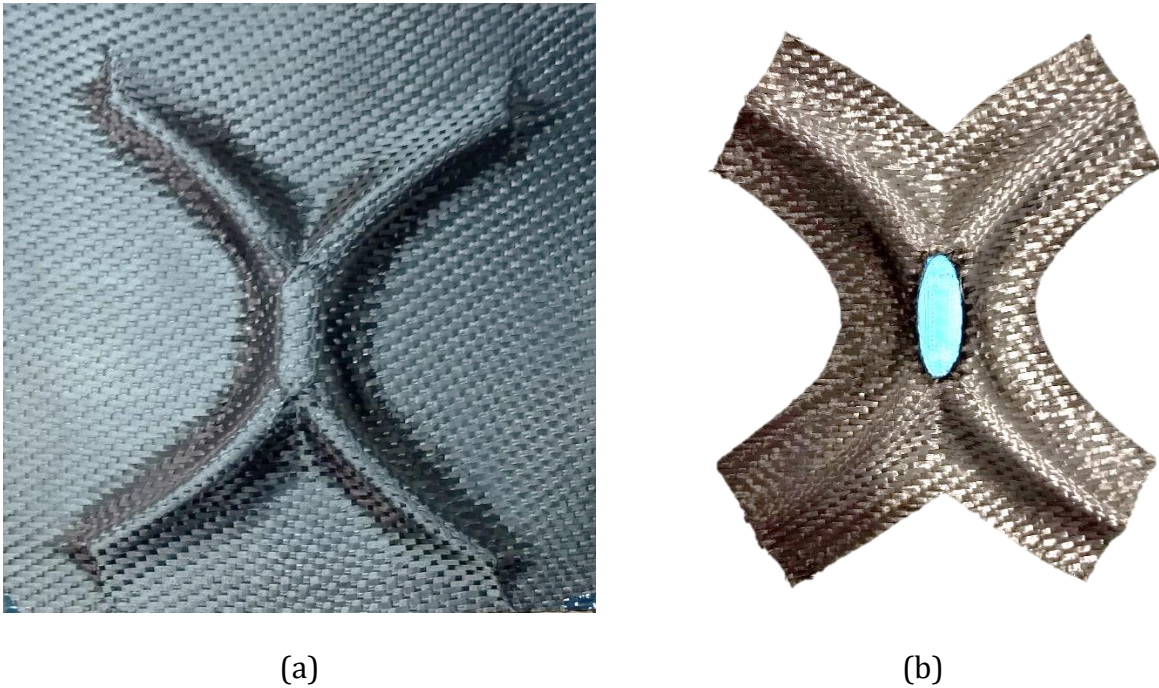


Figure 6.9. Preform after binder melting prior to trimming (a), net-shape preform after trimming operation.

Table 6.5. Fabrication parameters of X-shaped composite panel for study #1.

Parameter	Value
Tool	Aluminium plate
Resin	Epoxy System
Fibre architecture	Carbon – 5HS + Binder – 4540
Binder	Cytec 7720
Skin Layup	2 plies, non-consolidated
X-shaped stiffener	2 plies, preformed to stiffener shape
Preforming	Vacuum bag, 60 minutes @ 80°C
Injection temperature	25°C
Vacuum pressure	14.7 PSI absolute
Post cure	24h @ 25°C

Core Dissolution

For the core washout, the pump providing water circulation was equipped with a Y-junction to split the stream into two outlets. By using custom designed brackets, the outlets were mounted to the composite panel to force water directly into the opening of the stiffener structure. The dissolution setup as well as the water flow pattern throughout the stiffener are shown in Figure 6.10.

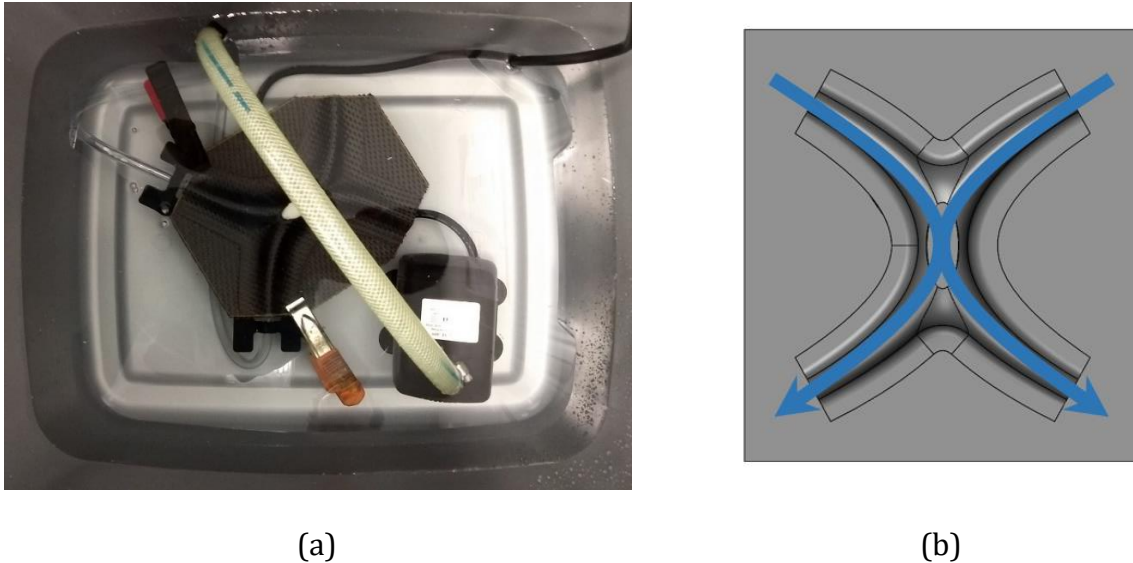


Figure 6.10. Dissolution setup for X-shaped stiffener. (a) Panel submerged and connected to water inlets. (b) Flow pattern through stiffener during dissolution.

The water was heated beforehand to achieve a temperature of 42°C at the beginning of the dissolution process. Due to limitations in this setup, no active water heating was possible.

The length of the washout cycle was 30 minutes, and upon completion the core structure was completely removed as determined by visual inspection. The water temperature had dropped at the end of the cycle to 36.7°C.

Results & Discussion

Figure 6.11 shows the final X-shaped stiffened panel after all dissolution and trimming operations have been completed. Overall, the first attempt at fabricating the X-shaped structure was successful. The core withstood the infusion process without visible

deformation and was not infiltrated by resin. The cut-out section on the top yielded the desired net-shape edge finish.



Figure 6.11. X-shaped composite panel – Study #1.

Two different part defects had been encountered. First, a large dry area on the skin was located directly underneath the stiffener in the corresponding shape. This dry spot issue is common with cores in infusion processes. While the flow media placed on top of the structure allows for resin impregnation throughout the part, the section of reinforcement trapped between the flat mould and flat bottom of the stiffener lacks proper resin impregnation. This defect is shown in Figure 6.12-(a).

Secondly, excessive resin accumulation occurred at the four ends of the core as shown in Figure 6.12-(b). Due to the drastic change in geometry, namely from the raised stiffener section to the flat panel, bridging in the vacuum bag lead to resin accumulation at each stiffener end. As part of study #1, the ends of the panel had been trimmed to yield a clear cut, however, for future panels and applications, the bag bridging and resin accumulation needs to be addressed.



(a) Dry areas underneath the stiffener.



(b) Excessive resin accumulation due to bag bridging at stiffener ends.

Figure 6.12. Fabrication defects in X-shaped stiffened panel.

6.2.5 Study #2

The second study of the X-shaped stiffener attempts to improve on the manufacturing defects encountered in Study #1. The core geometry was redesigned, as well as adjustments to the composite fabrication process have been made. The additive manufacturing as well as the dissolution process have not been altered and are identical to those in Study #1.

Core Design & Fabrication

Compared to Study #1, the core design remains mostly identical with the addition of three new features. To mitigate the dry spot issue, a flow media pattern was integrated into the base of the core. Rather than adding a separate flow media that will be challenging to remove once the structure is moulded, the pattern is directly printed into the core. To address the issue of resin accumulation due to vacuum bag bridging at the end sections of the stiffener, a smooth transition section was added to occupy the area of potential bridging. Lastly, the transition area between the legs of the stiffener was increased for easier draping. The

original designed featured a comparably small radius, inducing wrinkles and warpage of the preform. All added design features are shown in Figure 6.13.

The 3D printing of the redesigned core was successful; however, the flow pattern channel width was reduced compared to the design. Compression of the first layer in the 3D printing process and the associated expansion of the bead width lead to a reduction in channel width. Nevertheless, the flow channels remained present and fabrication proceeded.

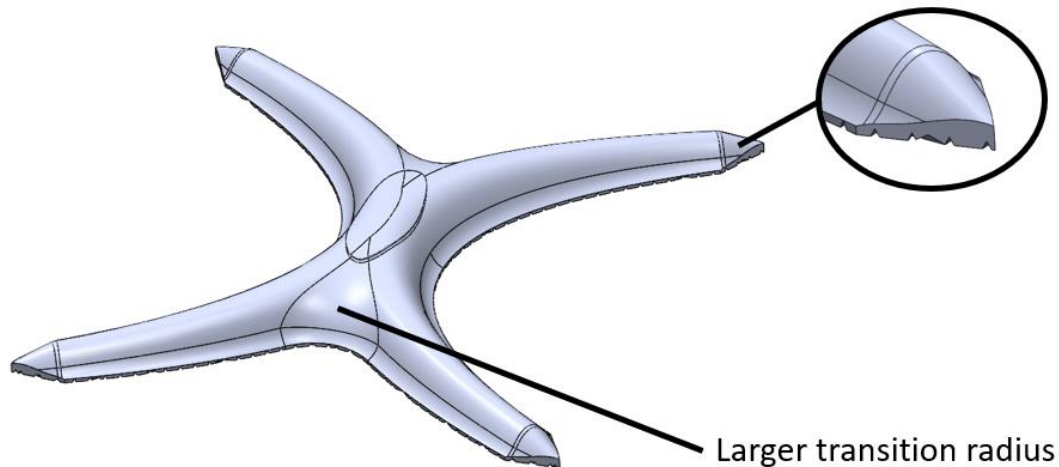


Figure 6.13. Redesigned X-shaped stiffener for Study #2. Added features include smooth end sections and larger transition radius between stiffener legs.

Composite Fabrication

The composite fabrication process was kept identical to Study #1. The only change made was in terms of fibre architecture and preforming process. The thick 6k-5HS reinforcement was replaced by lighter 3k-4HS carbon reinforcement, while the total ply number was kept identical. All manufacturing parameters are listed in Table 6.6.

Table 6.6. Fabrication parameters of X-shaped composite panel for Study #2.

Parameter	Value
Tool	Aluminum plate
Resin	Epoxy System
Fibre architecture	Carbon – Plain Weave – 3k
Binder	EMS D1365
Skin Layup	2 plies, non-consolidated
X-shaped stiffener	2 plies, preformed to stiffener shape
Preforming	Vacuum bag, 60 minutes @ 80°C
Injection temperature	25°C
Vacuum pressure	14.7 PSI absolute
Post cure	24h @ 25°C

Results & Discussion

The composite structure after demoulding is shown in Figure 6.14. The core was not removed at this stage. As with Study #1, no major issues during the moulding process occurred. Investigating the dry-spot defect seen in the previous study, the flow pattern had significantly reduced the dry area. However, as shown in Figure 6.15, small patches of dry fibre were still present. This might be due to the aforementioned reduction of the flow pattern in the 3D printing process.



Figure 6.14. X-shaped composite panel with sacrificial core – Study #2.

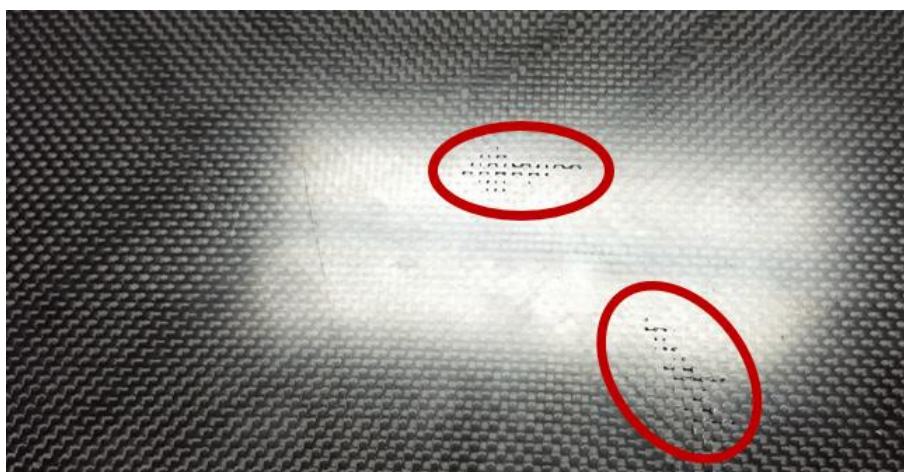


Figure 6.15. Resin starvation on skin of X-shaped stiffened panel Study #2.



(a) After demoulding.



(b) Resin cracks after flexing of panel

Figure 6.16. Resin rich stiffener ends of X-shaped stiffened panel Study #2.

Inspecting the ends of the stiffener, an overall reduction in resin accumulation was found. However, pools of resin were still visible all around the stiffener ends as shown in figure Figure 6.16-a. Small bridges in the bag resulted in heavy resin accumulation at the foot of the sacrificial core. On attempt to flex the panel, these sections fractured as shown in Figure 6.16-b. After core washout, these areas will still be present causing defects on the surface of the part.

Lastly, according to visual inspection, the consolidation of the fibre reinforcement to the sacrificial core was not ideal. The less flexible plain weave demonstrated more spring-back, resulting in more bridging of the bag. Therefore, the structure was generally more resin rich as in Study #1, especially at the junction of the stiffener and the skin.

Concluding, a further design iteration is required to eliminate both, the dry area as well as the resin rich stiffener ends.

6.2.6 Study #3

For the third study, the core geometry was redesigned once more as well as adjustments to the composite fabrication process were made. The additive manufacturing as well as the dissolution process have not been altered and are identical to those in Study #1.

Core Design & Fabrication

The only changes to the core made compared to Study #2 was a redesign of the flow media pattern and of the stiffener ends as shown in Figure 6.17. To increase the resin flow through the flow media, the pattern density and depth was increased. The redesign of the end section included an additional ridge to obtain a clear cut at the end of the stiffener and to further reduce resin accumulation.

Fabrication and sealing of the redesigned core was successful; including the flow pattern.

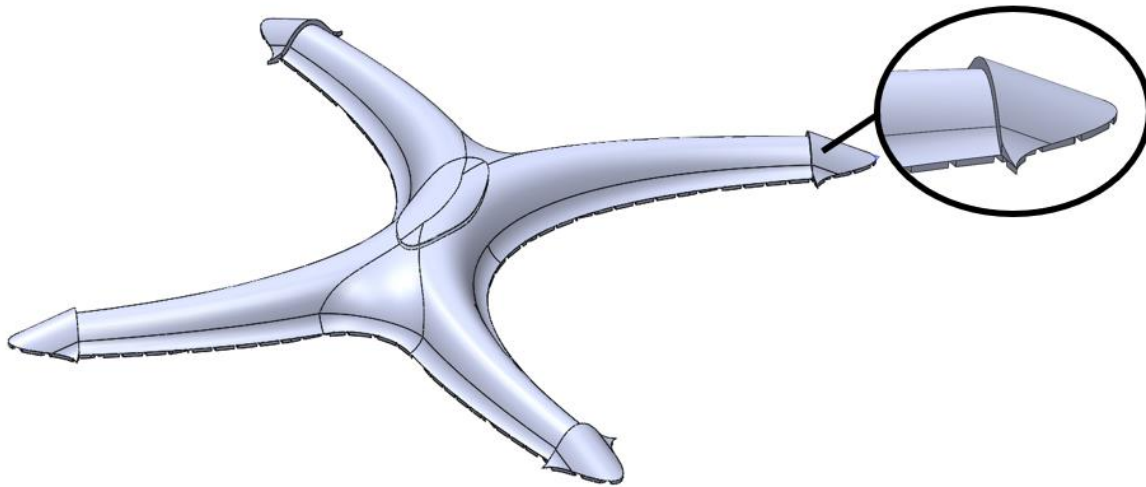


Figure 6.17. Redesigned X-shaped stiffener features for Study #3.

Composite Fabrication

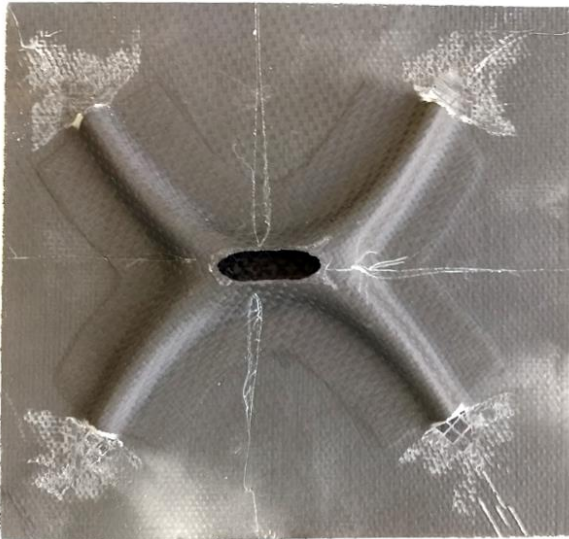
The composite fabrication process was reverted to the one used in Study #1 and materials and parameters are listed in Table 6.5. The only change was made to the bagging procedure. Additional pleads were added that align with the legs of the stiffener to further prevent any resin rich areas at the stiffener ends.

Results & Discussion

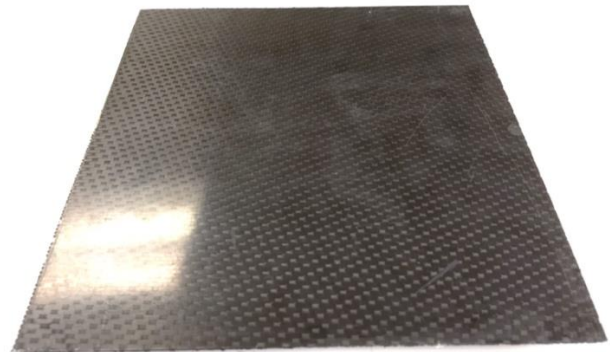
The composite structure after demoulding and washing out the sacrificial core is shown in Figure 6.18. The demoulding and wash-out of the core were successful. Upon inspection, no visual defects were identified. The redesigned flow pattern was able to avoid any resin starved areas, yielding a well impregnated skin as shown in Figure 6.18-b.

Furthermore, the resin accumulations at the stiffener ends were significantly reduced and the core could be removed without damage to the surround skin. However, a few post-finishing operations were necessary to remove any excess resin, as seen by the white, sanded areas around the stiffener exits. Figure 6.19 compares the fabricated stiffener opening to an opening on a structure manufactured using a conventional elastomeric mandrel. Although the stiffener ends in this study show missing fibre at the outermost end, the overall moulding quality between the two samples is comparable. Lastly, by reverting back to the easier to

draped 5-Harness reinforcement architecture, the same moulding quality was achieved without showing any resin rich areas on the stiffener.



(a) Hollow stiffened section after core removal

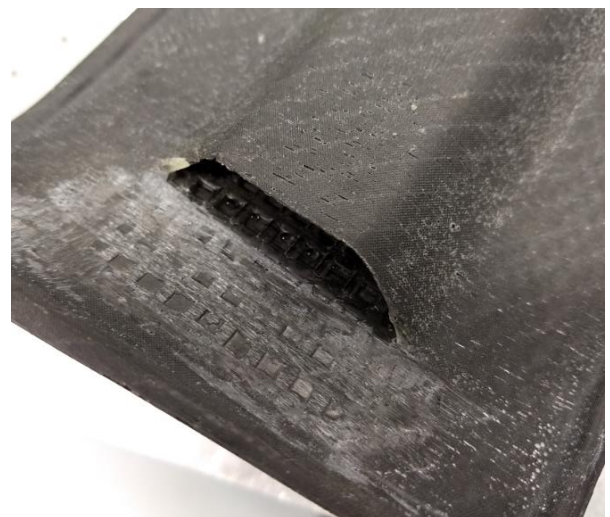


(b) Skin side without any visual defects.

Figure 6.18. Results of X-shaped composite panel – Study #3.



(a) X-shaped stiffener – Study #3.



(b) Conventionally fabricated reference structure.

Figure 6.19. Comparison of fabrication quality of stiffener ends.

In conclusion, the X-shaped stiffener study proofed that through three design iterations, it was possible to design a 3D printed sacrificial core which integrates a flow media pattern as well as features that enable moulding of net-shape cut-outs. While the integrated flow media pattern resolves the dry area defect, it also causes a resin rich interface. Compared to a conventional removable flow media, the integrated media slightly increases the total weight of the structure. This is a common issue with complex removable cores and must be seen as a trade-off for increased core complexity. Furthermore, it was shown that the proposed 3D printed core technology is capable of moulding stiffened structures with comparable quality to parts industrially fabricated using conventional core technologies.

7 COST ANALYSIS

This chapter presents the cost analysis conducted for different core technologies. As discussed in Chapter 1, one of the motivations for this work is to develop sacrificial core technologies that offer a competitive and ideally lower price point than current manufacturing processes. This chapter will first cover the methodology used to assess the price of the different technologies presented. Then, by using a T-shaped structure as a case study, the associated costs for the manufacturing of the core materials are calculated. The goal of this chapter is not only to compare the cost of the presented sacrificial technology to alternative sacrificial cores, but also to provide means to analyze which core technology is best suited for an application case.

7.1 Methodology

The cost model presented is a simple model for the financial feasibility analysis of a technology. Several studies and models are covered in the literature for assessing the fabrication cost of composite structures [33-35]. The following outlines the several cost categories and summarizes the calculations used to determine the cost of production.

The cost associated with integrating a new technology in a manufacturing process can be separated into two main categories, namely the investment and the production cost.

7.1.1 Investment

Investments are costs associated with one-time purchases with the goal of generating returns. Investments are spendings coupled to a certain technology or process rather than being coupled to a specific project or application. In this context, the investment is generally equipment, for example the purchase of a 3D printer. The cost of investment can vary drastically and must therefore be evaluated for each specific case. For example, the production facility might already have invested in equipment that is not used to its full capacity and hence additional investment can be skipped. This makes the general evaluation

on investment cost challenging, and although listed in the following, is not considered when assessing the cost of different fabrication methods.

7.1.2 Production cost

The production cost (PC) of a part can be separated into two categories, namely non-recurring cost and recurring costs.

$$\textbf{Production cost} = \sum \textbf{Non – recurring cost} / \textbf{unit} + \sum \textbf{Recurring cost} \quad \textbf{Eqn. 1}$$

In this context, non-recurring costs (NRC) are one-time costs coupled to a specific project or application. These costs are purchases that must be made for each specific project, but generally do not re-occur throughout the production run. For example, this includes tooling that cannot be used for fabricating anything else but a single product. Furthermore, non-recurring cost also includes the cost of research and development as well as engineering. For simplicity, the engineering cost is omitted in this work. The NRC must be amortized throughout the lifetime of the production run, and hence the NRC per product unit is used to calculate production cost.

$$\sum \textbf{NRC} / \textbf{unit} = \sum \textbf{NRC} / \textbf{production quantity} \quad \textbf{Eqn. 2}$$

Recurring costs (RC) are costs associated with each manufactured product. RC is defined as the price to fabricate one unit and includes material cost (MC), consumable cost (CC) as well as labour (LC) and burden cost (BC).

$$\textbf{RC} (\$/\textbf{unit}) = \sum \textbf{MC} + \sum \textbf{CC} + \sum \textbf{LC} + \sum \textbf{BC} \quad \textbf{Eqn. 3}$$

To estimate material and consumable cost accurately, material losses must be accounted for. The material amount that ends up in the final product is referred to as effective material, while the material scraped during the fabrication process is referred to as lost material. The quantity of lost material is calculated by determining a loss percentage and applying it to the effective material used in the manufacturing of the product.

$$\textbf{Lost material (volume)} = \textbf{Effective material (volume)} \times \textbf{Loss\%} \quad \textbf{Eqn. 4}$$

$$\begin{aligned} \textbf{Lost consumables (volume)} \\ = \textbf{Effective consumables (volume)} \times \textbf{Loss\%} \end{aligned} \quad \textbf{Eqn. 5}$$

The material and consumable cost is based on the volume price of the material and the amount of material processed.

$$MC (\$/unit) = (\sum Effective material + \sum Lost material) \times material price (\$/volume) \quad \text{Eqn. 6}$$

$$MC (\$/unit) = (\sum Effective consumables + \sum Lost consumables) \times consumable price (\$/volume) \quad \text{Eqn. 7}$$

Burden cost, also referred to as overhead, is the cost associated with running the production facility. Simplified, burden costs are all expenditures that are not related to fabricating a specific product. Burden lumps several factors into a “per hour per area” cost and includes for example the property cost of the facility, the insurance and the electricity. For example, if a machine takes a certain amount of time to manufacture a part without the need for any human attention, the labour cost might be zero. However, the burden will still be contributing to the recurring cost. Burden cost is challenging to estimate accurately and heavily depends on location as well as the production facility. In this work, an estimated value of burden cost is determined based on the equipment footprint.

The labour and burden cost are usually calculated from hourly rates.

$$Labour cost = \sum Labour time \times Labour rate (\$/hour) \quad \text{Eqn. 8}$$

$$Burden cost = Cycle time \times Burden rate of equipment (\$/hour) \quad \text{Eqn. 9}$$

Although this type of cost assessment is simple, it provides the necessary means to compare the production cost of different manufacturing processes without overcomplicating the analysis with unnecessary detail.

7.2 Cost assessment

7.2.1 Case Study

The case study selected for the cost assessment is the T-shaped omega geometry shown in Figure 7.1. The cross-section of the stiffener is constant, and the stiffener can be manufactured using a multi-part elastomeric mandrel, hence does not require a sacrificial mandrel. Furthermore, this simple shape is easy to manufacture using a casting process and does not feature any fine details. This specific geometry was therefore chosen as a benchmark structure since it can be fabricated with several core technologies. Although not covered in this work, it was used to fabricate several benchmarks and evaluate the technical feasibility of different sacrificial core geometries in combination with resin transfer moulding. Therefore, labour and manufacturing effort were measured rather than estimated.

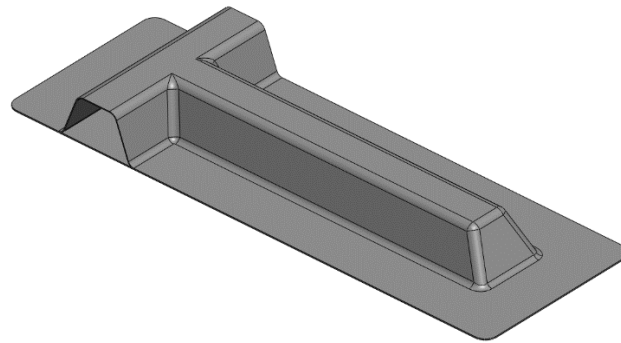


Figure 7.1. Omega benchmark structure selected as case study for the cost analysis.

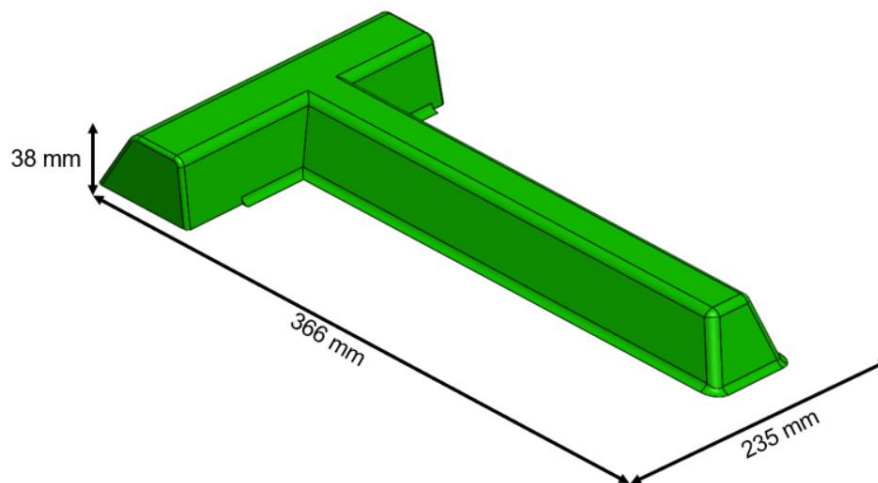


Figure 7.2. Core geometry with dimensions used for cost analysis study.

The overall dimension of the core is 235 mm by 366 mm by 38 mm as shown in Figure 7.2. Since only the cost associated with the core structure is evaluated and not the entire composite manufacturing process, only the core volume is of interest. The calculated bulk volume of the core is $989.7 \times 10^3 \text{ mm}^3$.

7.2.2 Process Analysis

The cost assessment is split by fabrication process, namely cores by casting and cores by fused deposition modelling. Each process has different non-recurring costs and labour steps and must therefore be investigated on its own.

To evaluate labour and burden cost, standard rates are set for all processes, which are listed in Table 7.1.

Table 7.1. Standardized cost rates.

Rate	Cost
Labour cost	35.00\$ / hour
Burden cost - Oven	5.00\$ / hour
Burden cost – 3D printer	3.23\$ / hour

7.2.2.1 Cast cores

Cast cores refer to all core technologies that use a low temperature, low pressure casting process. This study includes plaster-based sacrificial cores and cast foam flyaway cores.

The non-recurring cost of this technology is the required casting tool. There are several options to manufacture the casting tool, such as CNC milling, 3D printing or fabricating a *splash*. A *splash* is a copy of the resin transfer moulding tool fabricated by a manual casting procedure. However rather than copying the exact same geometry, an offset is integrated to accommodate for the composite thickness. While the casting of a *splash* is a manual procedure that doesn't require any costly machining operations, it is a multi-step process that involves the casting of at least two geometries.

For this analysis, two tooling options were investigated. First an aluminum tool machined using a 5-axis machining centre, and secondly, a *splash* made with a urethane-based resin system. The estimated cost of each tool is shown in Table 7.2. It should be noted that the selection of tooling material is highly influenced by the production rate and production run length. For example, a 3D printed polymer tool might be the cheapest options. However, it might have to be refurbished or replaced throughout longer runs, making it less feasible for high production volumes.

Table 7.2. Cost of casting tools for sacrificial cores via casting.

	Material	Process	Total Cost
Concept #1	Aluminum 6061	5-axis CNC milling	\$1803.00
Concept #2	Urethane Resin	Manual casting	\$850.04

To calculate the recurring cost, the casting process must be analyzed. The several steps required to fabricate one sacrificial core by casting are shown in Figure 7.3.



Figure 7.3. Process steps for casting a sacrificial core.

First, the tool is cleaned from any residue and prepared with a release agent to ensure the cast core will release easily. Then, the casting material is prepared. This often involves mixing two components together, for example the plaster base with water or the epoxy base with hardener. Subsequently the tool is closed, and the material is cast into the tool. Once the casting step is completed, the core is either cured at room temperature or in an oven. Once the material is cured, the core is demoulded from the tool. Lastly, if required, the core is sealed by wrapping the core in Teflon tape.

The associated fabrication cost for each step for the plaster-based and the cast foam cores are shown in Table 7.3. For comparison, an elastomeric mandrel made from silicone is included as well. Table 7.4 outlines the material cost for each technology.

It should be noted that the burden cost was only applied when a process required the use of equipment, such as an oven. If the core was cured at room temperature, the burden cost was neglected. Furthermore, the burden cost for equipment was amortized over a total of six cores in order to use the equipment's full production capability.

Table 7.3. Fabrication cost analysis of cast cores.

		Tool preparation	Casting	Cure	Demoulding	Sealing	Total time	Total cost
Plaster-based core	Labour (min)	5	10	0	5	30	50	\$29.17
	Burden (min)	0	0	135	0	0	135	\$11.21
	Material (\$)	\$1.39	\$24.57	\$0.00	\$0.00	\$8.05		\$34.01
							Fabrication total	\$74.39
Cast foam	Labour (min)	5	10	0	5	0	20	\$11.67
	Burden (min)	0	0	60	0	0	60	\$4.98
	Material (\$)	\$1.39	\$12.96	\$0.00	\$0.00	\$0.00		\$14.35
							Fabrication total	\$31.00
Elastomeric core	Labour (min)	5	10	0	5	0	20	\$11.67
	Burden (min)	0	0	0	0	0	0	\$0.00
	Material (\$)	\$1.39	\$70.64	\$0.00	\$0.00	\$0.00		\$72.03
							Fabrication total	\$83.70

Table 7.4. Material cost analysis of cast cores

Plaster-based core	Material	Quantity		Loss %	Loss Quantity		Total quantity		Cost/Unit		Cost
	Release agent	20	ml	50%	10	ml	30	ml	\$0.046	\$/ml	\$1.39
	Plaster material	989.7	cm ³	20%	197.94	cm ³	1187.64	cm ³	\$0.021	\$/cm ³	\$24.57
	Teflon Tape	0.1039	m ²	25%	0.026	m ²	0.130	m ²	\$61.99	\$/m ²	\$8.05
Cast foam	Release agent	20	ml	50%	10	ml	30	ml	\$0.046	\$/ml	\$1.39
	Cast foam	989.7	cm ³	10%	98.97	cm ³	1088.67	cm ³	\$0.016	\$/cm ³	\$17.09
Elastomeric core	Release agent	20	ml	50%	10	ml	30	ml	\$0.046	\$/ml	\$1.39
	Silicone	989.7	cm ³	10%	98.97	cm ³	1088.67	cm ³	\$0.065	\$/cm ³	\$70.64

The analysis results for recurring cost are graphically summarized in Figure 7.4.

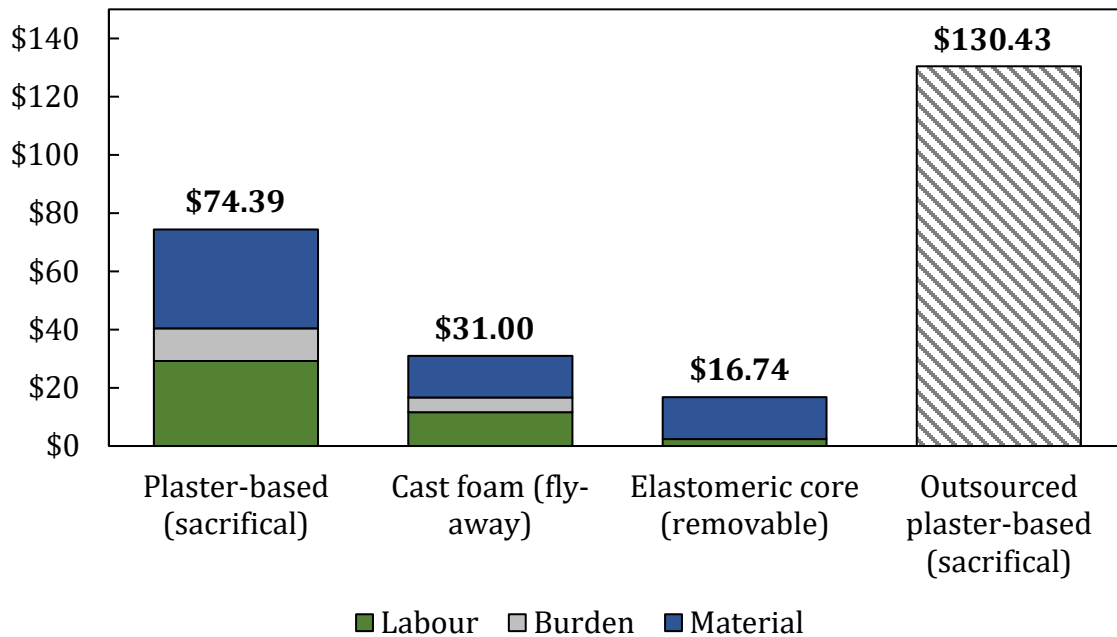


Figure 7.4. Comparison of recurring cost analysis results for cast cores.

The elastomeric core is the option with the least recurring cost of \$16.74. Although the manufacturing cost is \$83.70 per core, this cost is distributed over the lifetime of the core, which is estimated to last at least five fabrication cycles. The cast foam core is with \$31.00 almost double that price and the second most affordable option. The in-house manufactured plaster-based core and the outsourced plaster-based core follow with a recurring cost of \$74.39 and \$130.43, respectively. The cost composition of the cast foam and plaster-based cores are similar, with almost equal amounts in labour and material cost, and only a small percentage of burden. The high labour cost of the plaster-based core is due to the additional step of warping the core with Teflon tape.

The outsourced plaster-based core is shown for reference. The casting and sealing of the core are done by an external supplier and the core is delivered ready to be used for composite moulding. The large price difference indicates that significant fabrication cost can be saved when manufacturing in-house compared to contracting a third-party manufacturer, provided the process knowledge and fabrication capabilities are available.

7.2.2.2 Sacrificial cores by additive manufacturing

The 3D printed sacrificial cores included in this cost analysis are four cores with different materials made by fused filament fabrication as well as one core 3D printed from a silica-based material.

The non-recurring cost point is one of the most favourable aspects of additive manufacturing. The 3D printing process does not require any type of tooling such as the casting process and has therefore virtually zero non-recurring cost. While this is often seen as a big advantage for development and the fabrication of prototypes, it is also a big cost advantage for smaller production runs. A high non-recurring cost for any type of fabrication tool, such as the aluminum tool in the casting process, requires a large initial investment by the customer. If, by any chance, the product geometry is altered, or the manufacturing process is switched, the non-recurring cost cannot be retrieved, and it might have to be spent again. Seldomly, a change to existing tooling is feasible, rendering this need for tooling inflexible. Eliminating the non-recurring cost is therefore a critical competitive advantage. Not only is the risk of tool investment removed, but also the time from design to production start is significantly shortened.

Further advantages are cycle time improvement and the on-demand manufacturing advantages. Being able to produce multiple geometries on the same additive manufacturing equipment without the need to install a tool, can reduce cycle time immensely. Often, the installation of a tool is labour intensive and error-prone, generally increasing the effective cycle time per part. In addition, in an effort to minimize tool changes, the same product is often produced in larger quantities and stocked. Additive manufacturing allows for swift product changes and virtually on-demand manufacturing, enabling lean stocking of products and therefore reducing burden cost.

To evaluate the recurring cost of the additive manufactured part, again the entire process cycle must be investigated. The processing steps are shown in Figure 7.5.

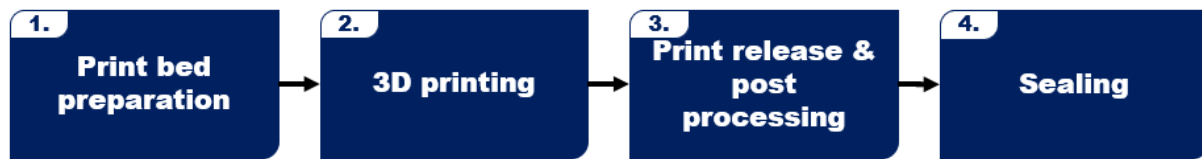


Figure 7.5. Process steps for fabrication of 3D printed cores.

The first step is to prepare the print bed of the 3D printer. This is a maintenance step and involves checking for any debris from the last print and wiping the bed with a cleaning agent.

The next step is the 3D printing of the geometry. After the print is completed, the print is released from the build platform and the necessary post-processing is done. Post-processing involves the manual trimming of excess material, if any, and the removal of support structure if present.

The last step is the sealing of the core. Available sealing options are the previously discussed *water sealing approach*, brush on sealers or wrapping the core in Teflon tape.

It should be noted that one-time setup steps, such as programming the printer, are omitted in this analysis. As mentioned earlier, these would fall into the category of engineering as part of the non-recurring cost.

The fabrication cost analysis for the four selected sacrificial cores is outlined in Table 7.5.

Table 7.5. Fabrication cost analysis of 3D printed sacrificial cores.

		Print bed preparation	3D printing	Print release & post processing	Sealing	Total time	Total cost
FDM A	Labour (min)	2	2	10	10	24	\$14.00
	Burden (min)	0	792	0	60	852	\$43.88
	Material (\$)	0	\$21.18	0	0		\$21.18
						Fabrication cost	\$79.07
FDM B	Labour (min)	2	2	10	10	24	\$14.00
	Burden (min)	0	792	0	60	852	\$43.88
	Material (\$)	0	\$37.95	0	0		\$37.95
						Fabrication cost	\$95.83
FDM C	Labour (min)	2	2	10	10	24	\$14.00
	Burden (min)	0	792	0	60	852	\$43.88
	Material (\$)	0	\$55.22	0	0		\$55.22
						Fabrication cost	\$113.10
FDM D	Labour (min)	2	2	10	30	44	\$25.67
	Burden (min)	0	792	0	0	792	\$42.64
	Material (\$)	0	\$71.58	0	2.80		\$74.38
						Fabrication cost	\$142.69
Ceramic core	Labour (min)	0	0	0	30	30	\$17.50
	Burden (min)	0	0	0	0	0	\$0.00
	Material (\$)	0	\$39.03	0	2.80		\$41.83
						Fabrication cost	\$59.33

The material cost for cores fabricated by fused deposition modelling is calculated based on the infill percentage, the scrap rate, and the material cost. In this analysis, the infill percentage was set to 15% and the scrap rate was estimated at 5% of the material. Using the volume of the core, the required material is estimated.

$$V_{total} = V_{core} \times (P_{infill} + P_{scrap}) \quad \text{Eqn. 10}$$

$$V_{total} = 989.7 \text{ cm}^3 \times (15\% + 5\%) = 197.94 \text{ cm}^3$$

$$V_{total} = \text{Total material required}$$

$$V_{core} = \text{Core volume}$$

$$P_{infill} = \text{Infill percentage}$$

$$P_{scrap} = \text{Scrap rate}$$

Using the specific material cost, the core material cost is then estimated. The results are shown in Table 7.6.

Table 7.6. Material cost for 3D printed cores.

	Cost/unit		V_{total}	Material cost
FDM - A	\$0.107	\$/cm ³	197.94 cm ³	\$21.18
FDM - B	\$0.192	\$/cm ³		\$37.95
FDM - C	\$0.28	\$/cm ³		\$55.22
FDM - D	\$0.36	\$/cm ³		\$71.58

The fabrication of the ceramic core was outsourced to a service centre and the associated material cost is unknown. Hence, the material cost was set to the price of the final supplied core and no labour or burden cost is calculated.

The estimations of the recurring costs are graphically summarized in Figure 7.6.

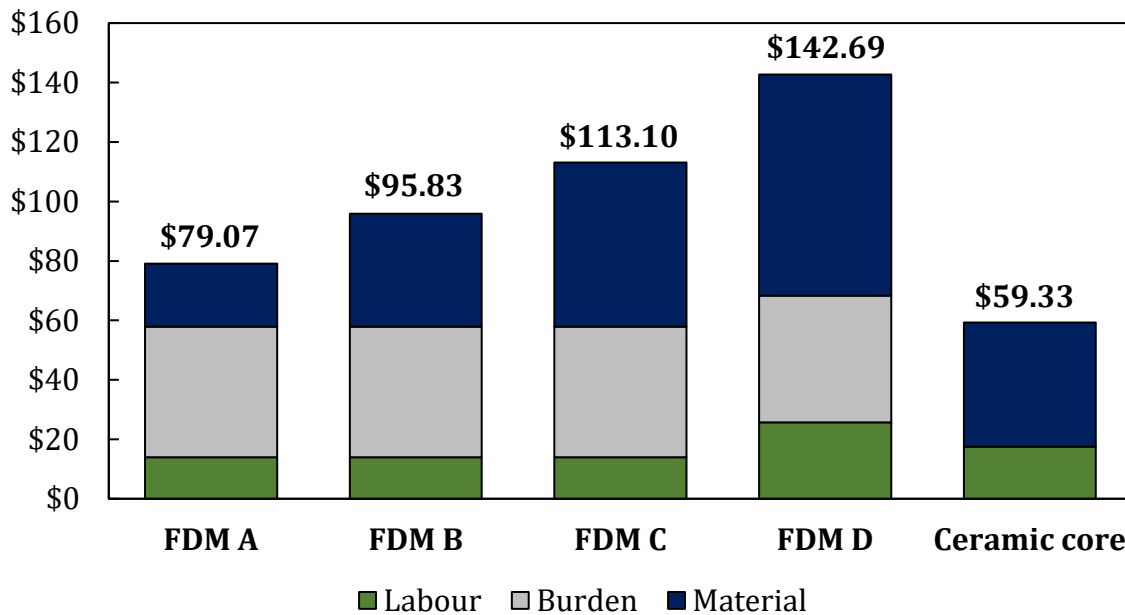


Figure 7.6. Comparison of recurring-cost analysis results for 3D printed cores.

For the FDM cores, the labour and burden cost are equal for material FDM-A to FDM-C, with a slight increase in labour cost for FDM-D, due to the difference in sealing process used. The largest difference between FDM cores is the material cost. The trend of higher material cost is directly correlated to the increase of achievable operating temperature of the core. FDM-A material has the lowest fabrication cost with \$79.07 per core, however, also has the lowest temperature resistance and is the most difficult material to print. Contrary, FDM-D has the highest temperature resistance and the highest price with \$142.69 per core.

Lastly, it should be noted that the burden occupies a large percentage of the fabrication cost due to the relatively slow fabrication process. For the FDM cores, the 3D printing time was estimated at 13 hours and 12 minutes. A decrease in burden cost for a specific facility will therefore significantly impact the fabrication cost of a 3D printed core.

For comparison, a 3D printed ceramic core was graphed as well. Although supplied by a third-party manufacturer, the ceramic core has the lowest fabrication cost with \$59.33.

7.3 Cost Comparison

To determine which technology of core fabrication becomes financially feasible, the non-recurring and recurring cost must be compared and assessed based on the desired business case, which dictates the required production volume in a given time frame. The fabrication cost for a low and high production volume is graphed in Figure 7.7 for all sacrificial cores technologies assessed.

The tooling chosen for the cast cores in this comparison is the aluminum mould at a price of \$1803.00, which translates to the offset in the graph for the three technologies requiring this NRC.

First off, for production volumes below 25 units, using additive manufacturing technology is consistently more cost effective than a cast sacrificial core, independent of material choice. Above this volume, the higher cost additive technologies become more expensive than the lower cost casting methods. The 3D printed ceramic core is the cheapest option independent of volume, due to its non-existing NRC and lowest RC overall. Comparing the plaster-based cast core with the lowest cost FDM-A core, the FDM-A core remains more cost effective up to a volume of 360 units, at which point the NRC of the cast core is amortized and the core becomes the financially more feasible alternative. The outsourced plaster-based core is rendered as the most expensive option up until a volume of around 160 units, at which point the highest cost FDM-D core has the most expensive price point.

Although this analysis cannot be a direct comparison since each technology has its own merits and disadvantages, it places the additive technologies in the same price category as cast cores for low volume productions. Up to a volume of 360 units cores fabricated via fused deposition modelling remain competitive to cast alternatives, and even for slightly larger production volumes do not become unfeasible.

To conclude, although the correct core technology for each application is mainly driven by their technical feasibility, this analysis suggests that additive manufacturing is not only limited to prototype fabrication but can offer a competitive price point for low to medium production volumes.

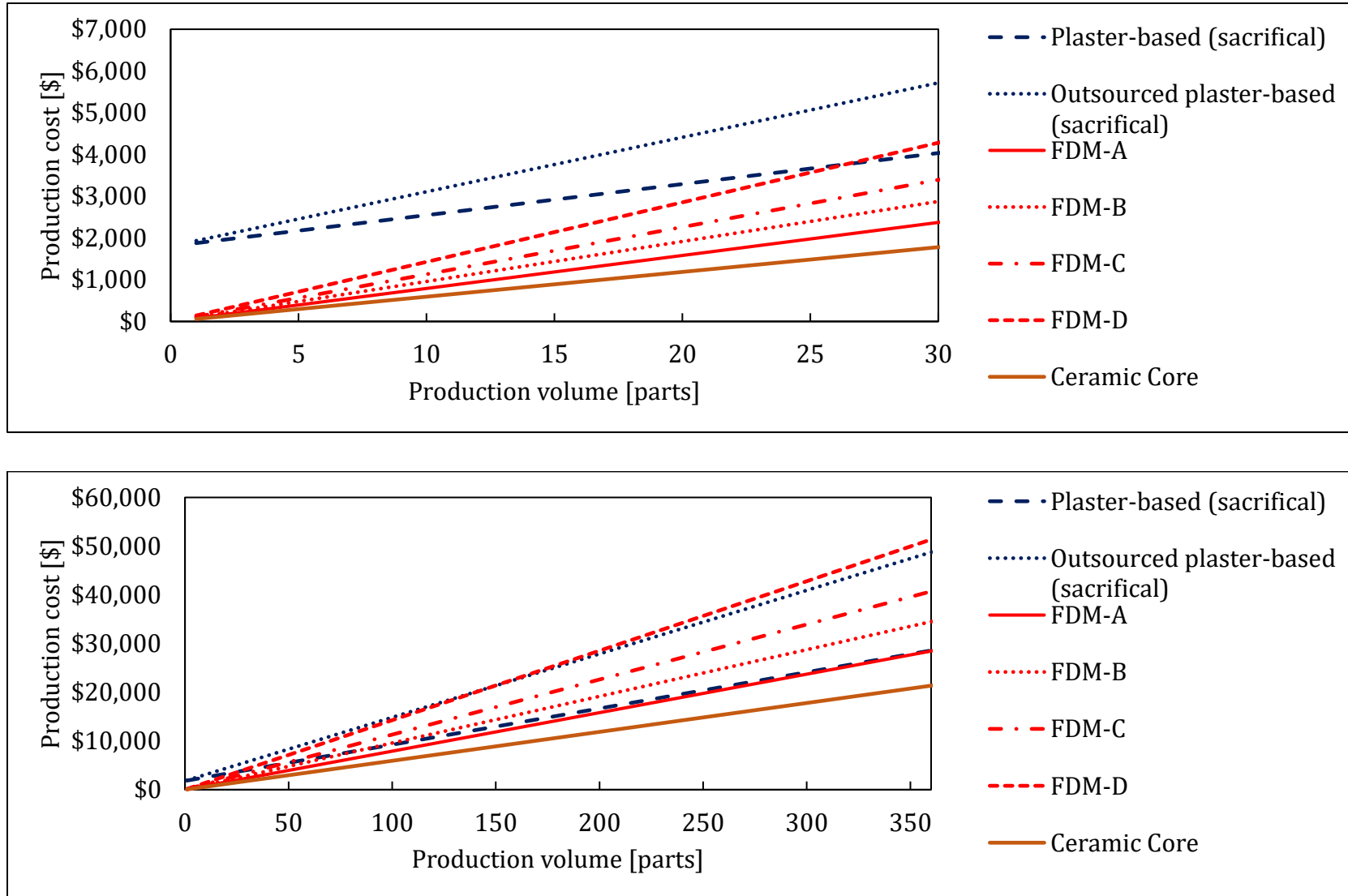


Figure 7.7. Production cost versus production volume for sacrificial core technologies. Low volume production ranging from 0-30 parts (top) and medium volume production ranging from 0-350 parts (bottom).

7.4 Key Findings

This chapter covered the cost considerations and conducted a cost analysis for sacrificial cores fabricated by casting and additive manufacturing. This analysis suggests a way to approach the cost assessment for additive manufactured cores and how to determine if a technology is a financially feasible option. Key findings of this analysis are listed below:

Cast cores

- Cast cores require significant investment due to non-recurring tooling cost
- Cast flyaway cores offer a lower price point compared to sacrificial cast cores
- Plaster-based sacrificial cast cores are the most expensive cast cores to fabricate
- Internal manufacturing of plaster-based cores compared to outsourcing reduces fabrication cost significantly

Additive manufactured cores

- Elimination of non-recurring cost makes additive manufacturing a flexible fabrication process
- Cores fabricated via fused deposition modelling generally have the highest recurring cost
- Burden cost can contribute up to 50% to recurring cost of FDM cores
- Fabrication cost of FDM cores is mainly driven by material cost
- FDM material cost increases with increase in operational temperature of the material

Conclusion

- Additive manufactured cores offer competitive price points to cast sacrificial cores for low to medium production volumes (100-500 units).
- Traditional processes, such as elastomeric cores, remain the lowest cost option when technically applicable.

8 CONCLUSIONS & FUTURE WORK

As composite structures become increasingly more complex in the aerospace industry, novel manufacturing technologies that offer a competitive price point become of interest. With current fabrication methods relying on labour-intensive and costly multi-part assemblies, the development of a one-shot, net-shape moulding process gains traction as an attractive method to manufacture complex composite structures. To enable such a process, the integration of cores, especially of sacrificial nature to create hollow structures, becomes imperative. With advancements of additive manufacturing methods and soluble polymers, 3D printed sacrificial cores show great potential as the next generation of freeform cores. The objective of this work was to investigate, and if necessary, develop novel core technologies that combine 3D printed sacrificial cores with liquid moulding of composites. Specifically, a solution is proposed that uses fused deposition modelling in conjunction with soluble PVOH-copolymers to enable the fabrication of hollow complex composite structures.

8.1 Conclusions

Throughout the course of the work presented, soluble polymers have been characterized, and a functional method was evaluated and presented for the fabrication of 3D printed sacrificial cores. Significant progress has been made on the integration of commercially available PVOH-copolymers as soluble cores used in the fabrication of composite structures by liquid moulding. Figure 8.1 outlines the advancements that have been covered throughout this thesis.

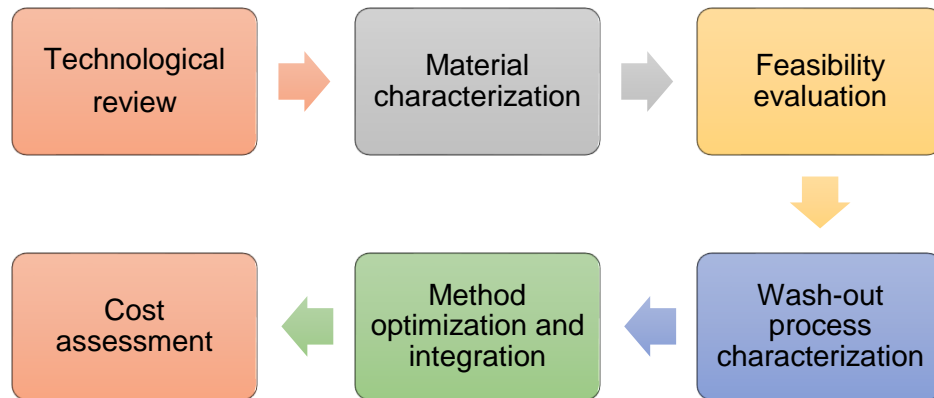


Figure 8.1. Workflow of covered work.

In the first section, a comprehensive review of core technologies that are currently offered on the market was conducted. Suitable and financially feasible technologies for liquid moulding were identified and potential challenges were discussed. The result was the following conclusions:

- No commercially available core solutions are offered specifically tailored to liquid moulding
- Cast foam cores offer promising solutions for low-weight, permanent cores
- Sacrificial plaster and ceramic based cores are well established but lack robust implementations for liquid moulding
- PVOH-based soluble polymers combined with 3D printing offer high potential for the development of a sacrificial core technology.

Based on the results of the technology review, a process for the implementation of 3D printed sacrificial cores were proposed. To determine the material limitations of PVOH-copolymers, material characterization was conducted, including the determination of the operational temperatures, the mechanical strength and the coefficient of thermal expansion. The results were compared to commercially offered core solutions and the application field was discussed. The following conclusions were drawn:

- PVOH-copolymers have an upper temperature limit of 64 °C and hence are only applicable for low temperature composite moulding processes

- 3D printed sacrificial materials offer significantly higher strength than commercially available sacrificial cores, improving handling and reducing deformation
- Polymer based cores exhibit significantly higher CTE than ceramic or plaster-based cores.

Having investigated the material capabilities and limitations, a feasibility study of three sacrificial core materials was conducted to verify the suitability of the selected technologies with liquid moulding. The proposed 3D printed sacrificial core process was validated, along with a cast plaster core and a commercial 3D printed ceramic core. The following was found:

- Cast plaster cores and 3D printed ceramic cores are fragile and highly porous, making them not well suited for applications with liquid moulding
- The developed 3D printed sacrificial core technology is suitable for moulding hollow composite structures with liquid moulding
- 3D printed PVOH-copolymer cores can be robustly sealed from resin infiltration using a water spray sealing process
- Wash-out of PVOH-copolymer cores is difficult and lengthy.

While the developed core technology was validated to be technically feasible, challenges regarding the washout of the core were encountered. To overcome these difficulties, the next step was the development and analysis of an optimized washout process.

By experimentally measuring dissolution rates of the polymers for different conditions, two different washout processes, namely agitated water and ultrasonic cleaning were investigated. Although it has proven to be difficult to accurately measure and predict the dissolution rate of 3D printed cores, it was found that water at elevated temperatures yields the fastest washout rate.

The next phase implemented the discussed washout methods and focused on the fabrication of demonstrator structures. By designing and manufacturing a complex panel, the agitated washout process was deemed as the more suitable approach. Subsequently, a simple stiffened panel was designed and fabricated to validate the moulding capabilities of the developed 3D printed sacrificial core process. The following conclusions were drawn:

- The proposed process is capable of moulding complex composite structures fabricated by liquid moulding
- The composite quality achieved is comparable to structures fabricated with conventional core technologies

Lastly, a cost assessment method was proposed, and the fabrication cost of different core technologies were analyzed. The assessment revealed the following:

- Additive manufacturing is a flexible fabrication process by eliminating non-recurring cost
- The recurring cost of the proposed 3D printed cores is higher than traditional cast core technologies
- 3D printed cores offer competitive price points to other technologies for low to medium production volumes.

The overall objective of this work was achieved by delivering and validating a flexible and financially feasible fabrication process of sacrificial cores, that is suitable for manufacturing low volumes of complex composite structures using liquid moulding.

8.2 Future Work

Significant efforts are required before the proposed process can be implemented for production of aerospace structures. Future work, that would improve and further validate the 3D printed sacrificial core method developed, include the following:

- A dimensional accuracy analysis of the PVOH-copolymers cores and the resulting composite part is suggested. Although the dimensional accuracy assessment of 3D printed parts has been covered in the literature [19], no study has been done on PVOH-copolymer cores. Next to determining the dimensional tolerance of the core, the tolerance of the final composite structure should be investigated to ensure no minor deformations of the core have occurred during the moulding process.
- Microscopic analysis of the moulded composite is suggested to be performed to ensure no contamination of the washout core into the matrix has occurred. Visible artefacts of apparently trapped core have been found in some structures fabricated,

however, not all. A possible link to excess moisture in the core causing this contamination must be investigated.

- To apply this process in a production environment, the development of a washout cell is required. While the washout setup presented is functional, a more feasible system including a recycling approach to filter and extract the dissolved polymer from the solvent, is worth investigating.
- All structures fabricated in this work were made with low pressure infusion processes. The proposed sacrificial core should be tested with resin transfer moulding processes that have a completely enclosed rigid cavity and apply higher pressures to the core.

The future developments and investigations suggested are believed to be key components to bring the developed process to the level required to be suitable for the targeted production of complex aerospace structures.

9 REFERENCES

1. Tomblin, J., *Overview of Composite Material Trends in Aviation Manufacturing*. 2006, National Institute for Aviation Research (NIAR) National Institute for Aviation Research (NIAR).
2. Hale, J., *Boeing 787 from the Ground Up*. 2006, Boeing.
3. Levesque, M., *COMP-1601 - Research Proposal*. 2016.
4. Kruckenberg, T.M. and R. Paton, *Resin transfer moulding for aerospace structures*. 1998.
5. Clever, H.A. and M.T. Johnson. *Development of an FST/OSU passing rigid polyurethane foam for the aerospace industry*. in *SAMPE Long Beach 2016 Conference and Exhibition, May 23, 2016 - May 26, 2016*. 2016. Long Beach, CA, United states: Soc. for the Advancement of Material and Process Engineering.
6. Stöger, A.Z.W., *In-Mold Foamed Cores for Lightweight Design*. Kunststoffe International, 2015. **2015/10**.
7. Synfoam. *Flame Retardant Closed Cell Syntactic Resin System*. Available from: http://synfoam.com/Products/SynFoam_LFR.
8. *Foam core impresses in aircraft study*. Reinforced Plastics, 2014. **58**(6): p. 31-33.
9. Du, H., et al., *Shape memory polymer S-shaped mandrel for composite air duct manufacturing*. Composite Structures, 2015. **133**: p. 930-938.
10. Tooling, S. *Smart Bladders*. Available from: <http://www.smarttooling.com/products/smart-bladders>.
11. Hammami, A. and A. Al Zarouni, *Investigation of the RTM/Bladder Molding Process*.
12. Vaidyanathan, R., et al., *Water soluble tooling materials for complex polymer composite components and honeycombs*. SAMPE Journal, 2003. **39**(1): p. 22-33.
13. Vaidyanathan, R., et al., *Water soluble tooling materials for filament winding and VARTM*. SAMPE Journal, 2005. **41**(4): p. 40-55.
14. AG, A.C.L., *Autoclave Application with Aquacore 1024*.
15. Gibson, I., D.W. Rosen, and B. Stucker, *Additive manufacturing technologies : rapid prototyping to direct digital manufacturing*. 2010.
16. Goodship, V., B. Middleton, and R. Cherrington, *Design and Manufacture of Plastic Components for Multifunctionality : Structural Composites, Injection Molding, and 3D Printing*. 2016.
17. Merriman, D.J., *3D PRINTED PROTOTYPE AND WATER WASHOUT TOOLING FOR COMPOSITES*. 2014, The ExOne Company.
18. Li, H., et al., *Modeling and characterization of fused deposition modeling tooling for vacuum assisted resin transfer molding process*. Additive Manufacturing, 2015. **7**: p. 64-72.
19. Schniepp Timothy, J., *Design guide development for additive manufacturing (FDM) of composite tooling*. 2016.
20. Stratasys. *Ultem 1010*. Available from: <http://www.stratasys.com/materials/search/ultem1010>.
21. Stratasys, *ST-130 - Technical Data Sheet*.

22. Stratasys. *ST-130 Sacrificial tooling material*. Available from: <http://www.stratasys.com/materials/search/st-130>.
23. Verbatim, *BVOH (Butenediol vinyl alcohol co-polymer) for use with 3D printers – water-soluble support material for complex 3D printed objects*.
24. Filaments.ca, *PVA Filament*.
25. e3D-Online. *Scaffold Soluble Support Filament*. Available from: <https://e3d-online.com/scaffold-filament-3d-printing-spoolworks>.
26. Lakshman Narender, S., *3D printed dissolvable molds for composite applications*. International SAMPE Technical Conference, 2016. **2016**.
27. manufacturingguide.com, *Fused Deposition Modeling, FDM*.
28. International, A., *ASTM D695-15, Standard Test Method for Compressive Properties of Rigid Plastics*. 2015.
29. Gardiner, G. *HP-RTM on the rise*. 2015; Available from: <https://www.compositesworld.com/articles/hp-rtm-on-the-rise>.
30. Thouin, M., H. Ghiasi, and L. Lessard, *Design of a carbon fiber bicycle stem using a novel internal bladder resin transfer molding technique*. Advanced Composites Letters, 2010. **19**(1): p. 51-60.
31. Duran, C., *Experimental desktop 3D printing using dual extrusion and water-soluble polyvinyl alcohol*. Rapid Prototyping Journal, 2015. **21**(5): p. 528-34.
32. Lehnert, L.H., P., *Additive Manufacturing of Polyvinyl Alcohol Mandrels for Complex Composite Structures*. International SAMPE Technical Conference, 2018. **2018**.
33. Haffner, S., *Cost modeling and design for manufacturing guidelines for advanced composite fabrication*, in Massachusetts Institute of Technology. Dept. of Mechanical Engineering. 2002: Massachusetts Institute of Technology.
34. Ma, W., *Cost Modelling for Manufacturing of Aerospace Composites*. 2011, Cranfield University.
35. Tong, R., *Cost Analysis on L-Shape Composite Component Manufacturing in Mechanical and Industrial Engineering* 2012, Concordia University